Faculdade de Engenharia da Universidade do Porto

Development of Polymeric Nanoparticles Loaded with Efavirenz Targeting Central Nervous System through Microfluidic Platforms

Cláudia de Freitas Martins

June, 2017

U.PORTO
FEUP FACULDADE DE ENGENHARIA
UNIVERSIDADE DO PORTO

MEB - MESTRADO EM ENGENHARIA BIOMÉDICA **2016/2017**

A Dissertação intitulada

"Development of Polymeric Nanoparticles Loaded with Efavirenz Targeting Central Nervous System Through Microfluidic Platforms"

foi aprovada em provas realizadas em 07-07-2017

o júri

Presidente Prof. Doutor Fernando Jorge Mendes Monteiro
Professor Catedrático do Departamento de Engenharia Metalúrgica e de Materiais da FEUP - U.Porto

Prof. Doutor José Carlos Márcia Andrade
Professor Auxiliar do Instituto Universitário de Ciências da Saúde

Doutor Bruno Filipe Carmelino Cardoso Sarmento
Investigador do Instituto de Engenharia Biomédica da INEB - U. Porto

O autor declara que a presente dissertação (ou relatório de projeto) é da sua exclusiva autoria e foi escrita sem qualquer apoio externo não explicitamente autorizado. Os resultados, ideias, parágrafos, ou outros extratos tomados de ou inspirados em trabalhos de outros autores, e demais referências bibliográficas usadas, são corretamente citados.

Autor - Cláudia de Freitas Martins

Faculdade de Engenharia da Universidade do Porto

“Be fearless in the pursuit of what sets your soul on fire”

Jennifer Lee

Abstract

The human immunodeficiency virus (HIV) is a lentivirus responsible for HIV infection and acquired immunodeficiency syndrome (AIDS). This virus uses the central nervous system (CNS) as reservoir, especially the brain, which turns it as a promising target to fight this pathology. The antiretroviral efavirenz (EFV), applied in the HIV therapy, is usually not able to reach the CNS due to the difficulties in surpass the blood-brain barrier (BBB). Nanoparticles (NPs) hold tremendous potential in overcome the BBB, demonstrating to be an effective drug delivery system to the CNS. Since the conventional bulk approaches to produce NPs lack a precise control over the final properties of the nanosystems, microfluidic platforms emerged as a prospective solution to circumvent this drawback, providing much more uniform and tunable formulations.

In this work, a formulation of EFV-loaded poly(lactic-co-glycolic acid) (PLGA) NPs was produced through an innovative microfluidic platform, using the nanoprecipitation technique. In comparison with the conventionally-performed nanoprecipitation, the nanoformulation obtained through the microfluidic platform resulted in reduced NPs average size (133.0 nm for the conventional method; 72.8 nm for microfluidics), comparable NPs polydispersity index (0.090 for the conventional method; 0.086 for microfluidics), and less negative surface charge (-28.0 mV for the conventional method; -14.1 mV for microfluidics). This decrease in size is an advantageous feature for brain-targeted drug delivery. With microfluidics, higher EFV association efficiency (32.7 % for the conventional method; 80.7 % for microfluidics) and drug loading (3.2 % for the conventional method; 10.8 % for microfluidics) were obtained. The robustness of the microfluidic method was successfully demonstrated by a scaling experiment, which proved that physico-chemical properties of NPs were not affected by changes in the final volume of batches. The microfluidics-associated EFV-loaded nanosystem also demonstrated to be constituted by homogeneous round-shaped particles, containing a residual amount of the organic solvent used in the production methodology and with a sustained *in vitro* drug release profile over time from their matrix. The EFV-loaded NPs proved to be safe to BBB endothelial cells (hCMEC/D3 cell line) and brain parenchyma neuron cells (ND7/23 cell line), providing protection compared to the free drug. Hemolysis studies demonstrated a nonhemolytic behavior of the NPs, which presented only approximately 1-2 % of hemolysis and did not cause morphological changes in red blood cells. The microfluidics-associated EFV-loaded PLGA NPs were further functionalized with a transferrin receptor-binding 12-amino acids peptide, using the carbodiimide chemistry. Herein, Bradford test and nuclear magnetic resonance analysis suggested an effective surface functionalization of NPs. Finally, functionalized NPs were able to interact with BBB endothelial cells, and EFV permeated through a BBB *in vitro* model. Therefore, the work developed in the scope of this dissertation confirmed the advantages of microfluidics over conventional methodologies in the loading of the anti-HIV drug EFV in PLGA NPs, which presented suitable properties to be possibly administered by the intravenous route, in order to target the BBB.

Resumo

O vírus da imunodeficiência humana (VIH) é um lentivírus que está na origem de uma infeção viral e da síndrome da imunodeficiência adquirida (SIDA). O Sistema Nervoso Central (SNC) é um reservatório viral do VIH por excelência, principalmente o cérebro, o que o torna num alvo promissor para o combate desta patologia. O antirretroviral efavirenz (EFV), usado na terapia do VIH, apresenta geralmente uma capacidade reduzida de atingir o SNC devido à dificuldade em ultrapassar a barreira hematoencefálica (BHE). As nanopartículas (NPs) têm um elevado potencial nesta área, demonstrando ser capazes de ultrapassar a BHE e eficazes sistemas de entrega de fármacos para o SNC. Dado que as metodologias de produção de NPs baseadas em metodologias convencionais estão ligadas à carência de um controlo exato sobre as propriedades finais dos nanossistemas, as plataformas associadas à tecnologia de microfluídos surgem assim como uma possível solução para contornar esta problemática, providenciando formulações mais uniformes e versáteis.

Neste trabalho, uma formulação de NPs de ácido poli(láctico-co-glicólico) (PLGA) carregadas com EFV foi produzida por uma inovadora plataforma associada à tecnologia de microfluídos, com recurso à técnica de nanoprecipitação. Por comparação com a nanoprecipitação executada por metodologia convencional, a nanoformulação obtida pela execução da mesma técnica num ambiente microfluídico apresentou um tamanho médio inferior (133.0 nm para o método convencional; 72.8 nm para a tecnologia de microfluídos), uma comparável polidispersão das NPs (0.090 para o método convencional; 0.086 para a tecnologia de microfluídos) e uma carga superficial menos negativa (-28.0 mV para o método convencional; -14.1 mV para a tecnologia de microfluídos). A diminuição do tamanho médio das NPs é uma característica vantajosa no que diz respeito à entrega de fármacos direcionada para o cérebro. A tecnologia de microfluídos permitiu obter resultados melhores relativamente à eficiência de associação do fármaco (32.7 % para o método convencional; 80.7 % para a tecnologia de microfluídos) e dosagem do mesmo (3.2 % para o método convencional; 10.8 % para a tecnologia de microfluídos) nas NPs. A robustez do método implementado para a produção de NPs a partir da tecnologia de microfluídos foi comprovada com sucesso através de uma experiência de "scaling", que provou que as propriedades físico-químicas das NPs não são afetadas pela alteração do volume final da formulação. O nanossistema carregado com EFV resultante da tecnologia de microfluídos também demonstrou ser constituído por partículas homogéneas e de forma arredondada, contendo apenas uma quantidade residual do solvente orgânico usado aquando da sua produção, e com uma libertação "in vitro" do fármaco controlada a partir da sua matriz, ao longo do tempo. Numa segunda fase, as NPs carregadas com EFV obtidas pela tecnologia de microfluídos demonstraram não apresentar citotoxicidade em células endoteliais da BHE (linha celular hCMEC/D3) nem em células neuronais do parênquima cerebral (linha celular ND7/23), providenciando proteção em comparação com o fármaco na sua forma livre. Os testes de hemólise evidenciaram o caráter não-hemolítico do nanossistema, sendo que este apresentou uma percentagem de hemólise de apenas cerca de 1-2 % sem causar alterações morfológicas em eritrócitos. De seguida, as

NPs de PLGA carregadas com EFV e produzidas pela tecnologia de microfluídos foram funcionalizadas através da química de carbodiimida com um péptido de 12 amino ácidos específico para ligação ao recetor da transferrina. O teste de Bradford e a análise de ressonância magnética nuclear foram efectuados e surgeriram a funcionalização superficial efetiva das NPs. Por fim, as NPs foram capazes de interagir com células endoteliais da BHE e o EFV permeou através de um modelo "in vitro" da BHE. Assim, o trabalho desenvolvido no âmbito desta dissertação confirmou as vantagens da tecnologia de microfluídos em relação às metodologias convencionais na incorporação do fármaco anti-VIH EFV em NPs de PLGA, que apresentaram propriedades adequadas para uma possível administração intravenosa, de forma a atingirem a BHE.

Acknowledgments

Ao meu orientador, Professor Bruno Sarmento, deixo o meu sincero agradecimento por me ter recebido no seu grupo e por ter marcado o início do meu percurso científico. Obrigada por todo o apoio e por acreditar em mim. Não poderia deixar de mencionar a boa disposição e otimismo que tão bem o caracterizam. Muito obrigada por tudo! Espero, verdadeiramente, que isto seja apenas o início.

Às minhas co-orientadoras, Francisca Araújo e Maria João Gomes, a quem devo um enorme agradecimento por toda a dedicação, paciência e bons conselhos. Francisca, pela compreensão, por todas as palavras de encorajamento, e, acima de tudo, pela amizade inesperada que construímos. Maria João, por me ter amparado nos tempos iniciais e por, mesmo longe, nunca ter deixado de me acompanhar. Obrigada por me terem ajudado a tornar a realização desta dissertação possível.

Ao Professor José Machado Da Silva, pela disponibilidade e prontidão no esclarecimento de qualquer dúvida.

À Virgínia Gonçalves, por ter sido tão prestável e amável comigo, recebendo-me sempre bem no seu laboratório.

Ao Carlos Fernandes, à Inês Gonçalves e à Tália Figueiredo, pela contribuição fundamental para o desenvolvimento do meu trabalho científico.

Aos meus colegas de grupo, pelo bom ambiente que me proporcionaram e espírito de entreajuda. Um especial obrigada ao José das Neves, pelos sábios conselhos, e à Rute Nunes, por ter sido bem mais do que uma "colega" cuja ajuda foi fundamental ao longo do meu mestrado.

Aos bons amigos que fiz no i3s/INEB, a quem devo um obrigada pelo companheirismo, apoio e momentos de diversão. Andreia Pereira e Inês Borges, pelas gargalhadas intermináveis. João Brás e Gonçalo Laranja, por serem uma verdadeira "lufada de ar fresco" nos momentos mais complicados. Micaela Querido, pela boa surpresa que foi a nossa amizade e por me ter guiado nos primeiros tempos. Patrícia Henriques, por ser a "coleguinha" do meu coração.

Aos amigos da cidade que irei sempre recordar com o maior dos carinhos, a minha Covilhã, por serem a prova de que a verdadeira amizade é mais forte do que qualquer distância. Não posso deixar de mencionar a Ângela Magalhães e a Daniela Dias, por todos os momentos inesquecíveis e por estar tão grata por os nossos caminhos se terem cruzado.

Aos meus amigos da Cidade Berço, por compreenderem a razão da minha ausência em alguns momentos importantes, sem nunca deixarem de me fazer sentir em casa. Às minhas amigas de infância, "Mirisaclauchi", por estarem ao meu lado todos estes anos. À Ana Costa, por prezar tanto a nossa amizade e pelas nossas agradáveis semelhanças na forma de pensar. À Vânia, pelos ensinamentos que ajudaram a moldar a minha postura, não apenas no ballet, mas também na vida.

Às Professoras Alcina Lobo, Armanda Gomes e Maria do Céu, por me terem incentivado sempre a dar o meu melhor e por me terem motivado em diferentes fases do meu percurso escolar. Obrigada!

E porque o melhor fica para o fim… aos meus pais e à minha irmã! Aos meus pais, pelo apoio incondicional, por serem o meu "porto seguro", por me darem tudo aquilo a que eles nunca tiveram direito… não há palavras que cheguem para expressar o quanto eu os admiro, o amor infinito que sinto por eles, o sentimento de gratidão pelo esforço que depositaram neste meu percurso académico. À minha irmã, o meu maior orgulho, por me compreender como ninguém, por saber sempre como me confortar nos momentos mais difíceis, por me querer tão bem. Não posso deixar de agradecer aos restantes familiares que contribuíram para o sucesso desta jornada.

Deixo ainda o meu agradecimento às instituições que me acolheram - FEUP, i3s/INEB e iinfacts/CESPU.

Cláudia Martins

Contents

List of figures

List of tables

Abbreviations and Symbols

List of abbreviations

^{1}H NMR	Proton nuclear magnetic resonance
6-C	6-coumarin
ABC	Adenosine triphosphate-binding cassette
AE	Association efficiency
AET	Active efflux transporter
AIDS	Acquired immunodeficiency syndrome
ANOVA	One-way analysis of variance
API	Active pharmaceutical ingredient
ART	Antiretroviral therapy
ARV	Antiretroviral
BBB	Blood-brain barrier
bFGF	Basic fibroblast growth factor
BLOOD-CSF	Blood–cerebrospinal fluid
BSA	Bovine serum albumin
CAT1	Cationic amino acid transporter 1
CD4	Cluster of differentiation 4
CD8	Cluster of differentiation 8
CMT	Carrier-mediated transporter
CNS	Central nervous system
CNT2	Concentrative nucleoside transporter 2
CPE	Central nervous system penetration effectiveness scoring system
CSF	Cerebrospinal fluid
CSF-BLOOD	Cerebrospinal fluid-blood
CSF:BP	Cerebrospinal fluid:blood plasma concentration ratio
DAPI	4',6-diamidino-2-phenylindole
DCM	Dichloromethane
DDS	Drug delivery system
DL	Drug loading
DLS	Dynamic light scattering
DMEM	Dulbecco's Modified Eagle medium
DMF	N,N-dimethylformamide

DMSO	Dimethyl sulfoxide
DNA	Deoxyribonucleic acid
DP	Drug/polymer ratio
DSDNA	Double-stranded deoxyribonucleic acid
EBM-2	Endothelial basal medium 2
ECM	Extracellular matrix
EDC	1-ethyl-3-(3-dimethylaminopropyl)carbodiimide
EDS	Energy-dispersive X-ray spectra
EFV	Efavirenz
EI	Entry inhibitor
EMA	European Medicine Agency
FACS	Fluorescence-activated cell sorting
FBS	Fetal bovine serum
FcR	Fc receptor
FDA	Food and Drug Administration
FSC-A	Forward scatter area
FSC-H	Forward scatter height
GA	Glycolic acid
GLUT1	Glucose transporter 1
HBSS	Hank's Balanced Salt Solution
hCMEC/D3	Immortalized human cerebral microvascular endothelial cell line
HEPES	4-(2-hydroxyethyl)-1-piperazineethanesulfonic acid
HIV	Human immunodeficiency virus
HIV-1	Human immunodeficiency virus type 1
HIV-2	Human immunodeficiency virus type 2
HPLC	High-performance liquid chromatography
HPMC	Hydroxymethylcellulose
IC50	50 % inhibitory concentration
IN	Integrase
INSTI	Integrase strand transfer inhibitor
ISO	International Organization for Standardization
LAT1	L-type amino acid transporter 1
LA	Lactic acid
LDA	Laser Doppler anenometry
MCT1	Monocarboxylate transporter 1
MES	2-(N-morpholino)ethanesulfonic acid
MFI	Mean fluorescence intensity
MTT	3-(4,5-dimethylthiazol-2-yl)-2,5-diphenyltetrazolium bromide
MWCO	Molecular weight cutoff
NC	Negative control
ND7/23	Mouse neuroblastoma × rat dorsal root ganglion neurone hybrid cell line
NHS	N-hydroxysuccinimide

NNRTI	Non-nucleoside reverse-transcriptase inhibitor
NP	Nanoparticle
NRTI	Nucleoside reverse-transcriptase inhibitor
NtRTI	Nucleotide reverse-transcriptase inhibitor
Papp	Apparent permeability
PBS	Phosphate buffered saline
PC	Positive control
PDI	Polydispersity index
PDMS	Polydimethylsiloxane
PGA	Poly(glycolic acid)
P-gp	P-glycoprotein
PI	Protease inhibitor
PLA	Poly(lactic acid)
PLGA	Poly(lactic-co-glycolic acid)
PR	Protease
PVA	Poly(vinyl alcohol)
PVCA	Poly(vinyl chloride-co-acetate)
PVPA	Phospholipid vesicle-based permeation assay
RMT	Receptor-mediated transporter
RNA	Ribonucleic acid
RT	Reverse transcriptase
SDS	Sodium dodecyl sulfate
SEM	Scanning electron microscopy
SSC-A	Sideward scatter area
TCR	T-cells receptor
TEER	Transepithelial electric resistance
TEM	Transmission electron microscopy
THF	Tetrahydrofuran
TMS	Tetramethylsilane
WGA	Wheat germ agglutinin
WHO	World Health Organization
Z-AVERAGE	Average size

List of symbols

ζ	Zeta
δ	Chemical shift value
R^2	Coefficient of determination value

Chapter 1

Introduction

1.1 Context and motivation

The central nervous system (CNS) is a well-protected structure by means of biological barriers, namely the blood-brain barrier (BBB). This barrier, which is mainly formed by endothelial cells that line cerebral microvessels, plays a key role in the maintenance of a precisely regulated CNS microenvironment [1]. However, the same mechanisms that protect this complex physiological system against dangerous compounds can also avoid brain-targeted drug delivery to be effective [2]. The conventional solutions offered to circumvent this problem are often associated with a neuroinvasive surgery [3].

Human immunodeficiency virus (HIV) infection and acquired immunodeficiency syndrome (AIDS) belong to a spectrum of conditions derived from the HIV. The HIV continues to be considered a major global public health issue since the virus attack specific types of immune cells, hence suppressing the immune system. Therefore, a lot of opportunistic infections or other diseases may appear and the body cannot act against them [4]. The HIV is characterized by a neurovirulent profile, thus being able to infect the brain, use the brain as reservoir, and cause severe CNS damage [5]. In consequence, the CNS is recognized as a sanctuary site for virus replication.

The emergence of antiretroviral therapies (ARTs) against HIV resulted in virus-associated morbidity and mortality decline [5], allowing infected individuals to improve their life quality and expectancy. Efavirenz (EFV) is an antiretroviral (ARV) approved by Food and Drug Administration (FDA) for HIV infection treatment [6]. This drug attaches and blocks a virus-specific enzyme, the reverse transcriptase (RT) [7-9]. However, the importance of ARVs to penetrate the CNS continues to be debated. After the administration of a drug, its distribution throughout the body depends on its physico-chemical properties and molecular structure [10]. In the case of EFV and other ARVs, the final amount of drug that reaches CNS is only a small fraction of the administered dose. This means that, during the path, they interact with biological barriers and healthy tissues, which are not involved in the process, even causing the loss of the drug efficacy and the arrival of undesirable effects [11]. This drawback can be circumvented by formulating the drug into an appropriate drug delivery system (DDS) which is defined as a “formulation or a device that enables the introduction of a therapeutic substance in the body and improves its efficacy and safety by controlling the rate, time, and place of release of drugs in the body” [12]. Furthermore, to achieve an efficient

pharmacological activity of the drug at the site of action it is necessary to recognize some important aspects, such as the interactions of the components of these systems with the biological environment, the stability of therapeutic agents, and the molecular mechanisms of cell-signaling involved in the pathophysiology of the disease under consideration. Drug delivery systems are usually associated with small size, reduced toxicity and modification of drug pharmacokinetics [11, 13].

Nanoparticles (NPs) are considered one of the most auspicious and versatile DDSs into regions of difficult access, like the brain, being able to provide protection to therapeutic agents while efficiently delivering them into the damaged areas [14]. For that reason, these novel approaches are able to face the challenge of crossing the protective barriers of the CNS [15], and also to prolong systemic drug circulation [16, 17]. Nanoparticles are considered a product of nanotechnology, which is the field of technology that aims to control, manipulate, study and engineer structures and devices in the "nanometer" size range [18]. The definition of nanomaterials may vary from the classical one, which considers any structure having at least one dimension value within the range 1-100 nm [19], to a more liberal interpretation, which considers any substance with particulate dimensions from 1 nm up to 999 nm. Considered the technology of the future by many, nanotechnology has applicability in a wide range of areas and is expected to open some new paths to fight and prevent diseases [20].

Different materials are used to produce NPs, as polymers (polymeric NPs, micelles, dendrimers), lipids (liposomes), viruses (viral NPs), metals, or even organometallic compounds (nanotubes) [21, 22]. Nowadays, polymeric NPs are most of the times preferred as DDSs due to their favorable properties for active pharmaceutical ingredients (APIs) loading and delivery. Particularly in this field, the biodegradable polymer poly(lactic-co-glycolic acid) (PLGA) has shown immense potential [23].

There are several techniques to produce NPs as DDSs, which are suitable for several applications. Among them, nanoprecipitation may be used to encapsulate EFV in PLGA NPs. The successful loading of drugs within the NPs core depends mostly on APIs properties, NPs materials composition, and the encapsulation method [23]. Techniques performed by conventional bulk methods using equipments as homogenizers or magnetic stirrers and vassels offer several limitations, such as the lack of precise control of NPs properties. Regulatory institutions such as FDA and the European Commission pointed out that one of the major restrictions to the actual application of current nanotechnology is, in fact, the lack of homogeneous formulations of NPs [24]. Therefore, microfluidic platforms emerged as potential candidates to produce drug-loaded NPs in a well-controlled process using the same techniques. Microfluidics is associated with a fine manipulation of process parameters, thus providing the optimization of NPs properties, including encapsulation efficiency of drugs in the systems and monodispersity of batches. This method is able to tightly control the local particle-formation environment in a continuous flow pattern [25].

1.2 Objectives

Herein, we aimed to develop a formulation of EFV-loaded PLGA NPs to target the CNS using the microfluidics technology. To the best of our knowledge, any microfluidic system to produce NPs with this polymeric matrix and to encapsulate this drug has been yet reported. Nanoprecipitation was the selected technique to perform drug encapsulation.

The tasks planned in this dissertation were:

- Production of EFV-loaded NPs by the conventionally-performed technique (including a modified version of nanoprecipitation);

- Production of EFV-loaded NPs by the technique performed through microfluidics using the co-flow and flow-focusing geometry of the fluids;
- Comparison of NPs obtained by the two methodologies regarding particles physico-chemical characteristics;
- Evaluation of the robustness of the microfluidic method in scale-down or scale-up NPs production;
- Analysis of the effect of microfluidics-associated EFV-loaded PLGA NPs on the metabolic activity of BBB endothelial cells and brain parenchyma neuron cells;
- Study of the hemolytic potential of the nanosystem obtained by microfluidics;
- Functionalization and characterization of NPs with a transferrin receptor-binding peptide;
- Evaluation of the interaction of functionalized NPs with BBB endothelial cells;
- Permeability study of NPs through a BBB *in vitro* model (including the evaluation of the model integrity).

The nanosystem should be intravenously administered, *a posteriori*.

The uppermost concept of this project was to develop ARV-loaded NPs using the microfluidic technology as a scalable methodology. Once the setup was defined, including the optimization of NPs final properties, to accomplish the desired purpose, the system underwent biological tests and was ameliorated to operate in the desired target, leading to a therapeutically effective treatment against the pathological case in study, the HIV.

1.3 Work structure

This dissertation was organised in five chapters.

Chapter 1, “Introduction”, was dedicated to explore the motivation for this work and the inherent main goals.

Chapter 2, “State of the Art”, was divided into seven sections: the first related to the CNS, where BBB was emphasized; in the second section, a brief reference to BBB *in vitro* models was stated; the third associated with HIV, in particular to the infection mechanism and the incidence in CNS; the fourth section presented a brief introduction to the HIV-based ART; in the fifth section the use of polymers as biomaterials to be implemented in NPs was discussed; on the sixth section, conventionally-performed methodologies were described, namely nanoprecipitation, that allows PLGA NPs development; the seventh and last section of this chapter was related to an innovative method used in the production of PLGA NPs, the microfluidics, and its applicability.

Chapter 3, where the “Material and Methods” of the practical work performed were presented in detail, so the experiments described can be reproduced by other researchers.

Chapter 4, “Results and Discussion”, stated the results obtained and respective discussion.

In the last chapter, “Conclusion”, the main findings of the developed work and future prospects were presented.

Chapter 2

State of the Art

2.1 Central nervous system

The CNS is composed by the brain and the spinal cord. These structures have sensitive cells which need accurate control of their biochemical and immunological milieu, in order to achieve an optimal functioning [26, 27]. Some disorders related to the CNS are neurodegenerative diseases as Parkinson's or Alzheimer's diseases, brain cancer, epilepsy, and severe infections as HIV [28].

There are three main boundaries in the brain that protect neuronal microenvironment: the blood–cerebrospinal fluid (blood-CSF) barrier, the BBB, and the cerebrospinal fluid-blood (CSF–blood) interface. Blood-CSF barrier is formed by epithelial cells of the choroid plexus; BBB is shaped through cerebral endothelium; and the CSF-blood interface is formed by superposition of dura mater and the avascular arachnoid epithelium [16, 29, 30].

For the purpose of this study, BBB was the main focus.

2.1.1 Blood-brain barrier

One of the barrier systems that protect and maintain the homeostasis of the CNS in all animals with a complex nervous system is the BBB [31]. The BBB main goal is to control the influx of blood-borne active molecules and cells to the brain [32]. However, BBB is a "bottleneck" in drug development for brain target, thus restraining the enlargement of CNS pharmacotherapeutics field [33].

The BBB covers almost all brain regions, with the exception of circumventricular organs, where blood-borne molecules diffusion across the vessel wall is allowed [34].

The BBB is composed by strongly linked brain microvascular endothelial cells through specific junctional structures [2, 31]. Astroglia, pericytes, perivascular macrophages, and a basement membrane (also known as basal lamina) surround BBB endothelial cells, thus contributing to the maintenance of BBB integrity [31]. Regarding anatomy and functionality, BBB is directly associated with brain parenchymal cells, such as neurons [34]. On Figure 2.1, the BBB structure and its environment are illustrated.

Endothelial cells delineate the brain microvessels. These cells interact with the surrounding astrocytes, pericytes and neurons, and together they build the so-called neurovascular unit [35]. Endothelial cells have highly selective functions due to the inter-endothelial junction network and a

particular assortment of transporters, which allow the controlled passage of substances through the BBB [36]. Endothelial cell-cell junctions include tight junctions, adherens junctions and gap junctions. All of these junctions result from the combination of membrane adhesive proteins that allow BBB cohesive structure [37, 38]. Adherens junctions are mainly responsible for regulating cell-cell contacts [39]; tight junctions regulate solutes and ions diffusion through the paracellular pathway [2, 31, 39]; and gap junctions, in turn, mediate intercellular communication by hemi-channels formation [38, 40, 41]. Besides junctions, the capillary endothelium is characterized by the lack of fenestrations, and almost absence of pinocytotic vesicles [34].

Astrocytes represent around 90% of overall brain mass [42]. They are crucial cells for BBB development and maintenance by secreting factors, which provide the adequate association between barrier cells and the establishment of strong tight junctions [43]. Among other functions, astrocytes are responsible for neurons support, and play a key role in different brain metabolic processes [44, 45].

Pericytes are contractile cells which encircle the brain capillaries, composed of relatively undifferentiated connective tissue [46]. Pericytes association to blood vessels regulates endothelial cells survival, migration, differentiation, proliferation, and vascular branching [47].

Perivascular macrophages are responsible for innate and adaptive immune responses in the brain [47]. Literature data suggest that this cell line derives from monocyte lineage [48].

In addition to BBB cellular components, the extracellular matrix (ECM) is also an important structural element. The CNS ECM is formed in the intracellular microenvironment and then secreted into the extracellular space, in order to develop a dense molecule network of proteins and glycans [49, 50]. It surrounds cells providing both structural and chemical support. The ECM offers anchorage points to cells and enables their spatial arrangement. Simultaneously, the matrix is a source of external stimulus that conduct the survival, differentiation, growth, and migration of cells [51]. The basement membrane is a continuous ECM structure connecting endothelial cells to astrocytic endfeet, and it is mostly known for its role in maintaining BBB integrity [51, 52].

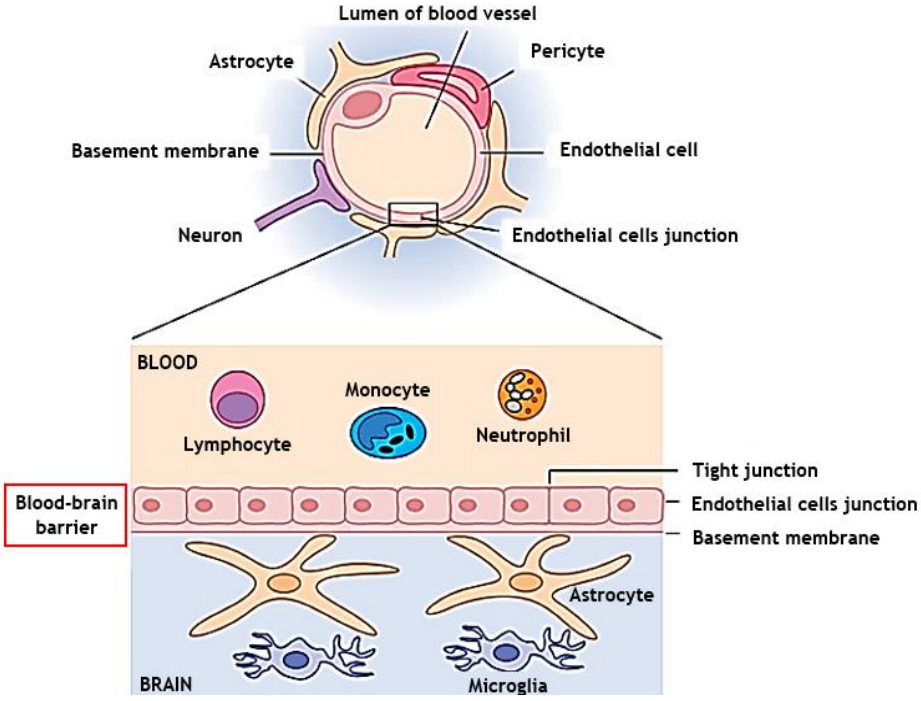

Figure 2.1 – Structure of the BBB. The principal feature of this barrier is the tight apposition of endothelial cells lining blood vessels in the brain. Adapted from [52].

Cells movement across BBB (eg, leukocytes) is a highly regulated process that requires cell- and tissue-specific mechanisms. These interactions involve a variety of intracellular and/or extracellular molecules and barrier structures, which include cytokines and their receptors, cell adhesion molecules, and tight junctions, among others [53].

The BBB is also an enzymatic barrier. These enzymes are responsible for neuroactive blood-circulating solutes metabolization, like drugs or nutrients, and they are often polarized between the apical and basolateral surface of endothelial cells [37]. Some examples of these enzymes are γ-glutamyl transpeptidase, alkaline phosphatase, and aromatic acid decarboxylase [54].

In general, there is a bidirectional impediment to free diffusion through the BBB [31]. In fact, only the lipid-soluble small molecules with a molecular weight < 400 Da [55] and < 8 hydrogen bonds formed with solvent water [33] are able to cross the BBB with significant relevance, when driven by a concentration gradient and in absence of active transport [34].

In addition to providing a physical barrier, both apical and basolateral surfaces of endothelial cells are able to express molecular efflux and/or influx carriers (Figure 2.2). These are classified in carrier-mediated transporters (CMTs), active efflux transporters (AETs), and receptor-mediated transporters (RMTs). CMTs and AETs are responsible for small molecules transport, whereas RMTs are responsible for large molecules transport [56].

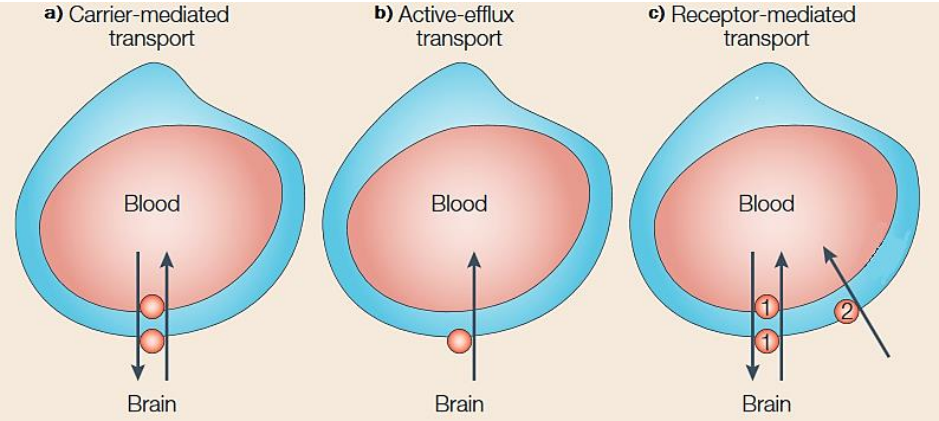

Figure 2.2 - BBB transporters. a) CMT; b) AET; c1) RMT transferrin receptor; c2) RMT Fc receptor. Adapted from [57].

Carrier-mediated transporters (Figure 2.2a) are expressed on both apical and basolateral BBB side, and thus they catalyze the bidirectional movement of polar nutrients between blood and brain, such as glucose, amino acids, monocarboxylic acids, choline, purine nucleosides, thyroid hormone and water-soluble vitamins [57]. Each molecule accesses a unique CMT system; this type of transport occurs through specialized stereospecific proteins, which means that they display significant structural requirements [57, 58]. Some examples of CMTs are glucose transporter 1 (GLUT1), monocarboxylate transporter 1 (MCT1), L-type amino acid transporter 1 (LAT1) and cationic amino acid transporter 1 (CAT1), or concentrative nucleoside transporter 2 (CNT2) [59].

Active efflux transporters (Figure 2.2b) are asymmetrically expressed on apical BBB side, and thus they mediate the unidirectional efflux of metabolic products and xenobiotics, which include drugs, from brain to blood [57]. Some examples of AETs structures are the P-glycoprotein (P-gp) transporter and other adenosine triphosphate-binding cassette (ABC) gene family members [60].

Receptor-mediated transporters (Figure 2.2c) consist on a group of peptide-specific receptors which can be expressed on apical, basolateral, or both BBB side [56, 57]. For example, on one hand

the transferrin receptor, represented with number 1 in Figure 2.2c, is a bidirectional system (expressed on both BBB side) [61]. On the other hand, the Fc receptor (FcR), represented with number 2 in Figure 2.2c, only promote the transport in the brain-to-blood direction (only expressed on apical BBB side) [62].

Besides transporters, BBB endothelial cells present several ion channels which are involved in brain homeostasis and barrier physiology [37].

The biggest challenge related to the treatment of diseases involving the CNS is the effective delivery of drugs across the BBB [2]. It is known that 100 % of large-molecule drugs and > 98 % of small-molecule drugs cannot surpass it [55]. Moreover, as previously mentioned, a successfully diffusion trough the BBB implies a drug lipid-soluble profile. Pharmaceutical industry has been trying to manipulate the BBB permeation by changing the water-soluble profile of drugs with therapeutic relevance for the CNS to a lipid-soluble one. However, this may rise variations in pharmacokinetic and chemical stability properties that enable successful therapies [63]. Besides size and solubility, drugs that are highly bound to plasma proteins are also less available to cross the BBB [64]. One possible solution to overcome these problems seems to be the exploitation of endogenous BBB transporters [55]. Drug structure can be modified to increase its affinity for one of several CMT or RMT systems that normally serves to mediate the brain uptake of natural molecules [63].

2.2 Blood-brain barrier *in vitro* models

Blood-brain barrier *in vitro* models present a useful tool to predict the ability of therapeutic compounds to permeate this biological barrier. This tool is also extremely important to study the effectiveness of nanotechnology-based products to deliver drugs across the BBB, hence allowing the identification of the optimal formulation parameters to be applied in *in vivo* studies [65].

In vitro models may be based on a cellular or non-cellular structure. Cellular-based models are able to express different physiological drug transport mechanisms and metabolic enzymes, allowing the inclusion and study of different permeability pathways [66]. Non-cellular-based models consist on artificial membranes, as phospholipid vesicle-based permeation assay (PVPA), and are only able to study the passive diffusion of drugs by passive transcellular-like permeability. Non-cellular models are cheaper, less time-consuming, easily reproducible, and do not present contamination problems compared to their cellular-based counterparts [67, 68]. However, cellular-based *in vitro* models are usually preferred since an ideal structure for a BBB *in vitro* model should comprise a morphology very similar to the *in vivo* cellular one, restrictive paracellular transport (well-defined tight junctions), expression of specific transporters, efflux mechanisms and enzymes [69]. Afterwards, the model should be able to closely mimic the *in vivo* environment of the BBB. It is important to mention that cellular-based BBB *in vitro* models also present disadvantages, as the associated costs of maintenance, time spent in cell culture, and difficulties in obtain reproducible results [68].

The simplest cellular-based BBB model consists on a monoculture of brain endothelial cells, the major cellular component of the BBB, cultured on an insert membrane (Transwell® system). Besides the simplicity, this model is considered appropriate for the initial screening of drugs permeability [69]. In order to increase the degree of resemblance with the biological structure of the BBB and its evironment, another cell types can be included, as astrocytes, neurons, or pericytes. They can be co-cultured in the basolateral compartment, either in contact (cultured in the basolateral side of

the insert membrane) or non-contact (cultured in the bottom of the well) [65]. Figure 2.3 demonstrates some examples of BBB *in vitro* models.

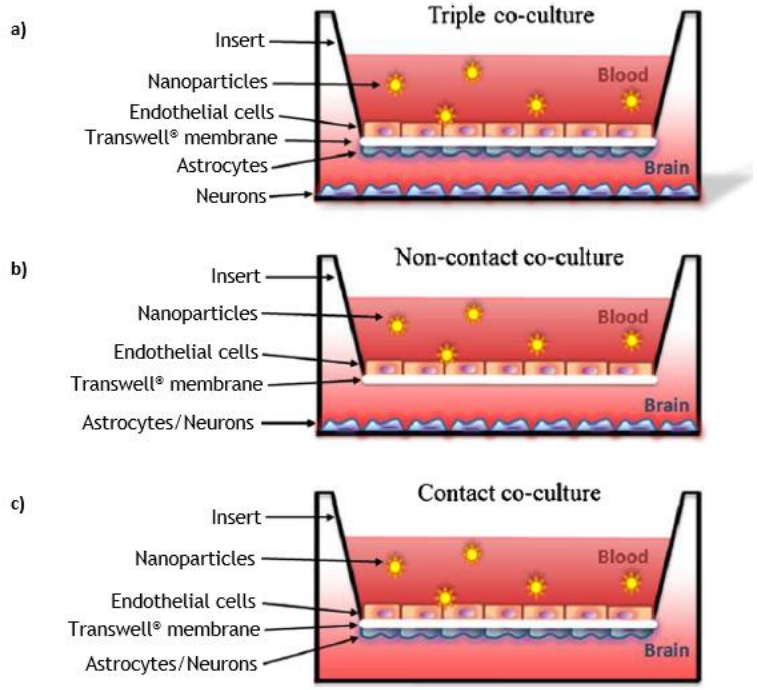

Figure 2.3 – Schematic representation of *in vitro* cell-based models of the BBB using Transwell® systems to be applied in permeability studies of nanotechnology-based products. a) Triple co-culture of endothelial cells, astrocytes and neurons; b) non-contact co-culture of endothelial cells and astrocytes or neurons; c) contact co-culture of endothelial cells and astrocytes or neurons. Adapted from [65].

Still, challenges remain. The *in vitro* models currently employed in the biomedical research field are far from the ideal structure, mainly due to the *in vivo* complexity of the BBB which is difficult to mimic. It would be important to improve these models, keeping a balance between the degree of resemblance, ease of development and applicability [65]

2.3 Human immunodeficiency virus

By the end of 2015, World Health Organization (WHO) estimated that 37 million people in the world were living with HIV [70]. HIV disease is caused by an infection with human immunodeficiency virus type 1 (HIV-1) or human immunodeficiency virus type 2 (HIV-2), which are retroviruses of the Retroviridae family, *Lentivirus* genus [71].

The virus infects and destroys immune cells, thus increasing susceptibility to infection and disease, and over time this can lead to AIDS [4].

The HIV is a blood-borne virus transmitted via sexual intercourse (vaginal, anal, or in a minor contribution, oral sex); shared intravenous drug paraphernalia (needles, syringes, or other sharp instruments); mother-to-child transmission when the mother is already HIV-positive, which can occur during pregnancy, childbirth or breast-feeding; and through blood transfusion [72, 73].

The HIV-1 is the most virulent type (commonly denoted only as HIV) [73]. Although the two types of virus share the same transmission routes, HIV-2 is not as easily transmitted as HIV-1. The HIV-2 takes more time from infection to AIDS, it has a longer latency period, and low or

undetectable plasmatic viral levels [74]. Moreover, HIV-1 is predominant worldwide, whereas HIV-2 is typically confined to West Africa [75, 76]. The mortality rate related to HIV-1-infected individuals is significantly higher than that related to HIV-2-infected ones [77]. Both HIV-1 and HIV-2 have an identical structure, and the virus-induced disease pathogenesis is also very similar [78].

2.3.1 Infection process

The HIV infects blood circulating cells containing HIV key receptors, which are mainly the CD4 (cluster of differentiation 4; immune cells receptor), but also CD8 (cluster of differentiation 8; co-receptor of T-cells receptor (TCR)), and various chemokine-receptors (HIV co-receptors). They help virus attachment to cells and promote the fusion of viral envelope with cell membrane. Therefore, virus capsule, which includes virus ribonucleic acid (RNA) and viral enzymes RT, integrase (IN), and protease (PR), enters the cytoplasm [79]. Each virus particle comprises two identical RNA copies of the genome [71]. After entry into the cell and due to the action of RT, the virus undergoes reverse transcription of its RNA genome into a double-stranded deoxyribonucleic acid (dsDNA). The IN then facilitates dsDNA integration into the host chromosome. By using the cellular replication machinery, provirus (HIV deoxyribonucleic acid (DNA)) replicates along with the chromosome when the cell divides [80]. Every time the provirus is transcribed, new viral RNA and proteins are produced using the host cell protein-making system [81]. The PR participates by processing the recently translated polypeptides into proteins, which are then assembled into viral particles [82]. At this point in time, the virus is able to bud out of the cell and proceed with its dissemination, acquiring a phospholipid envelope [83]. Figure 2.4 summarizes HIV infection process.

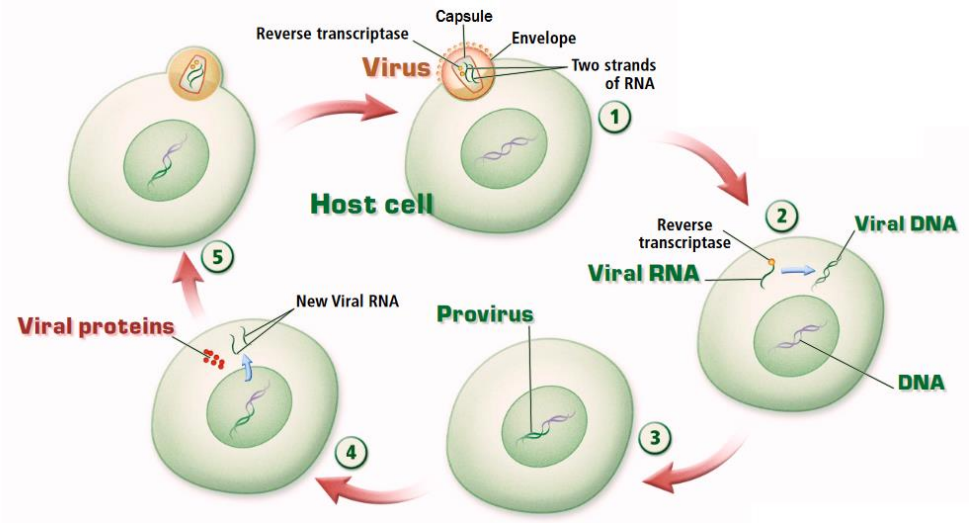

Figure 2.4 - HIV cell infection. 1) Virus and host cell membrane fusion; 2) viral RNA reverse transcription to DNA; 3) viral DNA incorporation into the host chromosome (provirus); 4) viral particles production; 5) viral particles bud out of the host cell. Adapted from [84].

2.3.2 Central nervous system invasion

The CNS is susceptible of infection by retroviruses of different species, especially by members of the lentiviruses family [85]. The HIV is a multisystem disorder that includes the CNS, among others human body systems.

The HIV is known to invade the CNS compartment from systemic circulation in an early stage of infection. This can be done through the blood-CSF barrier as cell-free viral particles [86], through

the infection of BBB endothelial cells or astrocytes and then transfer via these cells to the CNS, through the extracellular movement of the virus across a disrupted BBB [53], or through the BBB in form of peripherally infected leukocytes, mainly monocytes, a so-called "Trojan horse" mechanism [16, 86]. The last one is the most accepted model for HIV entry into the CNS (Figure 2.5) [87].

Several infected leukocytes circulate in the blood stream as an HIV effect. Simultaneously, there is a dysregulation of chemokines secretion and chemokines receptors in HIV-infected patients. This family of chemokines play a crucial role in the pathogenesis of the disease, facilitating leukocyte transmigration through the BBB to CNS in response to chemokine gradients [53]. Moreover, HIV increases the expression of adhesion molecules, which facilitates leukocyte binding and diapedesis across this barrier [88]. After crossing the BBB, HIV-infected cells propagate the infection within the CNS. Monocytes can become perivascular macrophages, and then produce new viral particles and spread productive HIV infection to neighboring microglia [89]. These two types of cells provide the site for HIV replication and evolution in the brain parenchyma [90]. They can also release a variety of neurotoxic host factors that contribute to neuronal injury [91] and activation of other CNS cells, such as astrocytes. When activated, astrocytes are able to increase the BBB permeability, and thus this leads to an increase in "Trojan horse" leukocytes influx [64]. Viral proteins expressed in the surface of HIV-infected cells appear to be responsible for the fusion of microglia and/or macrophages to result in the formation of giant multinucleated cells, the hallmark cells of brain parenchyma inflammation [79, 92]. Although neurons and oligodendrocytes are rarely infected [53], neuronal dysfunction throughout CNS, mainly related to axonal and dendritic pruning, is a very common HIV outcome [93].

In addition to the infection process, there are several complications associated with AIDS neuropathogenesis. This involves an inflammatory cascade which results from the modification of HIV-infected cells secretory functions, stimulated by the virus. They produce neurotoxic molecules, including cytokines and reactive oxygen species, that disrupt normal cellular functioning and modify neurotransmitters action [79].

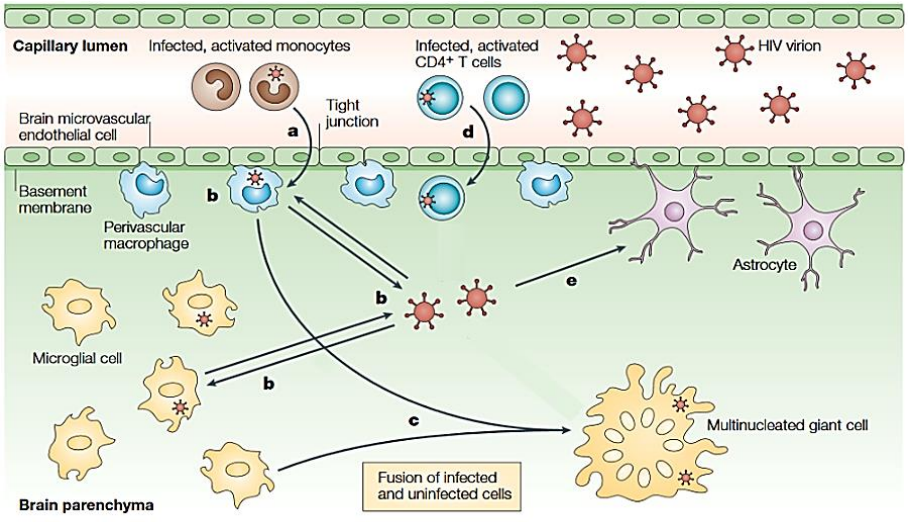

Figure 2.5 - "Trojan horse" mechanism. a) HIV enters the brain mainly through its presence in infected monocytes that migrate across the BBB; b) the virus that is produced in the brain compartment is mainly derived from monocytes which have differentiated into perivascular macrophages, but infected microglia can also contributes to the production of virus; c) the HIV-envelope glycoproteins expressed at infected cells surface are able to mediate cell-to-cell fusion, thus resulting in the formation of large multinucleated giant cells which produce virus; d) HIV can also enter the brain through its presence in infected CD4+ T cells; e) it is generally accepted that infection of astrocytes cells is not productive, and thus they do not contribute to viral replication. Adapted from [87].

2.4 Human immunodeficiency virus-associated antiretroviral therapy

The number of HIV-infected people enrolled in ARTs has been clearly increasing since 2005, at the same time as HIV-related deaths started decreasing (Figure 2.6) [70]. The HIV treatment involves taking medicines, known as ARVs, which slow the progression of the virus in human body, and thus they offer several life-saving and life-prolonging benefits to HIV-infected individuals. These drugs are usually given in combination, which is called an ART [94].

Regarding HIV infection clinical profile, ART became possible to turn a subacute lethal disease into a chronic ambulatory disease [95]. Current therapies are not able to eradicate the virus, thus ART goals are to achieve and maintain viral RNA at a low blood concentration, avoiding the formation of new viral particles and decelerating the damage to the host immune system [95-97].

The ART restores the immune function by increasing CD4 cells count and providing viral replication suppression to nearly undetectable levels, which can be maintained for years [95]. Consequently, this smooths HIV-related symptoms and prevents the appearance of opportunistic pathologies [79].

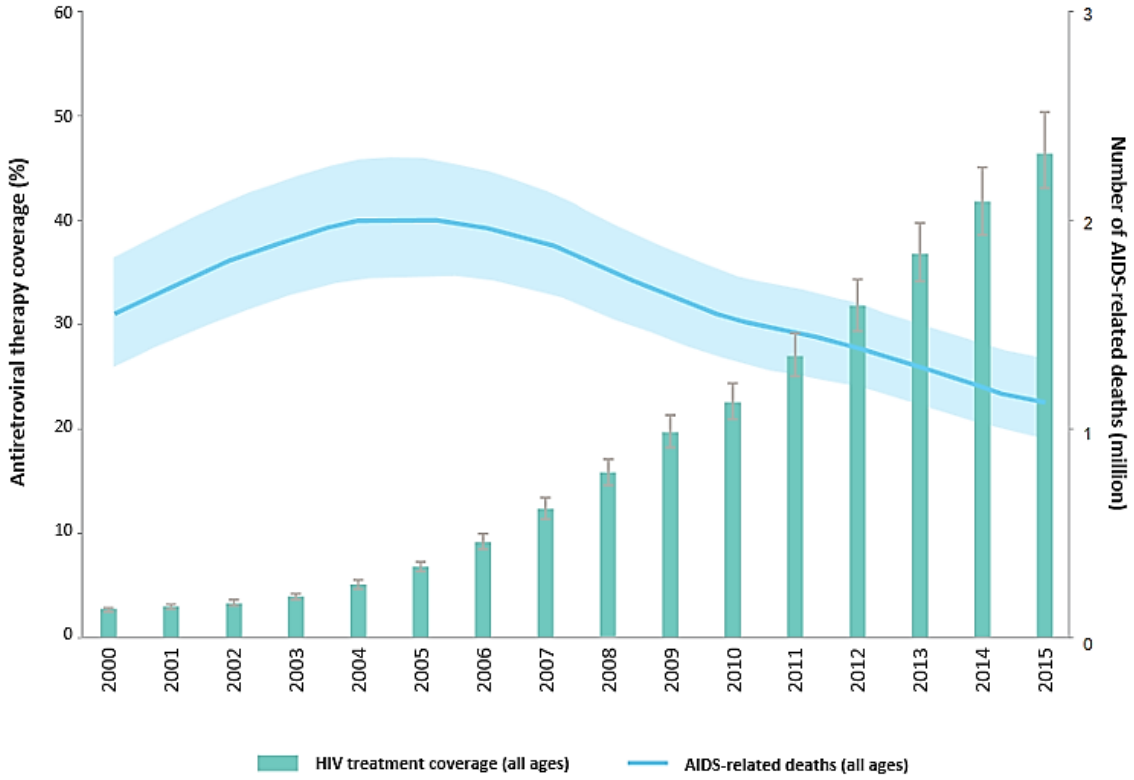

Figure 2.6 - Worldwide ART coverage and number of AIDS-related deaths between 2000 and 2015. Adapted from [70].

Antiretroviral therapies are based upon at least three anti-HIV medications that may belong to different drug classes [98]. The main ARV classes are nucleoside reverse-transcriptase inhibitors (NRTIs), nucleotide reverse-transcriptase inhibitors (NtRTIs), non-nucleoside reverse-transcriptase inhibitors (NNRTIs), integrase strand transfer inhibitors (INSTIs), protease inhibitors (PIs), and entry inhibitors (EIs) [99]. Table 2.1 summarizes their therapeutic action.

Table 2.1 — Properties of drugs commonly applied in HIV treatment.

Drug class	Drug action	References
NRTIs or NtRTIs	Analogues of nucleosides (NRTIs) or nucleotides (NtRTIs) which act as substrates for the RT. NRTIs and NtRTIs inhibit the enzyme by competing with endogenous nucleosides or nucleotides, respectively, for integration into the growing proviral DNA chain. Viral replication ceases without the presence of a hydroxyl group in the drug structure, hence avoiding the addition of another nucleoside (NRTI) or nucleotide (NtRTI).	[7, 8]
NNRTIs	These medicines are non-competitive inhibitors of the RT. They specifically bind to RT, near enzyme active site (allosteric inhibition). Consequently, the enzyme is locked in an inactive conformation and this reduces the binding of natural nucleosides.	[7-9]
INSTIs	Drugs that interact with IN catalytic core domain by combining with its divalent metal ions to form a chelate, hence blocking enzyme role in HIV pathogenesis.	[100, 101]
PIs	PIs inhibit the PR by mimicking the cleavage sites of retroviral polyprotein precursors and competing with them for the enzyme at a late stage of viral replication. Although HIV can still replicate in the presence of PIs, this leads to immature, non-infectious virus particles production.	[7, 102]
EIs	Drugs that are able to avoid entry of virus into host cells, affecting one of three phenomena: receptor binding, coreceptor binding, and membrane fusion. Currently, only compounds related to the last two strategies have been approved by FDA.	[103]

NRTI: nucleoside reverse-transcriptase inhibitor; NtRTI: nucleotide reverse-transcriptase inhibitor; NNRTI: non-nucleoside reverse-transcriptase inhibitor; INSTI: integrase strand transfer inhibitor; PI: protease inhibitor; EI: entry inhibitor.

2.4.1 Antiretroviral drug model: efavirenz

The 2016 WHO treatment guidelines for adult HIV-1 infection recommend the NNRTI EFV for a standard first-line ART, in combination with the NRTIs tenofovir and either lamivudine or emtricitabine [104].

Efavirenz, formerly known as DMP-266, is an antiviral drug and was approved by FDA in 1998, for use in combination with other ARV agents for HIV treatment [6]. This API, whose empirical formula consists on $C_{14}H_9ClF_3NO_2$ (Figure 2.7) [105], has a hydrophobic structure and a molecular weight of 315.68 $g.mol^{-1}$ [106-108]. According to the Biopharmaceutics Classification System, EFV is classified as a Class II API, which means that it is poorly soluble (aqueous solubility less than 10 mg/mL) and highly permeable across biological membranes [109].

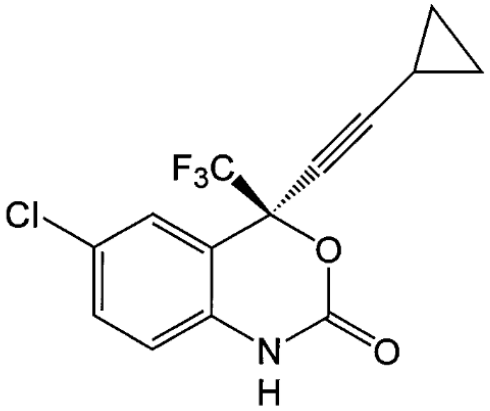

Figure 2.7 - Efavirenz structural formula. Reprinted from [110].

The pharmacokinetic of EFV appears to be similar between different genders and races. EFV is mostly metabolized in the liver to inactived hydroxylated metabolites, through a process involving the cytochrome P450 enzymatic system [111]. Following a single dose of 600 mg in adults, it is able to reach a peak plasma concentration of 4.1 mg/L in 3–5 h, and after multiple dosing, steady-state concentrations are achieved between 6 and 10 days [107]. Moreover, this drug has a poor bioavailability of nearly 40 % [106]. Serum EFV is highly protein bound (> 99 %), predominately albumin-bound, which hinders drug extravascular diffusion and allows its high intracellular and plasma concentration [107].

The ability of ARV drugs to reach the CNS (or to cross the BBB) can be evaluated based on two main complementary measures: cerebrospinal fluid:blood plasma concentration ratio (CSF:BP), also referred to as cerebrospinal fluid (CSF) penetration, and CNS penetration effectiveness scoring system (CPE) [112]. The choroid plexus allows drug movement from blood to CSF, and it is a leaky structure compared to the BBB. Drug entry into CSF is expected, a process that occurs through simple diffusion of the drug unbound form [107], and is not able to discriminate between drugs that cross, or not, the BBB [113]. This is the reason to consider not only one measure. CPE resulted from the studies of Letendre *et al*. [114, 115] and consists on a theoretical concept based on physico-chemical, pharmacokinetic and pharmacodynamic properties of each drug [116]. Its updated version is presented in four categories, ranging from 0 (worst CNS estimated penetration) to 4 (better CNS estimated penetration). Table 2.2 summarizes the CSF:BP and CPE for the main drugs applied to ARTs. As can be seen , the CSF:BP of EFV can vary between 0.003 and 0.01, and this drug belongs to CPE category 3 [117]. Although EFV levels in CSF are considered low, they are frequently above 50 % inhibitory concentration (IC50; API concentration where 50 % of viral replication is inhibited), which has the value of 0.5 ng/mL for this drug [64, 117].

There is no evidence of EFV association with any influx or efflux BBB transporters [118, 119].

Table 2.2 - CSF:BP and CPE for the main drugs applied to ARTs. Adapted from [16, 117].

Drug class	Drug	CSF:BP	CPE	References
NRTIs	Zidovudine	0.50	4	[120]
	Didanosine	0.21	2	[121]
	Stavudine	0.16-0.40	2	[122, 123]
	Lamivudine	0.06-0.23	2	[123, 124]
	Abacavir	0.18-0.36	3	[125]
	Emtricitabine	0.26	3	[126]
NtRTIs	Tenofovir	0.05	1	[126, 127]
NNRTIs	Nevirapine	0.63	4	[123]
	Efavirenz	0.003-0.01	3	[112]
	Etravirine	0.01	2	[128]
INSTIs	Raltegravir	0.01-0.61	3	[129]
	Dolutegravir	0.50	Not available	[130]
PIs	Saquinavir	≤ 0.002	1	[131, 132]
	Indinavir	0.11	4	[123]
	Atazanavir	0.002-0.014	2	[133]
	Fosamprenavir	0.012	2/3	[134]
	Darunavir	0.01	3	[135]
EIs	Enfuvirtide	Undetectable in CSF	1	[136]
	Maraviroc	0.025	3	[137]

CSF:BP: cerebrospinal fluid:blood plasma concentration ratio; CPE: central nervous system penetration effectiveness scoring system; NRTI: nucleoside reverse-transcriptase inhibitor; NtRTI: nucleotide reverse-transcriptase inhibitor; NNRTI: non-nucleoside reverse-transcriptase inhibitor; INSTI: integrase strand transfer inhibitor; PI: protease inhibitor; EI: entry inhibitor; CSF: cerebrospinal fluid.

2.5 Polymers as biomaterials: application in nanoparticles

A biomaterial can be defined as a "material intended to interface with biological systems to evaluate, treat, augment or replace any tissue, organ or function of the body" [138]. The most important requirement of a biomaterial is its biocompatibility, whose definition was provided by Williams in a consensus conference as follows "the ability of a material to perform with an appropriate host response in a specific application" [138]. It is associated to the response of the immune system after the introduction of the material and toxicity due to possible metabolites resulting from its degradation [139]. Biocompatibility is not expected as an intrinsic property of biomaterials. In fact, it depends on the biological environment and tolerability related to specific interactions with the tissues [140]. Another requirement desirable for a biomaterial is its biodegradability, which is a key parameter for its acceptance by regulatory authorities [141]. A biomaterial is called biodegradable when the products of its degradation are metabolizable in the body and excreted naturally afterwards [142].

Polymers are the most multifaceted class of biomaterials that are commonly applied in biomedical applications, ranging from surgical sutures to tissue engineering scaffolds, medical

implants, and DDSs [143]. Due to the versatility and ease with which they can be processed, polymers are quickly replacing other material classes, such as metals, composites, and ceramics for use as biomaterials [144]. Polymeric materials have a large molecular mass relative to their monomers, and thus, this contributes to their typical physical properties, including toughness, viscoelasticity, and a tendency to form amorphous structures [145]. Polymers are formed by long chains of repeated molecules via monomers polymerization [146]. Polymers chemical bonds consist of primary bonds, which are covalent bonds involving two atoms sharing electrons, and secondary bonds, which include van der Waals forces, hydrogen and ionic bonds [145].

Nanoparticles, as DDSs, built with polymeric biomaterials have gained attention from the scientific community as a result of their controlled and sustained release properties, subcellular size, feasibility of production and biocompatibility [147]. One desirable aspect in the field of NPs development is to use polymers already approved by FDA and European Medicine Agency (EMA) [148, 149]. In these nanosystems, the therapeutic substance may be encapsulated, adsorbed or dispersed in the NPs [150].

The first classes of polymers explored for NPs as DDSs were the non-biodegradable polyacrylics, poly(vinyl chloride-co-acetate) (PVCA) and polystyrene [146, 151]. The polymeric NPs built with these polymers do not disaggregate in the body and release drugs by passive diffusion in a slowly way [146]. Later on, polymeric NPs based on biodegradable materials were explored, since the polymers chains are capable of degrading *in vivo*, either enzymatically, non-enzymatically or both [146, 152]. Using these polymers, the production of a DDS, which releases an active agent during a predetermined time interval, is possible by selecting a specific polymer composition with a known rate of degradation [153]. Furthermore, the release is regulated by both passive diffusion of drugs and polymer breakdown [146]. In most of the cases, the products resulting from the degradation of these polymers are biocompatible and therefore toxicologically safe [152]. Some examples of biodegradable polymers are the poly(lactic acid) (PLA), poly(glycolic acid) (PGA), PLGA, polycaprolactones and polyacrylates [151].

Usually, polymeric NPs are classified into nanospheres and nanocapsules. Nanospheres are structures in which the drug is physically and uniformly dispersed in a matrix. Nanocapsules have a vesicular type structure in which a drug is confined to a cavity (liquid core) surrounded by a polymer membrane (polymeric shell) [55, 154]. This principle is demonstrated in Figure 2.8.

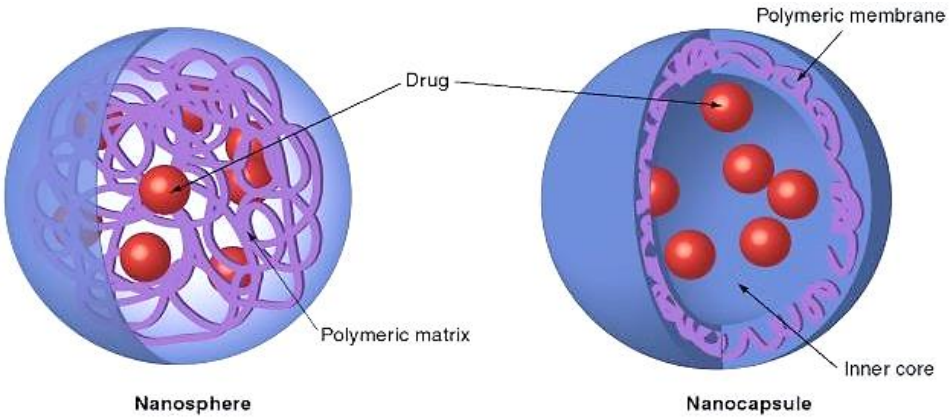

Figure 2.8 – The two types of polymeric NPs. Nanospheres present a polymeric matrix and nanocapsules present a vesicular-like structure. Reprinted from [155].

2.5.1 Poly(lactic-co-glycolic acid)

The PLGA is an aliphatic polyester copolymer of lactic acid (LA) and glycolic acid (GA), whose forms are usually identified by the ratio between these two monomers, also biodegradable [156]. They result from the hydrolysis of PLGA and are forwarded to natural metabolic pathways, as demonstrated in the Figure 2.9. In a biochemical point of view, the Krebs cycle is the mechanism responsible for LA and GA degradation and bioelimination inside the human body [23].

The arrangement of different GA building blocks originates PGA, which is the simplest linear aliphatic polyester. Still, PGA biomedical applications are limited due its low solubility and high rate of degradation yielding acidic products [157]. The arrangement of different LA building blocks originates PLA, and this polymer also belongs to the family of aliphatic polyesters [158]. Lactic acid can exist in optically active D- or L-enantiomers, and depending on the proportion of these enantiomers, PLA of variable material properties can be derived [159]. Lactic acid is more hydrophobic than GA, thanks to the presence of $-CH_3$ side groups. This means that it will absorb less water and present slower degradation rates [160]. Therefore, high ratios of LA:GA in PLGA compounds increase the time interval of degradability of this copolymer [152].

The properties of PLGA have turned it in one of the most attractive candidates in the field of biodegradable and biocompatible polymeric NPs as DDSs, since it has been considered the best tailored biomaterial for this purpose with respect to design and performance [152, 161-166]. This polymer can be processed into any shape and size, and can encapsulate biomolecules of a wide size range [167]. The application of PLGA in humans was already approved by FDA and EMA for the use in DDSs for parenteral administration, diagnostics and other applications of clinical and basic science research (cardiovascular diseases, cancer, vaccines and tissue engineering) [168, 169]. The PLGA has a good mechanical behavior [152], and it has also demonstrated low toxicity [23, 170]. This polymer degrades by hydrolysis of its ester linkages, through bulk or heterogeneous erosion, in aqueous environments [167].

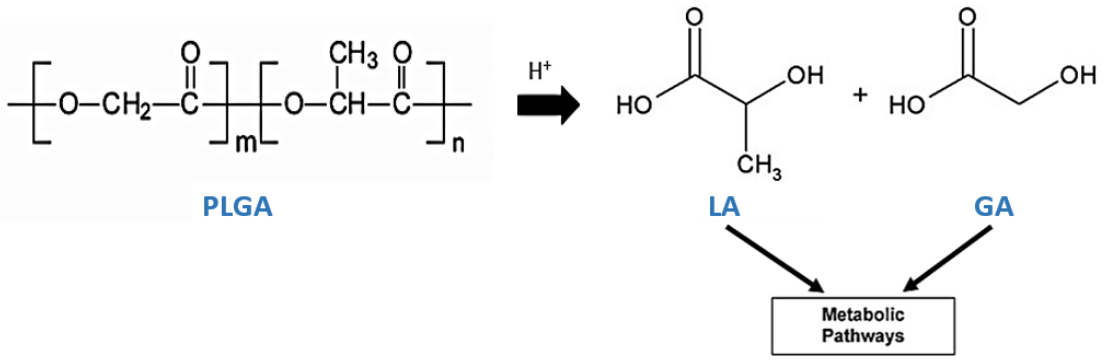

Figure 2.9 - Hydrolysis of PLGA in acidic medium. LA and GA are forwarded to natural metabolic pathways, such as the Krebs cycle. *m* and *n* are the number of GA and LA units, respectively. Adapted from [167, 170].

2.6 Conventionally-performed techniques to develop poly(lactic-co-glycolic acid) nanoparticles

In accordance with the classical nucleation theory, the two main steps involved in particulate systems development are nucleation and, then, particle growth. Both steps are triggered and strongly dependent on the mixing of the formulation components [171]. The rate and effectiveness of mixing will determine the size and size distribution of the generated particles. Therefore,

particles production method is crucial for their physico-chemical profile, which, in turn, will determine the behavior of the DDS [172].

One of the main strategies used in PLGA NPs formulations is the bottom-up approach. The bottom-up techniques are based on the growing of NPs from molecules in solution [173]. Among all the applicable procedures related to the bottom-up techniques, the nanoprecipitation is very usual for the encapsulation of hydrophobic drugs. For the purpose of this study, this technique will be focused.

2.6.1 Nanoprecipitation technique

The nanoprecipitation technique (also termed solvent displacement) as a way to produce NPs was first reported in a patent by Fessi and co-workers, in which they refer the production of spherical NPs with a size under 500 nm [174, 175].

Basically, two systems are needed: a semipolar solvent (commonly referred as water-miscible), in which both the polymer and the API are soluble (dispersed phase, organic phase or oil), and a non-solvent, miscible with the previous one but not allowed to dissolve neither the polymer nor the hydrophobic API (continuous phase, aqueous phase or water), consisting in a solution surfactant [162, 176, 177].

The choice of the organic solvent is decisive in developing a successful formulation of particles containing an API. Two main solvent features should be considered, namely the ability to dissolve both polymer and drug, and its toxicity if residual molecules are present in the final formulation [178]. Available solvents have been classified according to their toxicity on three classes: Class I (solvents to be avoided), Class II (solvents to be limited) and Class III (solvents with low toxic potential) [179]. For safety reasons and since there will always exist residual amounts of solvent in the final formulation [178], Class III solvents are the most suitable ones for physiological applications. Some examples of organic solvents commonly used in this technique are acetone, acetonitrile, N,N-dimethylformamide (DMF), tetrahydrofuran (THF), dichloromethane (DCM), and dimethyl sulfoxide (DMSO) [180].

In order to improve the production methodology, a surfactant should be added. Its role is to stabilize the nanosystem during the intermediate steps of the process and there are different possibilities for this component, such as TWEEN®, sodium dodecyl sulfate (SDS), polyvinyl alcohol (PVA), hydroxymethylcellulose (HPMC) or Pluronic® F-68 [181].

The first step consists in the preparation of the dispersed phase; here, the polymer and the API are mixed with a specific solvent. The second step consists in the preparation of the continuous phase, containing just the surfactant (non-solvent). Afterwards, the dispersed phase is slowly added to the continuous one [182].

The formation of NPs occurs spontaneously due to the inter-diffusion of the organic solvent into the surrounding continuous phase medium [162, 183]. This results in the decrease of interfacial tension between the two phases, a phenomena based on a constant formation of eddies of solvent at that local. Consequently, it can increase the surface area and lead to the formation of small drops of organic solvent [184, 185]. The magnetic stirring is considered a sufficient mechanical agitation procedure [176, 183, 184].

The nanoprecipitation is a straightforward method, results in an instantaneous formation of NPs, and is easy to perform [163, 176, 184]. Moreover, in general, this technique is associated with a better reproducibility compared to emulsion-based techniques.

2.7 Microfluidics: an alternative method to produce poly(lactic-co-glycolic acid) nanoparticles

Microfluidics is a multidisciplinary field intersecting science and technology, that deals with the manipulation of nanoliter volumes of fluids in channels ranging from tens to hundreds of micrometers [186]. A research boom in the field of microfluidics has been observed over the last years, and this technology demonstrated to be a useful tool to develop innovative drug delivery systems.

The application of microfluidics to the biological area started in 1950, when it appeared for the first time associated with gas chromatography and capillary electrophoresis experiments [187]. Nowadays, the devices built based on this concept demonstrate ability to address different domains of research, such as biological analysis [188], chemical synthesis [189], tissue engineering [190], or pharmaceuticals [191]. In the field of nanomedicine, different microfluidic approaches are being developed in order to produce DDSs, especially NPs [11, 192-197].

Alternatives to the conventional bulk methods that have been used to produce drug-loaded NPs emerged through the need for precise control of their properties. Some of the most common problems reported are the inability to control the mixing process [194]; poor drug loading [198] and consequent consumption of considerable amounts of expensive APIs to reach the desired therapeutic effect [199]; lack of reproducibility noted from batch-to-batch properties, namely in particles average size, size distribution, charge and drug release behavior [200]; and large polydispersity in size of particulate systems [201]. The monodispersity of NPs formulations is of major importance in determining the performance of particles as drug carriers, because it influences biodistribution, cellular uptake and drug release profile [195]. The outstanding outcomes in monodispersity of formulations associated with microfluidics are related to a better control of the steps involved in particles formation, nucleation and growth [171]. In the conventional methodology, stirring, shaking or sonicating are usually the mechanisms responsible to perform the mixing of the different phases. This involves an unstable ratio between the phases, heterogeneous environments and polydispersity of formulations. Moreover, the mixing is usually slow and incomplete, leading to adsorption of the polymers to aggregates of particles and a consequent increase in NPs final Z-average. In microfluidics, the mixing is usually faster than the time necessary to occur NPs nucleation and growth. Therefore, the polymer is not able to adsorb to recently-formed NPs, and ends up forming more particles with a smaller size [194, 202]. Besides the capability of obtaining a better control over the above mentioned parameters, recently microfluidic devices are gaining attention due to saving costs and time [11]. Furthermore, there is the possibility of varying key parameters, such as the flow rates, mixing time or channel diameters, in order to obtain formulations with tunable final properties [194]. Since the production process of NPs by microfluidics is continuous, this contributes to the reduction of batch-to-batch oscillations in relation to the final properties of the nanosystems [202]. The accurate manipulation of fluids and their laminar regimen inside the microchannels lead to the preservation of controlled hydrodynamic conditions, which are rapidly defined and kept during the process of formation of particles [171, 197]. Figure 2.10 illustrates some of the most appealing features of microfluidics to fabricate drug delivery carriers.

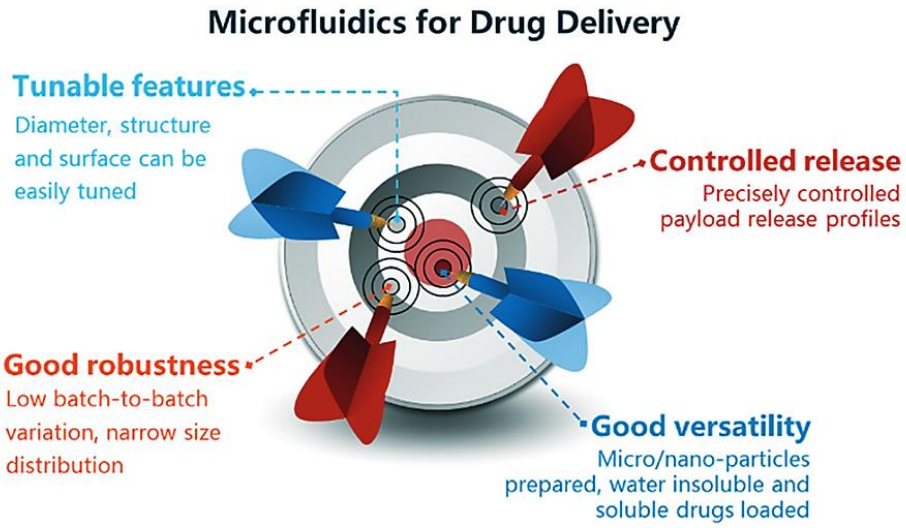

Figure 2.10 - Some of the most outstanding features associated with the microfluidic technology to produce drug delivery carriers. Reprinted from [202].

Yet, it is important to mention that big challenges remain. First of all, the translation from academic research to industry is a crucial step [186, 203] and this is only possible by turning this process into a scalable one. Generally, the reactors present small sizes and are associated with low flow rates [171]. Thus, the production could be scaled-up by introducing parallel microfluidic devices - only in this way it will be possible to reach units of rate production of kilograms per hour, instead of grams per hour [192, 197, 201]. In terms of performance, the danger of clogging of the channels with trapped small particles or precipitates is also a disadvantage [204].

2.7.1 Microfluidics platforms layout

A general microfluidics device should be constituted by a substrate, channels and pumps, such as syringe or peristaltic pumps, to generate pressure-driven flows through each channel [195, 203]. The typical materials used for the substrate are polydimethylsiloxane (PDMS), glass and silicon [187]. The channels used to introduce solutions into the device are called inlets. In opposition, the channels used to collect the recently formed particles from the device are called outlets [192, 196]. By increasing the number of the last ones, the production speed of NPs can be improved [192]. The inclusion of valves and reservoirs in the devices is also conceivable [204].

Microfluidic platforms may adopt different geometries, and the main ones are presented in Table 2.3.

Table 2.3 — Microfluidic platforms geometries.

Geometry	Design	Principle	References
Hydrodynamic flow-focusing	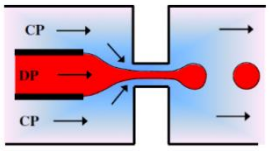	The flow-focusing geometry is associated with a combined two-phase flow that is forced to pass through a small orifice. In this case, the DP flows through the inner capillary, whereas the CP flows through the outer capillary in the same direction. Then, both fluids are forced to flow through a small orifice. In consequence, the CP exerts shear stress that forces the DP into a narrow thread. DP ends up breaking into particles inside or after the orifice.	[205, 206]
Hydrodynamic flow-focusing (adapted)	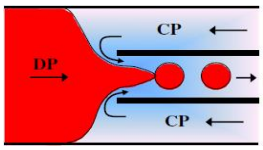	The two phases, CP and DP, are injected through the two ends of the same outer capillary but in opposite directions. Then, particles are collected from another, coaxially aligned, inner capillary. When the phases meet at the constriction place, the outer fluid may squeeze the inner fluid which breaks into spherical drops, and the DP may form a liquid thread in the core of the CP due to the symmetric shearing force imposed by CP.	[194, 205, 207-209]
Co-flow	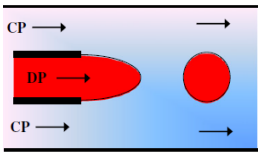	Two capillaries are coaxially aligned. The DP is injected through the inner capillary, whereas the CP is injected through the outer capillary but in the same direction. Drops are formed at the inner capillary orifice where the DP meets with the sheath CP, under the competition between shear force and surface tension provided by the outer phase.	[201, 205, 210-212]
T-junction	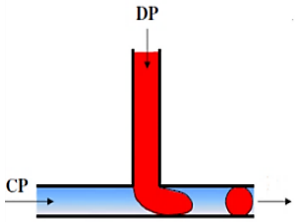	This microfluidic geometry is considered the simplest one. The CP is injected through the main channel, whereas the DP is injected through the perpendicular inlet channel. CP-induced shear stress and evolution of the emerging drop upstream pressure start distorting the DP in the downstream direction until its break up into a particulate system.	[205, 210]

Cross-junction (X-junction)	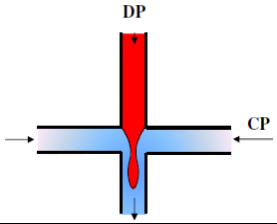	The two phases flow in perpendicular directions, which creates a focused DP in a CP stream.	[205, 210, 213]
Y-junction	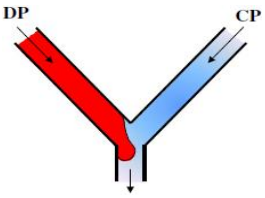	The two phases are injected through two separate inlets, and the product is removed using a common outlet.	[205, 214]

DP: dispersed phase; CP: continuous phase.

2.7.2 Droplet microfluidics

Although it will not be approached in this work, droplet microfluidics is an area extremely important in the field and thus it cannot be forgotten during this literature review section. Unlike the subject of this dissertation, which is focused on precipitation microfluidics and miscibility of the dispersed and continuous phase, droplet microfluidics, in turn, work in the basis of emulsions or immiscibility of the phases involved in NPs production [202, 215]. One of the most interesting applications of this type of microfluidics is the assembly of particulate systems with a core/shell structure, involving more than one emulsion. The co-flow, flow-focusing, and T-junction are the most used geometries in droplet microfluidics. Different or equal geometries can be combined in the same microfluidic chip, or the precursor phases can pass through different chips, originating complex layouts of the platforms or reactors which are used to produce these structures (Figure 2.11) [205]. Herein, three different fluids or phases are needed: the inner phase, the middle phase, and the outer phase. Particles resulting from these reactors present a core of inner phase surrounded by a shell of middle phase. Moreover, the outer phase has to be immiscible with the middle phase, and the middle phase has to be immiscible with the inner phase [216]. Nie *et al.* developed a microfluidic platform which combined the co-flow and flow-focusing geometries (Figure 2.11a) [217]; the primary emulsion was formed in the co-flow system at the inner capillary orifice where the inner phase met with the middle phase, and it was then focused in the orifice of the flow-focusing system by the outer phase. Utada *et al.*, in turn, established a different system but consisting on the combination of the same geometries (Figure 2.11c) [216]. Seo *et al.* manufactured a reactor which combined two consecutive flow-focusing systems (Figure 2.11b) [218]. The inner and middle phases were introduced in the first flow-focusing system, resulting in a primary emulsion. The thread of the primary emulsion was then focused in the orifice of the second flow-focusing system by the outer phase, where it broke and released the droplets. Abate *et al.* developed a platform combining two sequential cross-junction geometries (Figure 2.11d) [219]. The inner phase was injected into the central inlet, and the middle phase was injected into the side inlets of the first cross-junction system. The outlet of the first system, which contained the primary emulsion, fed the inlet of the second cross-junction system.

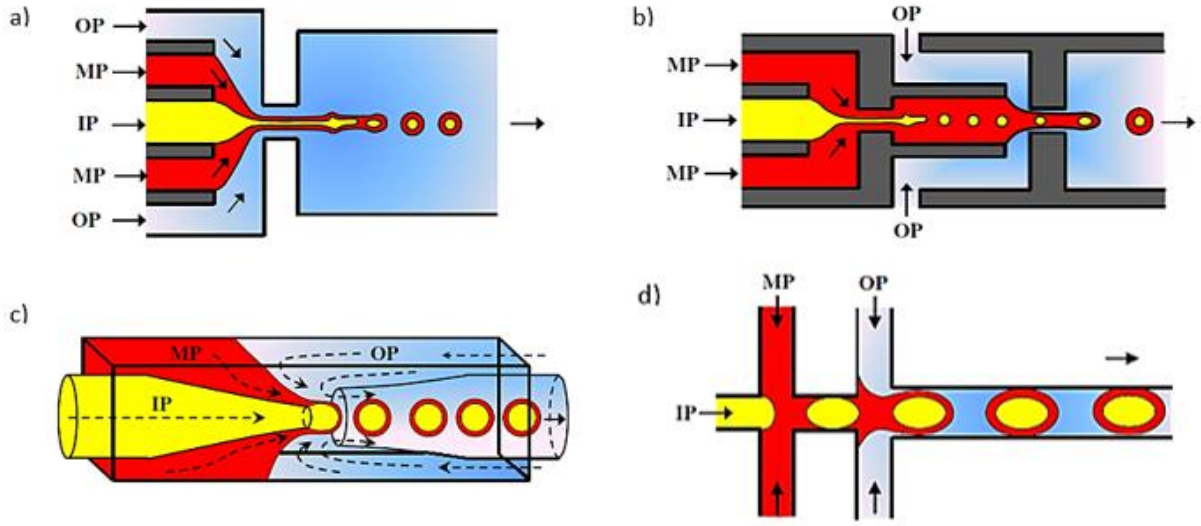

Figure 2.11 – Microfluidic platforms combining more than one geometry. a,c) co-flow and flow-focusing systems; b) two consecutive flow-focusing systems; d) two consecutive cross-junction systems. IP: inner phase; MP: middle phase; OP: outer phase. Adapted from [205].

Chapter 3

Materials and Methods

3.1 Materials and cell lines

PLGA (Purasorb PDLG 5004A; 50:50 lactic:glycolic molar ratio; molecular weight around 40 kDa) was kindly provided by Corbion. Immortalized human cerebral microvascular endothelial cell line (hCMEC/D3 cell line) was purchased from Cedarlane, and mouse neuroblastoma × rat dorsal root ganglion neurone hybrid cell line (ND7/23 cell line) was kindly provided by Dr. Pedro Moreno (Institute of Health Innovation and Research, University of Porto, Portugal). Transferrin receptor-binding 12-amino acids peptide (Thr-His-Arg-Pro-Pro-Met-Trp-Ser-Pro-Val-Trp-Pro) was purchased from Eurogentec.

TWEEN®-80, hydrocortisone, ascorbic acid, 4-(2-hydroxyethyl)-1-piperazineethanesulfonic acid (HEPES), basic fibroblast growth factor (bFGF), 3-(4,5-dimethylthiazol-2-yl)-2,5-diphenyltetrazolium bromide (MTT), glycerol, 6-coumarin (6-C), acetic acid glacial, 2-(N-morpholino)ethanesulfonic acid (MES), 1-ethyl-3-(3-dimethylaminopropyl)carbodiimide (EDC), N-hydroxysuccinimide (NHS), Histopaque, paraformaldehyde, sodium chloride, and bovine serum albumin (BSA) were acquired from Sigma-Aldrich; EFV from BDR Lifesciences; DMSO from VWR; endothelial basal medium 2 (EBM-2) and high glucose with ultraglutamine Dulbecco's Modified Eagle medium (DMEM) from Lonza; acetonitrile, Coomassie Reagent, and versene from Thermo Fisher Scientific; Triton X-100 from Spi-Chem; fetal bovine serum (FBS), penicillin-streotomycin, chemically defined lipid concentrate, Hank's Balanced Salt Solution (HBSS), rat tail collagen type I, and acetic acid, from Gibco; glutaraldehyde from AGAR Scientific; sodium cacodylate from Fluka; ethanol from Valente e Ribeiro, Lda; wheat germ agglutinin (WGA)-Alexa Fluor® 594 conjugate from Invitrogen; 4',6-diamidino-2-phenylindole (DAPI) and Vecstashield from Vector Laboratories, Inc.

Polyethylene tubes were purchased from Smiths Medical International Ltd.; syringes and needles from Henke-Sass Wolf; syringe pumps from Braintree Scientific, Inc.; tissue culture flasks from Orange Scientific; dialysis membrane (10,000 MWCO; Snake Skin® pleated dialysis tubing) from Thermo Fisher Scientific; well-plates and Transwell® cell culture inserts (transparent polyester membrane; 12-well plate format; 0.4 μm pore size) from Corning; black well plates from Greiner Bio-One; plastic tissue culture coverslips (13 mm) from Sarstedt; carbon adhesive tape from Ted Pella, Inc.; coverslips from VWR.

The microfluidic device was kindly provided by Dr. Hélder Santos (Division of Pharmaceutical Technology, Faculty of Pharmacy, University of Helsinki, Finland).

3.2 Conventional development of poly(lactic-co-glycolic acid) nanoparticles

Considering the nanoprecipitation technique, PLGA (20 mg) and EFV, in a drug/polymer ratio (DP) of 2.5, 5, 10 or 15 %, were dissolved in 1 mL of organic solvent (20 mg/mL of PLGA in organic solvent), acetone or DMSO, and directly injected with a needle (25G) into 20 mL of the surfactant solution, 1/2 % of TWEEN®-80 or 1/2 % of PVA in deionized water. Then, the solution was left under mechanical stirring for 3 h, at 200 rpm and room temperature, to ensure organic solvent diffusion.

For the modified nanoprecipitation technique, PLGA (80 mg) and EFV, in a DP of 15 %, were dissolved in 2 mL of organic solvent (40 mg/mL of PLGA in organic solvent), DMSO, and homogenized with 4 mL of the surfactant solution, 2 % of TWEEN®-80 in deionized water, by sonication (Sonics & Materials, Inc.) for 90 s at 70 % intensity. The resulting product was promptly poured in 7.5 mL of the surfactant solution, and kept under magnetic stirring for 4 h, at 300 rpm and room temperature, to ensure organic solvent diffusion.

Empty NPs (i.e., without EFV) for both techniques were also prepared using the same procedure but skipping the addition of EFV.

After production, NPs were washed three times with ultrapure water (ELGA system) and recovered by centrifugation (Beckman Avanti, JA2550 rotor, Beckman Instruments Inc.) or ultrafiltration using Amicon Ultra-15 Centrifugal Filter units (Millipore) with a molecular weight cutoff (MWCO) of 100 kDa. To better resuspend the formulation, if needed, samples were treated with glycerol or submitted to sonication (Sonics & Materials, Inc.) for 30 s at 30 % intensity.

3.3 Microfluidic development of poly(lactic-co-glycolic acid) nanoparticles

The microfluidic device was assembled by gathering borosilicate glass capillaries on a glass slide, as previously described [209, 220, 221]. Briefly, the chip was composed of two types of capillaries, for which the outer diameter of the cylindrical tapered capillary fitted the inner dimensions of the square capillary. One end of the cylindrical capillary (World Precision Instruments, Inc.), comprising an inner and outer diameters of around 580 and 1000 μm, respectively, was tapered using a micropipette puller (P-97, Sutter Instrument Co.) to a diameter of 20 μm; then, this diameter was enlarged to around 80 μm using a microforge (P-97, Sutter Instrument Co.). This cylindrical tapered capillary was placed into the square capillary, which had an inner dimension of around 1000 μm (Vitrocom), and coaxially aligned. A transparent epoxy resin (5 minute ® Epoxi, Devcon) was used to fix the capillaries.

The inner and outer fluids were injected separately into the chip through polyethylene tubes attached to syringes at constant flow rates controlled by syringe pumps.

The dispersed and continuous phases were poured into distinct syringes to be separately injected in the microfluidic device as the inner and outer fluid, respectively. Two fluids geometries were induced, namely the co-flow and flow-focusing. The dispersed phase consisted on a 20 mg/mL and 40 mg/mL mixture of PLGA in organic solvent, DMSO, for the co-flow and flow-focusing geometry, respectively, and a quantity of EFV corresponding to a DP of 15 %. The continuous phase

consisted on a surfactant solution, 2 % of TWEEN®-80 in deionized water, for both geometries. The particles were collected in plastic tubes containing 500 µL of a solution with the same composition of the continuous phase, in order to facilitate their deposition and consolidation. In the co-flow geometry, the inner and outer fluids were pumped into the microfluidic device at 2500 and 3750 µL/min, respectively. In the flow-focusing geometry, the inner and outer fluids were pumped into the microfluidic device at 1000 and 2500 µL/min, respectively. The production of NPs by microfluidics was run until reach a final volume of around 11.5 mL for the flow-focusing geometry and 20 mL for the co-flow geometry. Then, NPs suspensions were left overnight for solvent diffusion to occur (without magnetic stirring) and recovered by ultrafiltration.

Empty NPs (i.e., without EFV) for both geometries were also prepared using the same procedure but skipping the addition of EFV.

3.4 Characterization of nanoparticles

3.4.1 Mean particle size, size distribution and surface charge

Nanoparticles were characterized for their average size (Z-average) and polydispersity index (PDI) by dynamic light scattering (DLS), and zeta-potential (ζ-potential) through laser Doppler anemometry (LDA), using a Malvern Zetasizer Nano ZS instrument.

For these measurements, samples were diluted in an ionic solution of 10 mM sodium chloride.

3.4.2 Drug association efficiency and drug loading

To determine the association efficiency (AE) and drug loading (DL) of the developed nanosystems, the amount of EFV associated to the nanoparticles was indirectly estimated. This calculation was made by the difference between the total amount of EFV used to prepare the systems and the amount of EFV that remained in the aqueous phase, after nanoparticles isolation by ultrafiltration, according to Equations 3.1 and 3.2 [222].

$$AE\ (\%) = \frac{(Initial\ mass\ of\ EFV) - (mass\ of\ recovered\ EFV)}{Initial\ mass\ of\ EFV} \times 100 \quad (3.1)$$

$$DL\ (\%) = \frac{(Initial\ mass\ of\ EFV) - (mass\ of\ recovered\ EFV)}{Total\ mass\ of\ NPs} \times 100 \quad (3.2)$$

The amount of EFV was determined using a high-performance liquid chromatography (HPLC) method previously established [223]. Briefly, the quantification was performed by reversed-phase HPLC with ultraviolet detection using a Merck-Hitachi LaChrom® HPLC system (Merck, NJ). A Symmetry C8 column (5 µm, 4.6×250 mm; Waters, Milford, MA) with LiChrospher 100 RP-18 guard column (Merck) was used as stationary phase. Chromatographic runs were performed using an isocratic method and the mobile phase used was acetonitrile:acetate buffer 10 mM (57:43), pH 4.0, at a flow rate of 1 mL/min. Samples injection volume was 10 µL and the detection was at 247 nm. The method was linear in the range of 1-50 µg/mL.

3.4.3 Morphology and chemical screening

The morphological features of NPs were analyzed by transmission electron microscopy (TEM) with a JEOL JEM 1400 (JEOL Ltd.) microscope at an accelerating voltage of 120 kV. The energy-dispersive X-ray spectra (EDS) were collected for chemical analysis. Images were digitally recorded using a Gatan SC 1100 ORIUS CCD camera (Warrendale).

Samples were prepared by dropping 10 µL of NPs suspension onto a 300-mesh nickel grid. All samples were stained with uranyl acetate. Nanoparticles resulting from the microfluidic method of production were prior diluted ten times in water.

3.5 Microfluidic method: scaling experiment

Besides the above mentioned final volume of around 20 mL (standard scale), the production of EFV-loaded NPs using microfluidics by the co-flow geometry was also run until a final volume of 2 mL (scale-down) and 200 mL (scale-up). The settings and methodology used were the same described in Section 3.3, and the results for the scale-down and scale-up were, *a posteriori*, compared with the ones obtained for the standard scale.

3.6 *In vitro* release test

To ensure that the release assay would be performed in sink conditions, the solubility of EFV in 0.2 % of poloxamer in phosphate buffered saline (PBS) solution, pH = 7.4, was determined. Briefly, an excess amount of EFV (5 mg) was added to 3 mL of 0.2 % of poloxamer in PBS (to prepare a saturated solution), and placed for 15 min and 24 h in an orbital shaker incubator at 100 rpm and 37 ºC (IKA). Subsequently, the suspension was centrifuged at 10,000 *g* (Beckman Avanti, JA2550 rotor, Beckman Instruments Inc.) for 15 min, and EFV from supernatants was quantified through HPLC analysis.

For the release test, specifically, EFV loaded NPs (corresponding to 315 µg of drug) were added to 6 mL of 0.2 % of poloxamer in PBS solution, pH = 7.4, and then placed into an orbital shaker incubator, at 100 rpm and 37 ºC, during 24 h. Aliquots of 500 µL were collected at specific time points (0.25, 0.5, 0.75, 1, 1.5, 2, 2.5, 3, 4, 5, 7, 9, 23, and 24 h) during the assay, and the withdrawn volume was replaced with pre-heated 0.2 % of poloxamer in PBS solution. All the collected aliquots were centrifuged at 10,000 *g* for 15 min and the supernatant was used for HPLC analysis, in order to quantify the EFV released from NPs over time.

3.7 Nanoparticles labeling

The same protocol mentioned to produce EFV-loaded NPs by microfluidics and using the co-flow geometry was applied to obtain fluorescent NPs by encapsulating 6-C instead of the drug (in a 6-C/polymer ratio of 0.1 %). Following the same procedure applied to evaluate EFV-loaded NPs, 6-C loaded NPs were analyzed for their Z-average, PDI, ζ-potential. The AE and release profile of these NPs were also accessed, where 6-C was quantified through fluorescence (ex. 460 nm, em. 510 nm) using a plate reader (Synergy Mx, Biotek).

Previously to the release study, and ensuring that the assay would be performed in sink conditions, the solubility of 6-C in 0.1 % of TWEEN®-80 in PBS (pH = 7.4) was determined by

preparing a saturated solution. Briefly, an excess amount of 6-C (1 mg) was added to 5 mL of 0.1 % of TWEEN®-80 in PBS, and placed for 24 h in an orbital shaker incubator at 100 rpm and 37 ºC. Subsequently, the suspension was centrifuged at 10,000 *g* for 15 min, and the fluorescence of the supernatants was read in a plate reader.

The release assay was performed with a dialysis membrane. 6-C loaded NPs (corresponding to 1 mg of 6-C) were located inside the dialysis membrane, which was well closed at both extremities. The membrane was placed inside a beaker with 4 L of 0.1 % of TWEEN®-80 in PBS (pH = 7.4), with constant stirring (100 rpm) at 37 ºC. Samples of 1 mL were taken at time points of 0.5, 1, 2, 3, 4, 5 and 24 h, and their fluorescence was then quantified in a plate reader.

3.8 Nanoparticles functionalization and characterization

3.8.1 Functionalization process

The carbodiimide chemistry, or EDC/NHS coupling chemistry, was used to perform the covalent conjugation between the amine groups of a 12-amino acids peptide-binding transferrin receptor to the carboxyl group of NPs. This protocol was adapted from others previously described [209, 224].

Briefly, 1 mg of NPs was dispersed in 1 mL MES solution (10 mM; pH = 5.5) containing 3.14 µL of EDC (17 mM) and NHS (1.2 mg). The pH was adjusted to 5.5, and the mixture was stirred (300 rpm) for 45 min at room temperature in the dark. Then, the product was concentrated until the minimum possible volume by ultrafiltration, in order to remove the maximum amount of EDC and NHS, and ressuspended again in 1 mL MES solution (10 mM) at pH = 5.5. Since carboxyl groups of NPs were already activated, the peptide was added in a molar ratio of 1:10 in relation to PLGA. Afterwards, the mixture was kept stirring (300 rpm) at room temperature for 3.5 h in the dark. Finally, NPs were collected by ultrafiltration and characterized as previously mentioned (Z-average, PDI, and ζ-potential).

3.8.2 Bradford assay

The Bradford assay was used to indirectly quantify the amount of conjugated peptide to NPs, by measuring the free peptide in the supernatant resulting from the ultrafiltration after the functionalization process.

Briefly, 150 µL of Coomassie Reagent were added to the same volume of each standard or sample in a 96-well plate, and shaken during 30 seconds. Then, the plate was incubated for 10 minutes at room temperature, and the absorbance was measured at 595 nm in a plate reader. The results were simultaneously compared with a standard curve of BSA and the same peptide used for NPs functionalization, in concentrations ranging from 0 to 25 µg/mL. The AE of the peptide to the NPs was calculated according to Equation 3.3.

$$AE\ (\%) = \frac{(Initial\ mass\ of\ peptide) - (mass\ of\ recovered\ peptide)}{Initial\ mass\ of\ peptide} \times 100 \qquad (3.3)$$

3.8.3 Nuclear magnetic resonance analysis

To confirm the presence of the peptide in the formulation of functionalized NPs, proton nuclear magnetic resonance (^{1}H NMR) spectroscopic analysis was used for the detection of differences on spectra from non-functionalized and functionalized particles. Non-functionalized and functionalized empty PLGA NPs, as well as commercial PLGA used in the production process of NPs, were dissolved

(3 mg) in DMSO and placed on appropriate nuclear magnetic resonance tubes. The analysis were performed at room temperature on a Brüker AMX 300 spectrometer operating at 400.13 MHz, with every chemical shift value (δ; ppm) expressed relatively to tetramethylsilane (TMS) as an internal reference.

3.9 Cell culturing

Both hCMEC/D3 and ND7/23 were grown in tissue culture flasks (passage 38–50 and 11-21, respectively).

The hCMEC/D3 cell line was maintained in EBM-2 supplemented with FBS (5 %, v/v), penicillin-streotomycin (1 %, v/v), hydrocortisone (1.4 μM), ascorbic acid (5 μg/mL), chemically defined lipid concentrate (1/100, v/v), HEPES (10 mM) and bFGF (1 ng/mL). This last supplement was added extemporaneously in the culture medium.

The ND7/23 cell line was maintained in DMEM supplemented with FBS (10 %, v/v) and penicillin-streotomycin (1 %, v/v).

The cell cultures were kept in an incubator (CellCulture CO_2 incubator, ESCO) at 37 ºC with 5 % CO_2, in a water saturated atmosphere. Cell culture medium was changed every 2–3 days.

3.10 Nanoparticles-associated metabolic viability assay

The samples toxicity was assessed in the hCMEC/D3 and ND7/23 cell lines using the MTT metabolic viability assay.

A preliminary study was made to find the optimal cellular density of ND7/23 cell line. Cells were seeded in a 96-well plate in a concentration of 0.001, 0.005, 0.010, 0.015, 0.020, 0.040, 0.060, 0.080 and 0.100 $\times$ 10^6 cells/mL in supplemented DMEM. Then, MTT test was done according to manufacters' instructions, but cells were only incubated with medium, in order to further evaluate the resulting absorbances. The cellular density that proved to be the most appropriate one for the ND7/23 cell line was used for the seeding of these cells (0.015 $\times$ 10^6 cells/mL; 200 μL). For the hCMEC/D3 cell line, 200 μL of cells were seeded in a 96-well plate (0.04 $\times$ 10^6 cells/mL) in supplemented EBM-2. This cellular density was already described in a previous work [224].

After the seeding, cells were incubated during 24 h and then medium was removed and cells were washed with 200 μL of PBS. Thereupon, cells were incubated with free EFV, empty NPs, functionalized empty NPs, EFV-loaded NPs and functionalized EFV-loaded NPs, in concentrations of 100, 10, 1, 0.1, and 0.01 μM (in medium) determined in relation to the drug, for 24 h. Afterwards, solutions were discarded, cells were washed with 200 μL of PBS and then treated with 200 μL of MTT solution (0.5 mg/mL, in medium) per well, during 4 h in the dark. Formazan crystals, resulting from the reduction of MTT by viable cells, were solubilized with 200 μL of DMSO, under a 20 min slight shake, at 100 rpm and room temperature. Finally, absorbance was measured at 590 and 630 nm using a plate reader.

A negative control (NC), consisting on cells incubated with 1 % of Triton X-100 in medium solution, which has a detergent effect capable of disrupt cells (0 % of metabolic activity), and a positive control (PC), consisting on cells incubated only with medium (100 % of metabolic activity), were also prepared and treated similarly to the sample wells. Metabolic activity was expressed as a percentage compared to the controls according to the Equation 3.4.

$$Metabolic\ activity\ (\%) = \frac{Experimental\ value - NC}{PC - NC} \times 100 \quad (3.4)$$

3.11 Nanoparticles hemocompatibility assay

3.11.1 Quantification of hemolysis

The assay related to the quantification of hemolysis resulted from an adaptation of the protocol previously described by Pinto *et al.* [225]. Red blood cells were isolated from buffy coats (obtained from Immunohemotherapy Service, S. João Hospital, Porto, Portugal). Briefly, 2 mL of the buffy coat content were centrifuged (Eppendorf 5810R) over density gradient with 2 mL of Histopaque-1077 for 30 min at 400 *g* and room temperature, in accordance with the instructions of the manufacturer. After removal of the plasma upper layer, the lower layer containing red blood cells was washed three times with 8 mL of PBS (centrifugations for 30 min at 400 *g* and room temperature). Then, 100 µL of red blood cells in a concentration of 2×10^8 cells/mL were placed in eppendorf tubes. Next, 100 µL of free EFV, empty NPs, functionalized empty NPs, EFV-loaded NPs and functionalized EFV-loaded NPs were added to the tubes to obtain a final concentration of 50, 5, 0.5, 0.05, and 0.005 µM in PBS (concentrations determined in relation to the drug). Eppendorf tubes were incubated for 3 h at 100 g and 37 ºC. Afterwards, the tubes were centrifuged (Eppendorf 5417R) at 4000 rpm for 5 min to collect the supernatants, which were transferred (80 µL) to black polypropylene 96-well plates for absorbance reading, using a plate reader.

The PC, consisting on cells incubated with 1 % of Triton X-100 in PBS (100 % hemolysis), and NC, consisting on cells incubated only with PBS (lysis negative control; 0 % hemolysis), were also prepared and treated similarly to the sample tubes.

The hemoglobin value of the samples was calculated in accordance with Equation 3.5.

$$Hemoglobin\ value\ of\ sample\ (mg/dL) = \frac{[2 \times A_{415} - (A_{380} + A_{450})] \times 100 \times D_f}{E}, \quad (3.5)$$

where A_{380} is the absorbance value at 380 nm, A_{415} is the absorbance value at 415 nm, A_{450} is the absorbance value at 450 nm, Df is the dilution factor (that was 35), and E is the molar absorptivity of oxyhemoglobin at 415 nm (that is 79.46). The absorbance value at 415 nm corresponds to the Soret band absorption of hemoglobin, and the absorbance values at 380 and 450 nm correspond to the absorption of uroporphyrin, which falls under the same wavelength range.

Afterwards, the hemolytic potential of the samples was calculated in accordance with Equation 3.6.

$$Hemolysis\ (\%) = \frac{Hemoglobin\ value\ of\ sample}{Hemoglobin\ value\ of\ PC} \times 100 \quad (3.6)$$

The osmolarity of the formulations incubated with red blood cells were also determined at room temperature using a Micro-Osmometer M3320 (Advanced Instruments, Inc.).

3.11.2 Morphology of red blood cells

The assay related to the assessment of cell membrane integrity and morphology of red blood cells resulted from an adaptation of the protocol previously described by Shahbazi *et al.* [226] and was based on scanning electron microscopy (SEM) imaging. Briefly, and after the isolation of red

blood cells from buffy coats as described for the quantification of hemolysis, 1 mL of red blood cells in a concentration of 4×10^5 cells/mL in HBSS were seeded in 6-well plates containing plastic tissue culture coverslips. Then, NPs were added in 1 mL of HBSS to reach a final concentration of 50 µM. The plates were placed in an orbital shaker incubator for 3 h at 37 ºC and 100 rpm.

The NC, consisting on cells incubated only with HBSS (lysis negative control; 0 % hemolysis), was also prepared and treated similarly to the sample wells.

The cells were then fixed in 2.5 % glutaraldehyde in sodium cacodylate buffer (pH = 7.4) for 1 h, and dehydrated in increasing concentrations of 50, 70, and 100 % of ethanol for 5, 20, and 15 min, respectively. Finally, the coverslips were removed from wells, mounted on SEM supports using double sided carbon adhesive tape, and observed under SEM (FEI Quanta 400F). Before the SEM acquisition, samples were coated with gold/platinum under vacuum for 90 s, with a 15 mA current. An electron beam intensity of 10 kV and magnification ranging from 1000 to 15500 times were used.

3.12 Evaluation of cell-nanoparticle interaction

The quantification of the nanoparticles associated to hCMEC/D3 cells was evaluated using flow cytometry (fluorescence-activated cell sorting, FACS).

Cells were seeded in 6-well plates (0.28×10^6 cells per well in 1.5 mL of supplemented EBM-2) and were allowed to attach overnight. The cells were washed twice with pre-warmed 2 mL PBS pH 7.4, and then 1 mL of 6-C-loaded NPs in EBM-2, corresponding to 80 µg per well, were added to each well and incubated for 1 and 3 h at 37 ºC. After incubation, cells were washed twice with PBS and detached with versene. The cells were then washed twice with PBS and collected through centrifugation (Eppendorf 5810R) at 1300 rpm during 8 min. Finally, cells were ressuspended in 500 µL of PBS and placed in cytometer tubes.

The quantification was done using a FACS CANTO II cytometer (BD Biosciences), equipped with three laser with excitation of 405, 488 and 633 nm, where NPs were detected through the 488 nm channel. The results were analyzed using the software FlowJo vX.0.7.

3.13 Blood-brain barrier *in vitro* model

The guidelines to set up the BBB *in vitro* model used in this work were already reported in previous works [227, 228].

Briefly, to develop the BBB *in vitro* model, 2.5×10^4 cells/cm^2 of hCMEC/D3 cells (500 µL; supplemented EBM-2) were seeded on 12-Transwell® cell culture inserts. Previously to the seeding, the inserts were coated with 90 µL of a 50 µg/mL rat tail collagen type I in acetic acid solution (0.02 M) for 1 h, at 37°C, and then washed twice with PBS. The basolateral side of the wells were filled with 1.5 mL of supplemented EBM-2.

The system was maintained in the incubator at 37 ºC with 5 % CO_2 during 8 days, and medium was changed every 2 days. The hCMEC/D3 cells monolayer became confluent at the 8th day, which was the day appropriate to perform the permeability study.

The integrity of the cell monolayer was checked every 2 days by monitoring the transendothelial electric resistance (TEER) using an endothelial Volt–Ohm meter (Millicell® ER S-2; Millipore). The resistance value of an empty filter was subtracted from each measurement.

3.14 Evaluation of the blood-brain barrier *in vitro* model integrity

In order to evaluate the integrity of the BBB monoculture barrier, at culture day 8, the insert membranes presenting the hCMEC/D3 monolayer were stained and analyzed by confocal microscopy.

Insert membranes were fixed with 4 % paraformaldehyde in PBS for 10 min at room temperature, and washed three times with HBSS. After removal of HBSS, cell membranes were stained with 500 µL of 5 µg/mL Alexa Fluor® 594 WGA (apical compartment) in the dark during 20 min at room temperature. After, membranes were washed three times, 5 min each. Cell nuclei were then stained with 500 µL of 100 ng/mL DAPI (apical compartment) in the dark during 15 min at room temperature. After removal of DAPI, membranes were mounted on a glass slide in Vectashield and covered with a coverslip. The slides were observed using a confocal microscope (Leica Microsystems GmbH).

3.15 Permeability study

The permeability experiment across the cell monolayer (8th day of the BBB *in vitro* model) was performed in the apical-to-basolateral direction. After removing the cell culture medium, the basolateral compartment was filled with 1.5 mL of HBSS. Regarding the apical compartment, 500 µL of 10 µM of free EFV, EFV-loaded NPs, and functionalized EFV-loaded NPs diluted in HBSS were added (concentrations determined in relation to the drug). Then, the assay was conducted at 37 ºC using an orbital shaker incubator (100 rpm). At different time points (15, 30, 45, 60, 90, 120 and 180 min), 200 µL samples were taken from the basolateral side, and the same volume of pre-heated HBSS was added to replace the withdrawn volume. At the last time point, 200 µL samples were also taken from the apical side in order to quantify the amount of EFV which did not permeate through the membrane, and cell monolayers were treated with 1 % of Triton X-100 in PBS, in order to disrupt cells and quantify the amount of EFV internalized by them. All samples were used for HPLC analysis, in order to quantify EFV.

The integrity of the cell monolayer was checked during the permeability experiment by monitoring the TEER.

The permeability results were expressed in percentage of permeability and apparent permeability (Papp). Papp was calculated using Equation 3.7.

$$Papp = \frac{\Delta Q}{A \times C_0 \times \Delta t} \quad , \tag{3.7}$$

where C_0 is the initial concentration in the apical compartment of the insert, which was 3.16 µg/mL, A is the surface area of the insert (0.9 cm^2), Δt is the time during which experiment occurred in seconds (10800 seconds), and ΔQ is the amount of drug detected in the basolateral compartment in µg.

3.16 Statistical analysis

All the results were represented as mean ± standard deviation from a minimum of three independent experiments. Statistical analysis was performed by one-way analysis of variance (ANOVA) followed by a post hoc test (Tukey's honestly significant difference) to compare more than two groups. In case of comparison of two different groups, unpaired Student t-test was used.

Differences were considered significant at * $p < 0.05$, ** $p < 0.01$, or *** $p < 0.001$. All statistical analyses were performed with the software GraphPad Prism 5 (GraphPad Software Inc.).

Chapter 4

Results and Discussion

4.1 Conventional production of nanoparticles

Before moving forward to the microfluidics-based NPs production, some parameters had to be optimized for the conventional method, namely, the selection of the most appropriate recovering process after NPs synthesis, surfactant, organic solvent, and the introduction of possible attempts to improve the final characteristics of the nanosystems. The effect of each change on NPs properties was accessed by evaluating the Z-average, PDI, ζ-potential, AE and DL of the formulations.

Firstly, the production of NPs was run by means of the regular protocol for the conventionally-performed nanoprecipitation technique, using acetone and 2 % of TWEEN®-80 as the organic solvent and surfactant solution, respectively. Basically, the organic phase was added to the continuous phase, and this step was performed with a needle positioned directly into the core of the external phase (continuous) to prevent the occurrence of a superficial polymeric film [229]. The process is schematized in the Figure 4.1. The produced NPs were then collected by centrifugation using different speeds and times. Speeds of 10,000, 15,000, 20,000, 23,000, and 27,000 *g*, and centrifugation times of 15, 20, 30, 40, and 45 min were tested. NPs could not be ressuspended after ultracentrifugation, even trying slight speeds during a short period of time. Thereupon, in order to facilitate the resuspension of the formulation, the pellet was sonicated for 30 s at 30 % intensity. Still, the pellet was not perfectly ressuspended. As another strategy to facilitate the resuspension of the formulation, a glycerol bed in the bottom of the centrifugation tube was used. Once again, irreversible caking of the NPs occurred. Due to the impossibility of using ultracentrifugation while maintaining the formulation in viable conditions, the ultrafiltration was adopted to perform the recovering process in the next experiments.

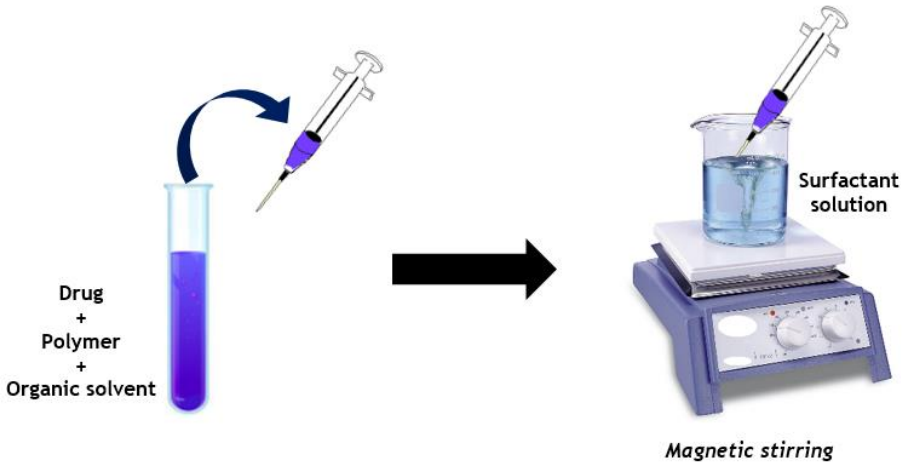

Figure 4.1 – Nanoprecipitation technique to produce NPs. The dispersed phase was added to the continuous phase, and then the product was stirred to promote organic solvent diffusion.

When performing the conventional nanoprecipitation technique with acetone and 2 % of TWEEN®-80, empty NPs with an approximately Z-average, PDI, and ζ-potential of 173 nm, 0.1, and -29 mV, respectively, were obtained (Table 4.1). Generally, the mean size of NPs for brain-targeted drug delivery should be up to 200 nm to enable endocytosis by capillary cells [230], and thus the formulation demonstrated to be satisfactory in respect to this issue. The PDI is an important formulation parameter because it affects NPs transport properties, biological activity and therapeutic efficiency [231]. Values of PDI up to 0.3 are described to be related with homogeneous populations of particles. However, PDI values higher than 0.3 usually mean the presence of a non-homogenous population and a presumable occurrence of NPs aggregation [232]. Herein, the formulation demonstrated to be homogenous. Also, the negative surface charge of the obtained NPs was expected, being consistent with the work of Stolnik *et al.* [233] who attributed this feature to the end carboxyl groups of PLGA. Then, EFV-loaded NPs were produced with the same composition, and different percentages of DP, namely, 2.5, 5, 10, and 15 %, were tested. The results are shown in Table 4.1. Although no relevant differences were observed in other parameters, the DP of 15 % was associated with the higher values of AE and DL. However, a maximum AE and DL of only 51 and 8 %, respectively, were obtained. Since these results implied a big loss of drug, a different percentage of TWEEN®-80, 1 %, was tested on the production process, while maintaining NPs composition and the DP of 15 %. Besides other differences perceived in NPs features, there was a significant decrease in AE (** $p < 0.01$) and DL (* $p < 0.05$), and therefore no improvements were seen by replacing 2 % of TWEEN®-80 (Table 4.1). For this reason, another surfactant solution, PVA, at two different concentrations of 1 and 2 %, was also tested, while maintaining again NPs composition and a DP of 15 %. Herein, both formulations containing PVA presented similar properties (Table 4.1). Apart from the significant increase in size (** $p < 0.01$) and charge (*** $p < 0.001$) regarding the formulation with 2 % of TWEEN®-80, an outstanding increase in AE and DL (*** $p < 0.001$) was also noted. However, this increase raised some doubts and the possibility of the interference of the collecting process of NPs, consisting on ultrafiltration, on these values was investigated. Since it was possible to observe a PVA mass attached to the filter, it was verified whether that could lead to retention of the non-associated drug, hence avoiding its detection on the supernatant afterwards. By ultrafiltrating a solution of free EFV in 2 % of PVA or TWEEN®-80, it was possible to observe that, in the formulations containing PVA, not all the drug was present on the supernatant in the end so, the emergence of false positive results related to this surfactant was

confirmed. Oppositely, the TWEEN®-80 demonstrated to be a reliable surfactant and thus it did not cause the previously described effect. Ultimately, and returning to the beginning, the next experiments were performed using 2 % of TWEEN®-80 as the surfactant solution and a DP of 15 %.

Table 4.1 - Optimization of the conventional process of fabrication of NPs. Results are presented as mean ± SD (n = 3).

Organic solvent	Surfactant (%)	DP (%)	Z-average (nm)	PDI	ζ-Potential (mV)	AE (%)	DL (%)
Acetone	-	-	173.4 ± 2.7	0.110 ± 0.010	-28.3 ± 3.3	-	-
	2 % TWEEN®-80	2.5	176.5 ± 2.5	0.081 ± 0.012	-23.8 ± 1.3	34.4 ± 9.7	0.9 ± 0.2 ***
		5	178.1 ± 2.3	0.079 ± 0.011	-24.1 ± 2.1	37.2 ± 6.0	1.8 ± 0.3 ***
		10	177.4 ± 2.2	0.084 ± 0.011	-26.2 ± 1.9	37.2 ± 3.3	3.6 ± 0.3 **
		15	180.2 ± 4.7	0.089 ± 0.015	-22.0 ± 1.6	40.9 ± 6.7	5.8 ± 0.9
	1 % TWEEN®-80	15	152.4 ± 2.5 **	0.077 ± 0.014	- 26.1 ± 1.7 *	26.4 ± 2.5 **	4.0 ± 0.4 *
	1 % PVA		207.9 ± 10.9 **	0.099 ± 0.036	- 0.7 ± 0.1 ***	98.5 ± 0.2 ***	14.6 ± 0.0 ***
	2 % PVA		204.3 ± 1.3 **	0.087 ± 0.012	- 0.6 ± 0.0 ***	97.3 ± 0.5 ***	14.4 ± 0.1 ***

DP: drug/polymer ratio; Z-average: average size; PDI: polydispersity index; ζ-Potential: zeta-potential; AE: association efficiency; DL: drug loading; PVA: poly(vinyl alcohol).
* $p < 0.05$; ** $p < 0.01$; *** $p < 0.001$ (comparison done in relation to NPs produced with 2 % of TWEEN®-80 and a DP of 15 %).

At this point of the work, some feedback about the capabilities of the microfluidic system, which will be explored in detail on the next section, started to being received. Since the main goal was to compare the final formulations obtained by the conventional with the microfluidic method, the reagents and respective concentrations were maintained between both methods. So, as will be

described later, there was a need to exchange the organic solvent involved on the production process of NPs, from acetone to DMSO. All the other formulation components and methodology were kept. The change of the solvent slightly affected the final properties of NPs produced by the conventionally-performed method, which will be discussed later on this chapter (Table 4.2; Section 4.3).

Finally, besides the regular nanoprecipitation, a new methodology based on a modified nanoprecipitation technique, including an extra sonication step, was introduced. This modified technique consisted of adding the dispersed phase to a small volume of continuous phase, followed by immediate sonication (first dispersion) and dilution of the resulting product in a bigger volume of continuous phase (second dispersion). R. Kulterer *et al.* [234] already described the influence of sonication on nanoprecipitation, concluding that it promotes the prompt disruption of the dispersed phase into small drops, right after reaching the continuous phase, and speeds up the intermixing process of the two phases. The first dispersion of the oil phase in a small quantity of surfactant solution with the sonication probe may promote a faster second dispersion, hence allowing a faster diffusion of that phase through the continuous one. In the regular nanoprecipitation, the single dispersion begins on the perimeter around the needle, and then it spreads to the periphery through a centrifugal gradient, which may lead to a slow diffusion of the dispersed phase through the continuous one. The aim inherent to this methodology was to obtain NPs with smaller dimensions when using the modified nanoprecipitation technique, since they are directly associated with a faster diffusion during the formation process of the particles. Moreover, the introduction of a modified nanoprecipitation methodology was important to verify if the microfluidic method would be able to surmount this improved version of the technique. Therefore, the results related to NPs properties will be discussed and compared between both methods later on (Table 4.2; Section 4.3).

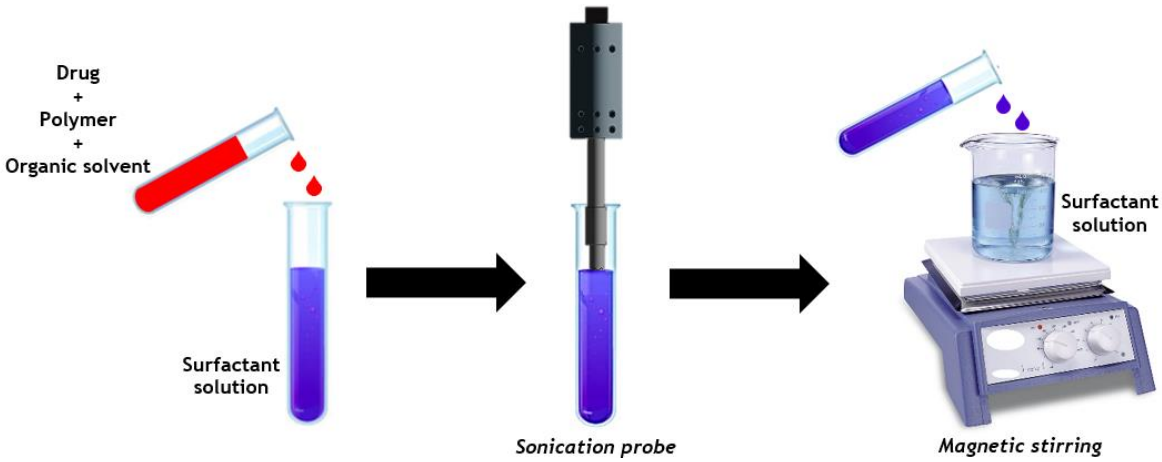

Figure 4.2 – Modified nanoprecipitation technique to produce NPs. This process involved two different dispersions of the organic phase in the aqueous one.

4.2 Nanoparticles production by microfluidics

The microfluidic platform was composed of a square capillary and a cylindrical tapered capillary. The outer diameter of the cylindrical tapered capillary fit the inner dimensions of the square capillary, facilitating the alignment of their axes.

The geometry of the microfluidic systems are designed to provide unique flow patterns. Herein, the co-flow and flow-focusing geometries were adopted to perform the nanoprecipitation technique

in the microfluidic chip. In order to compare the differences in NPs properties between the microfluidic and conventional methodology, the microfluidics-related results of the co-flow and flow-focusing geometries were compared with the conventional method-related results of the nanoprecipitation and modified nanoprecipitation techniques, respectively. Therefore, the microfluidic production was run until reach a final volume equal as the one obtained when performing the techniques by conventional methods, which is around 20 mL for the co-flow geometry, and 11.5 mL for the flow-focusing geometry. Moreover, PLGA and EFV in DMSO, and TWEEN®-80 concentrations used to perform the conventional method were exactly replicated in the microfluidic method.

In the co-flow geometry (Figure 4.3), the dispersed phase (inner fluid) flowed inside the inner cylindrical capillary, while the continuous phase (outer fluid) flowed between the inner and outer cylindrical capillaries in the same direction, resulting in the formation of the NPs. The two fluids co-flowed in parallel directions, and underwent mixing by well-defined diffusion after met each other.

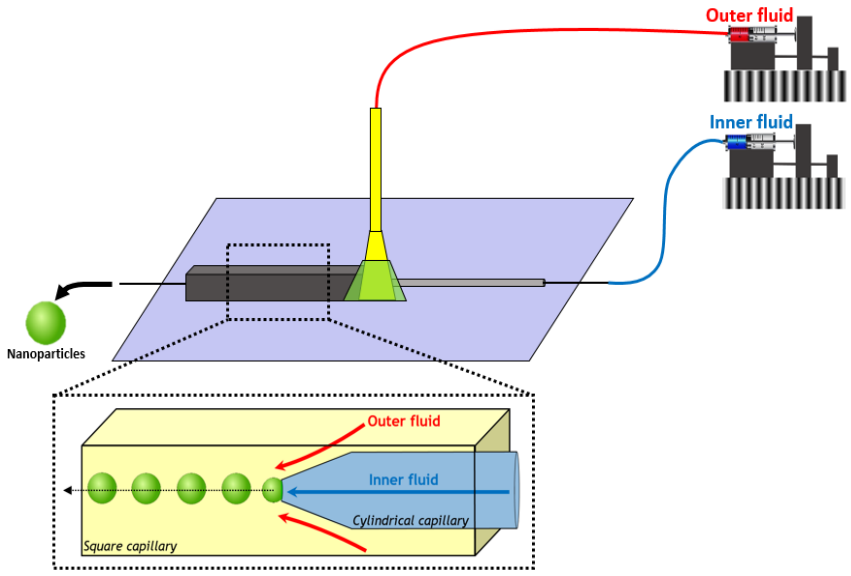

Figure 4.3 – Co-flow geometry in the microfluidic platform.

In the flow-focusing geometry (Figure 4.4), the dispersed phase (inner fluid) was injected into the left extreme of the square capillary, whereas the continuous phase (outer fluid) was injected in the opposite direction through the interstices between the right extreme of the square capillary and the cylindrical capillary. The two fluids flowed oppositely, and underwent mixing by well-defined diffusion after met each other. Moreover, the stream was forced to pass through the tapered tip of the cylindrical capillary and consequently narrow its shape. This resulted in the formation of the NPs.

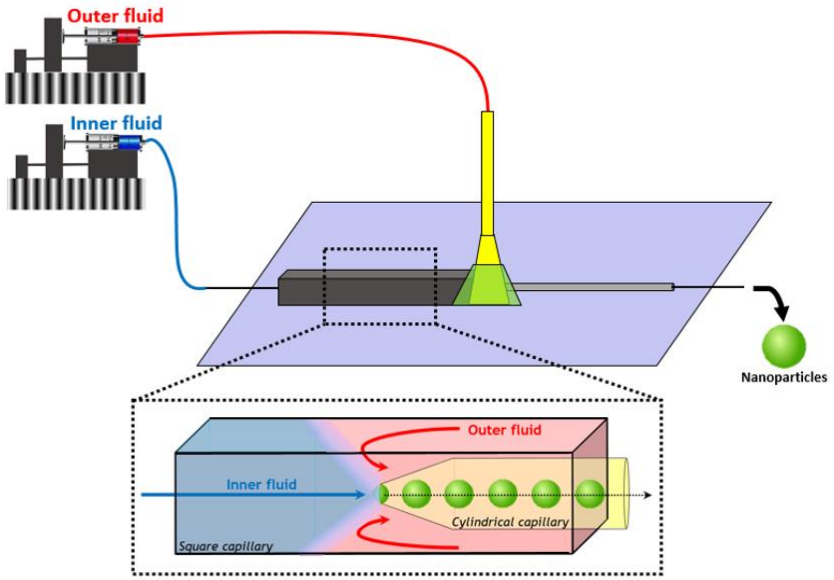

Figure 4.4 – Flow-focusing geometry in the microfluidic platform.

Different types of preliminary assays were made to optimize the process conditions and find the most appropriate setup to produce NPs by microfluidics. In terms of organic solvents, the production was initiated using acetone, as described in Section 4.1. However, it caused several issues related to clogging of the microfluidic chip, especially for the concentration of 40 mg/mL of PLGA, used as the inner fluid when adopting the flow-focusing geometry. Therefore, there was a need to change the organic solvent, and thus DMSO was selected to proceed with NPs development (the methodology was uniformed in order to use DMSO in every process of NPs production). DMSO prevented the emergence of clogging phenomena in the microfluidic chip, and, in addition, it belongs to solvents Class III, which is known by its low toxic potential, being widely used in the pharmaceutical field [235]. Afterwards, the effect of different inner and outer fluid flow rates on NPs size, PDI and ζ-potential was accessed for each fluids geometry adopted. The main goals were to achieve a size of NPs similar or lower than the ones obtained by the conventional method, the lowest possible value for PDI, and a ζ-potential of NPs similar to the ones obtained by the conventional method. Besides NPs properties, the time necessary to complete one batch of NPs was also taken into account. The effect of each combination of inner and outer fluid flow rate was translated in different values of Z-average, PDI and ζ-potential. Firstly, it is important to mention that, for both geometries and for all fluids flow rates tested, the ζ-potential did not vary significantly. Regarding the co-flow geometry, in test a), different outer fluid flow rates with a fixed inner fluid flow rate were experienced (Figure 4.5a). The flow rates of 20 µL/min and 50 µL/min for the inner and outer fluid, respectively, were considered the most adequate combination after this test, due to the lowest value obtained of PDI. In test b), the flow rates ratio derived from 20 µL/min (inner fluid) and 50 µL/min (outer fluid) was fixed, and then the flow rates were changed maintaining this proportion (Figure 4.5b). Herein, the flow rates of 1500 µL/min and 3750 µL/min for the inner and outer fluid, respectively, were considered the most adequate combination; besides this combination did not present the lower NPs size, it was verified that these flow rates were associated with the lowest value of PDI. In test c), the outer fluid flow rate of 3750 µL/min was fixed, and the inner fluid flow rate was altered (Figure 4.5c). The flow rates of 2500 µL/min and 3750 µL/min were selected for the inner and outer fluid, respectively, because it seemed that, from these values on, Z-average and PDI reached a minimum limit. Thus, for the co-flow geometry,

the inner and outer fluid flow rates were definitely stipulated as 2500 and 3750 µL/min, respectively. Regarding the flow-focusing geometry, in test a), the outer fluid flow rate was changed, while maintaining a fixed inner fluid flow rate (Figure 4.6a). The flow rates of 20 µL/min and 800 µL/min for the inner and outer fluid, respectively, were considered the most adequate combination, due to the acceptable low value of Z-average and PDI, in this context; moreover, these highest values of flow rates meant the faster production of NPs. In test b), the flow rates ratio derived from 20 µL/min (inner fluid) and 800 µL/min (outer fluid) was fixed, and then the flow rates were proportionally changed (Figure 4.6b). Herein, the flow rates of 62.5 µL/min and 2500 µL/min for the inner and outer fluid, respectively, were considered the most adequate combination, due to the lowest value of PDI and the acceptable value of Z-average. In test c), the outer fluid flow rate of 2500 µL/min was fixed, and the inner fluid flow rate was altered (Figure 4.6c). The flow rates of 1000 µL/min and 2500 µL/min were selected for the inner and outer fluid, respectively, because a low value of PDI and a satisfactory value of Z-average were reached. Thus, for the flow-focusing geometry, the inner and outer fluid flow rates were definitely stipulated as 1000 and 2500 µL/min, respectively.

Later on, the NPs resulting from these selected arrangements of fluids flow rates were analyzed in terms of their properties (Table 4.2; Section 4.3).

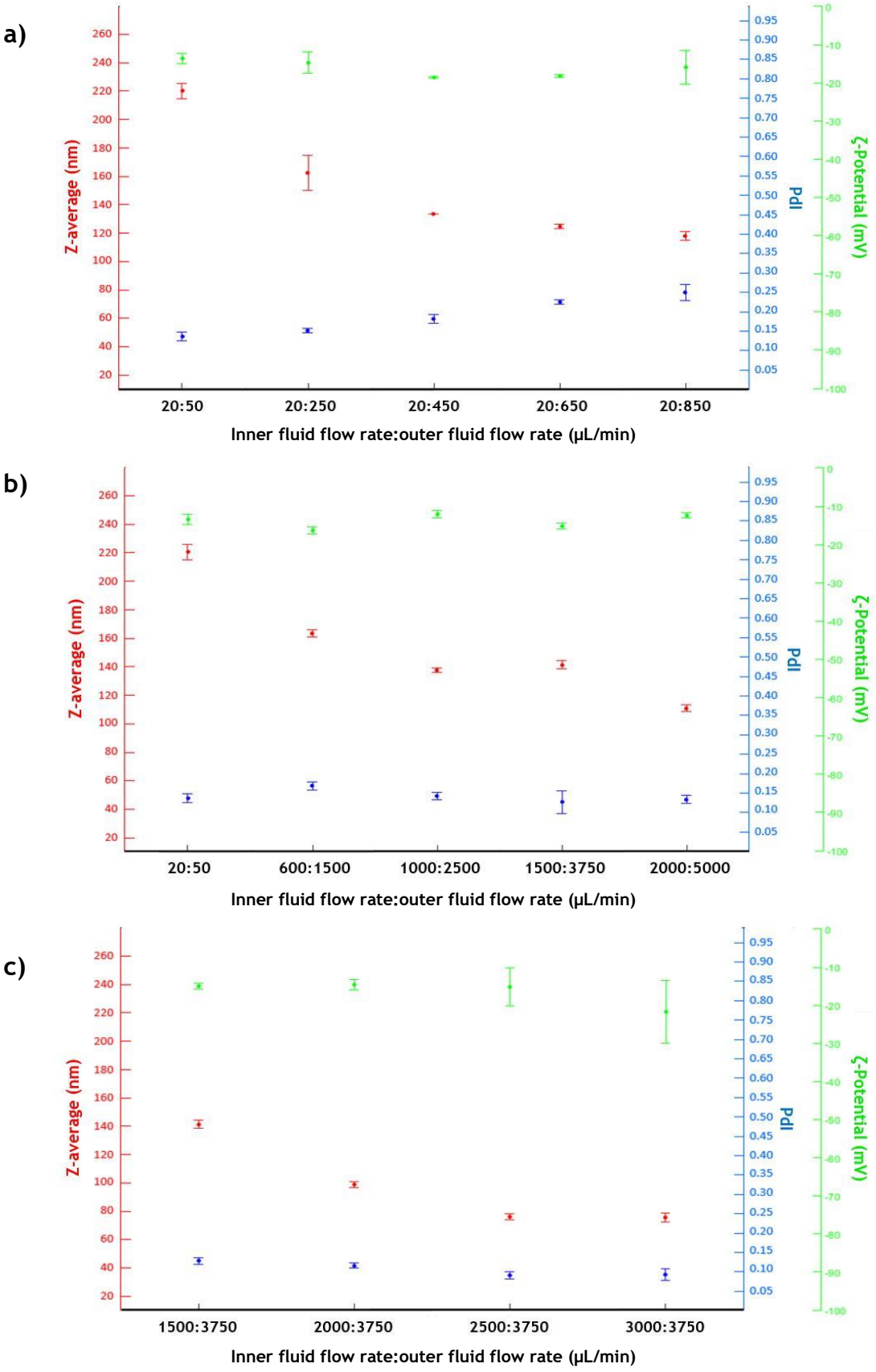

Figure 4.5 – Optimization of the flow rates in the microfluidic chip for the inner and outer fluid during the performance of the co-flow geometry.

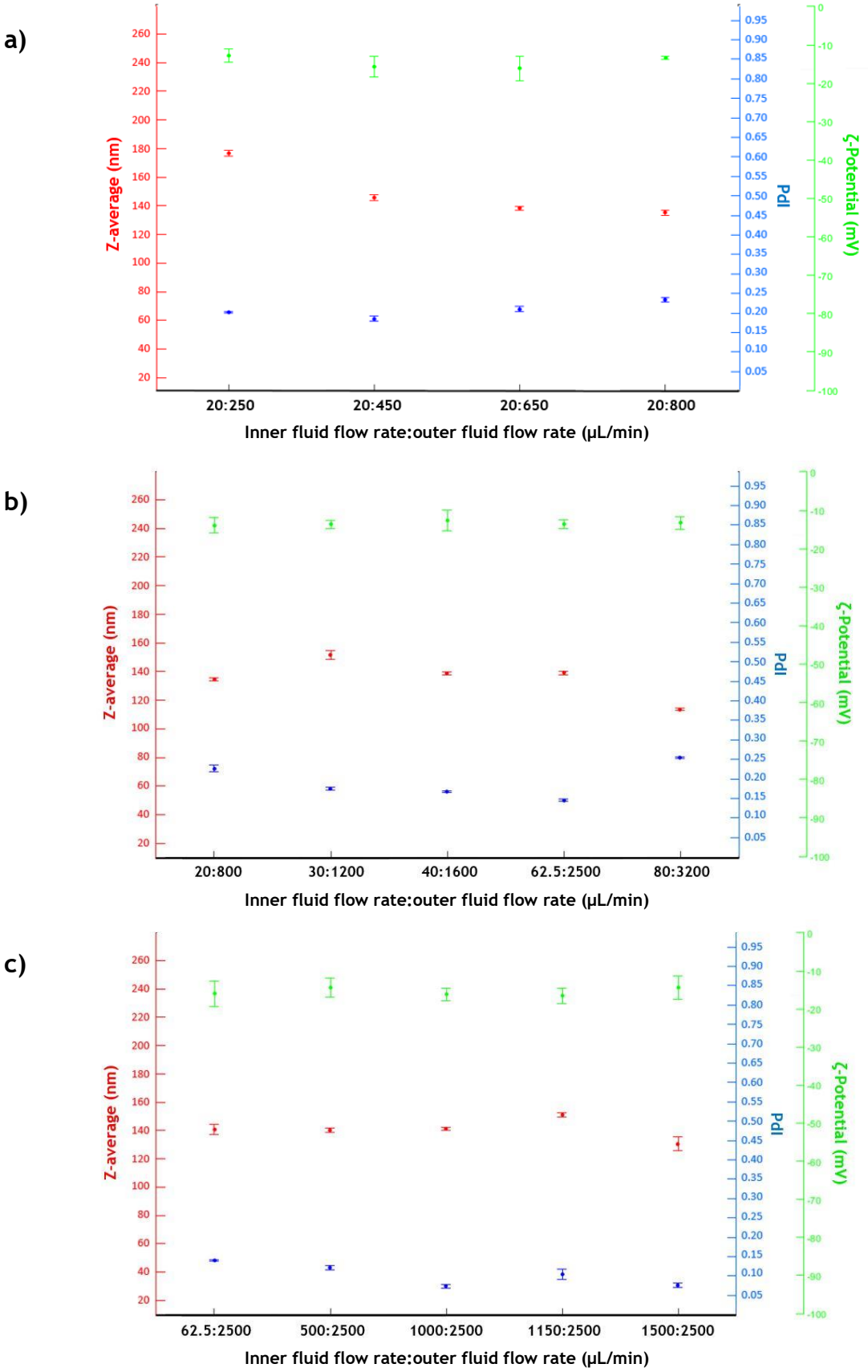

Figure 4.6 – Optimization of the flow rates in the microfluidic chip for the inner and outer fluid during the performance of the flow-focusing geometry.

4.3 Conventional and microfluidic method: comparison of nanoparticles properties

After production, EFV-loaded NPs formulations were evaluated for Z-average, PDI, ζ-potential, AE, DL, morphology, and chemical profile. As mentioned above, microfluidics-related results of the nanoprecipitation tecnhique performed through the co-flow and flow-focusing geometry were compared with the conventional bulk method-related results of the technique and modified technique, respectively.

4.3.1 Average size, polydispersity index and surface charge

The results for the evaluation of the obtained NPs in relation to their Z-average, PDI, and ζ-potential were depicted in Table 4.2.

All of the obtained formulations presented NPs which met the requirement of a Z-average under 200 nm, which is important to accomplish the brain-targeted drug delivery [230], as mentioned above. For the nanoprecipitation technique (test 1), the size of NPs obtained by microfluidics (around 70 nm) was significantly lower ($^{***}p < 0.001$) compared to the conventional methodology (around 133 nm). Considering the modified nanoprecipitation technique (test 2), NPs size results were not significantly different between the two production methods. Furthermore, NPs produced by microfluidics using the co-flow geometry consisted on the only nanosystem which presented a Z-average lower than 100 nm. It is well known that lower sizes of NPs enable longer blood half-time [236]. Moreover, Gao *et al*. injected polymeric drug-loaded NPs with sizes of 70, 170, 220 and 345 nm into rats (at the same dose), and proved that NPs with a size smaller than 100 nm led to the highest drug level in the brain; the authors associated the size of 70 nm with an easier endocytosis of NPs by vascular endothelial cells of the BBB [237].

In relation to PDI of NPs, results were not significantly different between the different approaches (for both test 1 and 2). However, it is necessary to highlight that the microfluidic technology was able to provide PDI values as low as the ones obtained by the conventional methodology (around 0.1). This was expected since particles narrow size distribution is commonly associated with microfluidics [238].

Regarding formulations ζ-potential, results demonstrated a significant increase in surface charge ($^{**}p < 0.001$) when performing NPs production by microfluidics, instead of the conventional methodology. This may be explained by an increase in the quantity of TWEEN®-80 associated with the particles when they were produced using the microfluidic approach, hence retaining a less negative charge [239]. Still, all formulations presented a negative ζ-potential, which is due to the PLGA profile [233], as mentioned before.

Empty and EFV-loaded NPs presented similar properties in relation to the mentioned physico-chemical parameters.

4.3.2 Association efficiency and drug loading

In order to define the amount of drug associated to the NPs, the quantification of EFV was carried out by HPLC and indirectly calculated (Equations 3.1 and 3.2). New calibration curves were set in the beginning of every experiment to verify the feasibility of the method proposed to detect EFV. This curve was constructed based on standard solutions freshly prepared in acetonitrile, thus considering the mobile phase of the method and the solution in which the NPs were analyzed, as well. The calibration curve comprised a range of EFV concentrations from 1 µg/mL to 50 µg/mL, at

equally spaced intervals. In Figure 4.7 is possible to find a model for this curve. The obtained calibration curves always presented a coefficient of determination value (R^2) between 0.990 and 0.999, which demonstrated the feasibility of the method [240].

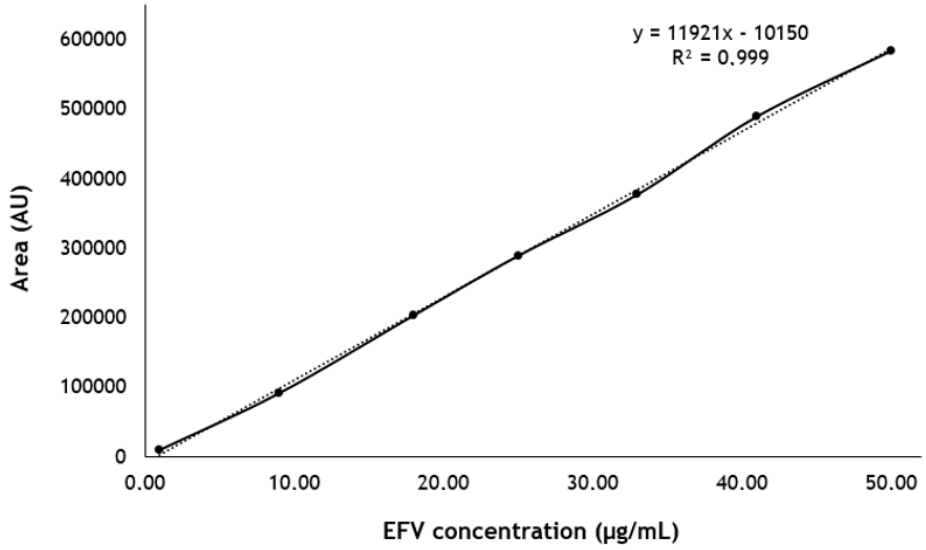

Figure 4.7 – Standard curve calibration for EFV quantification using HPLC.

The results for the evaluation of the obtained NPs in relation to AE and DL are depicted in Table 4.2.

Regarding the nanoprecipitation technique (test 1), microfluidics-associated AE was significantly higher (around 80 %; $^{***}p < 0.001$) compared to the conventional methodology, with a difference of around 50 %. Moreover, DL experienced a significant increase ($^{***}p < 0.001$) in microfluidics-produced NPs (around 11 %) in comparison to the conventional method (around 3 %). Literature data attributed reduced drug loss to fewer steps involved in microfluidics-assisted NPs production compared to sequential conventional mixing of multiple phases [241]. The selected combination of inner and outer flow rate allowed matching drug flow with drops generation, thus contributing to a better drug entrapment. Liu *et al*. attributed AE and DL differences between the two methods to the fixed higher volume ratio between the continuous and dispersed phase in microfluidics, instead of a gradual increase in the ratio of these two phases during the conventional NPs synthesis process [212]. It is well known that changes in the ratio between the two phases affect drugs distribution in NPs matrix [242]. Moreover, it is probable that a slower solvent diffusion in microfluidics might promote less simultaneous drug migration out of the particles during the fabrication process, creating a coefficient which did not favor EFV presence in the continuous phase. This is in accordance with the work of Liu *et al*. [202], who referred that microfluidics reduces the movement of molecules from the dispersed to the continuous phase, hence promoting the effectiveness of drug entrapment. NPs formulations associated with low AE and DL values imply the administration of large amounts of non-therapeutic excipients to reach a clinically relevant drug dose which is associated with side effects emergence [243, 244]. These two parameters are of extreme importance when developing drug delivery nanosystems.

Considering the modified nanoprecipitation technique (test 2), the obtained AE and DL were not significantly different between the two implemented methods, conventional and microfluidics; these results demonstrated that the microfluidic method is not able to improve these features in comparison to the conventional one.

Table 4.2 - Properties of NPs resulting from different approaches. In the test 1, NPs resulting from the conventionally-performed nanoprecipitation were compared with the ones resulting from microfluidics using the co-flow geometry. In the test 2, NPs resulting from the conventionally-performed modified nanoprecipitation were compared with the ones resulting from microfluidics using the flow-focusing geometry. Results are presented as mean ± SD (n = 3).

Test	Method/ technique or geometry	NPs type	Z-average (nm)	PDI	ζ-Potential (mV)	AE (%)	DL (%)
1	Conventional/ nanoprecipitation	Empty	134.0 ± 2.7	0.092 ± 0.009	-27.4 ± 3.1	-	-
		EFV-loaded	133.0 ± 3.6	0.090 ± 0.010	-28.0 ± 2.4	32.7 ± 1.0	3.2 ± 0.1
	Microfluidics/ co-flow	Empty	70.9 ± 3.2 ***	0.085 ± 0.003	-15.0 ± 1.6 **	-	-
		EFV-loaded	72.8 ± 4.9 ***	0.086 ± 0.004	-14.1 ± 2.3 **	80.7 ± 8.3 ***	10.8 ± 1.1 ***
2	Conventional/ modified nanoprecipitation	Empty	134.4 ± 3.9	0.083 ± 0.008	- 24.3 ± 1.9	-	-
		EFV-loaded	137.3 ± 6.6	0.084 ± 0.006	- 23.9 ± 1.6	65.6 ± 2.5	6.2 ± 0.2
	Microfluidics/ flow-focusing	Empty	145.1 ± 3.0	0.075 ± 0.012	-14.8 ± 1.6 **	-	-
		EFV-loaded	146.8 ± 4.8	0.075 ± 0.010	-15.0 ± 1.9 **	56.9 ± 2.0	2.8 ± 0.1

DP: drug/polymer ratio; Z-average: average size; PDI: polydispersity index; ζ-Potential: zeta-potential; AE: association efficiency; DL: drug loading; NP: nanoparticle; EFV: efavirenz.
** $p < 0.01$; *** $p < 0.001$ (comparison done between the same NPs type inside each test group).

In conclusion, the performance of the nanoprecipitation technique by microfluidics using the co-flow geometry demonstrated to be indeed advantageous to develop EFV-loaded NPs. Besides providing comparable features of NPs to the ones obtained by the conventional methodology regarding PDI, and a smaller Z-average compared to the conventional procedure, the microfluidic method allowed significant better results of drug association efficiency and loading. Still, performing the nanoprecipitation technique by microfluidics using the flow-focusing geometry did not present any improvement in comparison to the conventional method.

The next stage of the work consisted on the evaluation of NPs morphology and chemical screening, comparing the outcomes of the conventionally-performed nanoprecipitation technique with the microfluidics-assisted nanoprecipitation using the co-flow geometry.

4.3.3 Morphology and chemical screening

The TEM analysis was performed for EFV-loaded PLGA NPs produced by nanoprecipitation using both conventional and microfluidic methods (co-flow geometry). The results are demonstrated in Figure 4.8.

Data revealed round-shaped particles with relatively smooth surfaces. Moreover, no apparent morphological differences were found between NPs resulting from the two production methods.

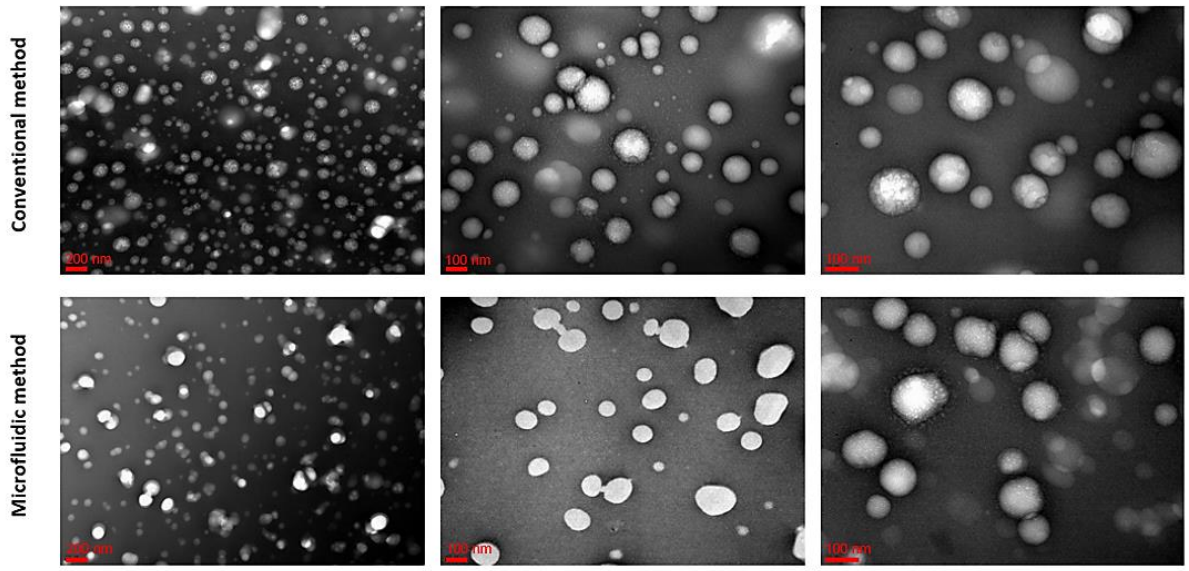

Figure 4.8 – TEM images of EFV-loaded PLGA NPs produced by the conventional and microfluidic method. From left to right, each column of images corresponds to a different magnification, namely, 50000, 100000, and 150000 times.

The EDS capability of TEM was used for elemental mapping of PLGA NPs produced by nanoprecipitation using both conventional and microfluidic method (Table 4.3). A single NP was focused, scanned and analyzed for its elemental composition. As expected, the results confirmed the presence of carbon and oxygen atoms in all formulations of NPs in similar levels, resulting from the presence of the polymer and the surfactant used in the production process. Moreover, it was possible to detect sulfur, which is characteristic of DMSO, and fluorine, which is characteristic of EFV (Table 4.3). In relation to the sulfur element, a significant difference (*** $p < 0.001$) was observed between empty NPs produced by the two methods, demonstrating a higher content of DMSO within NPs produced by microfluidics, in comparison to the conventionally-produced ones. However, for the EFV-loaded NPs, no differences in the DMSO content were found between the two methods of fabrication. This can be attributed to the higher affinity of DMSO to the water presented in the continuous phase of the NPs compared to the EFV, leading to a competitive and faster diffusion of the solvent out of the NPs, while the drug was efficiently entrapped within the nanosystem. It is well-known that DMSO has an high hydrogen bonding affinity for water [245]. Still, the higher level of DMSO found in the empty NPs produced by microfluidics may raise some issues related to a possible organic solvent-associated toxicity, which, in turn, may hinder the progression of the formulations to a commercially available product. However, the following *in vitro* cell

viability tests will confirm if this level of solvent is biologically relevant to cause cytotoxicity. Moreover, as a possible solution to remove the solvent from the microfluidics-produced empty NPs, an extra step based on dialysis could be added in the end of the fabrication process [246]. In relation to the fluorine, a significant difference (* $p < 0.01$) was observed between EFV-loaded NPs produced by the two methods. The microfluidic method allowed the formation of NPs with detectable levels of fluorine approximately two times higher than the conventional method. This is in good accordance with the results obtained for the AE and DL of the formulations, revealing the successful association of EFV with NPs when using the microfluidic method of production.

Table 4.3 - EDS analysis of PLGA NPs produced by nanoprecipitation using both conventional and microfluidic method. Results are presented as mean ± SD (n = 5).

Element	Associated substance	NPs		Average atomic (%)
		Type	Method of production	
S	DMSO	Empty	Conventional	0.02 ± 0.03
			Microfluidic	1.09 ± 0.10 ***
		EFV-loaded	Conventional	0.04 ± 0.02
			Microfluidic	0.02 ± 0.03
F	EFV	EFV-loaded	Conventional	0.15 ± 0.10
			Microfluidic	0.37 ± 0.07 *

S: sulfur; F: fluorine; DMSO: dimethyl sulfoxide; NP: nanoparticle; EFV: efavirenz.
* $p < 0.05$; *** $p < 0.001$ (comparison done between the same NPs type inside each associated substance group).

At this point of the work, NPs resulting from the nanoprecipitation technique performed by microfluidics using the co-flow geometry demonstrated to have a suitable profile to accomplish the purpose of this work in relation to physico-chemical characteristics. Thus, this formulation was the selected one to proceed with the next experiments.

4.4 Microfluidic method: scaling experiment

The aim of the scaling experiment was to understand the system behavior when the formulation final volume was decreased or increased ten times, and the scaling outcomes on NPs properties, regarding their Z-average, PDI, ζ-potential, AE and DL.

Microfluidic methods are usually designed as systems which are easily adapted to allow different scalings while maintaining the same properties of the final product. On the first hand, scale-down is important to diminish the need for expensive and time consuming large scale studies. One the other hand, scale-up is important to achieve a high throughput of NPs production, and it is the first step into a potential industrial application.

Therefore, the production of EFV-loaded NPs by microfluidics was run until a final volume of formulation of around 2 mL (scale-down) and 200 mL (scale-up). Then, these results were compared with the ones obtained for the 20 mL final volume (standard scale), already presented in the previous section. The results are shown in Table 4.4.

Table 4.4 - EFV-loaded NPs properties corresponding to the scale-down, standard scale, and scale-up. Results are presented as mean ± SD (n = 3).

Method	Z-average (nm)	PDI	ζ-Potential (mV)	AE (%)	DL (%)
Scale-down	75.5 ± 2.2	0.087 ± 0.003	-13.0 ± 1.5	86.2 ± 7.6	11.5 ± 1.0
Standard scale	72.8 ± 4.9	0.086 ± 0.004	-14.1 ± 1.3	80.7 ± 8.3	10.8 ± 1.1
Scale-up	73.2 ± 8.0	0.080 ± 0.004	- 12.8 ± 1.8	87.6 ± 5.7	9.9 ± 0.5

Z-average: average size; PDI: polydispersity index; ζ-Potential: zeta-potential; AE: association efficiency; DL: drug loading.

No significant differences were found between formulations with different final volumes. Thus, the microfluidic system was able to form NPs with a consistent and reproducible structure, independently of the formulation volume. These findings proved the robustness of the microfluidic method, hence demonstrating the feasibility of the microfluidic chip to perform scaling experiments and produce batches of NPs with different volumes. Herein, the versatility of the microfluidic technology was proved.

4.5 *In vitro* release test

Previously to the release profile, the solubility of EFV in 0.2 % of poloxamer in PBS after 15 min and 24 h was determined to assure the presence of sink conditions. The value obtained for the solubility of EFV in this medium was 0.29 and 0.36 mg/mL for 15 min and 24 h, respectively. Herein, the addiction of a surfactant, poloxamer, to the PBS solution aimed to increase the solubility of the drug in the medium and to prevent a possible adsorption of EFV on the container surface [247]. Since EFV is a hydrophobic drug, the low values obtained for its solubility in the aqueous solution were expected [248].

The release profile of EFV from PLGA NPs (Figure 4.9) was characterized by an initial rapid burst effect, with around 30 % of the drug being recovered from the medium in the first 30 min. An additional 20 % of EFV content was relatively slow released up to 9 h, and then the release ceased. This release behavior of drugs from PLGA NPs was frequently reported in the literature [249-252]. The mechanism responsible for the release of EFV from this DDS was a junction of the diffusion of the drug through the PLGA, and also polymer surface or bulk degradation, erosion, and swelling [253]. Moreover, it is known that the initial burst release is an outcome of the amount of drug which is near or attached to particles surface [254]. Oppositely, the amount of drug which is contained within the NPs core is usually released during a more prolonged period of time. The PLGA nanosystems are able to present this sustained release behavior since its internal structure is very well compacted, hence avoiding water penetration from the medium and promoting a relatively low drug diffusion out of NPs [255].

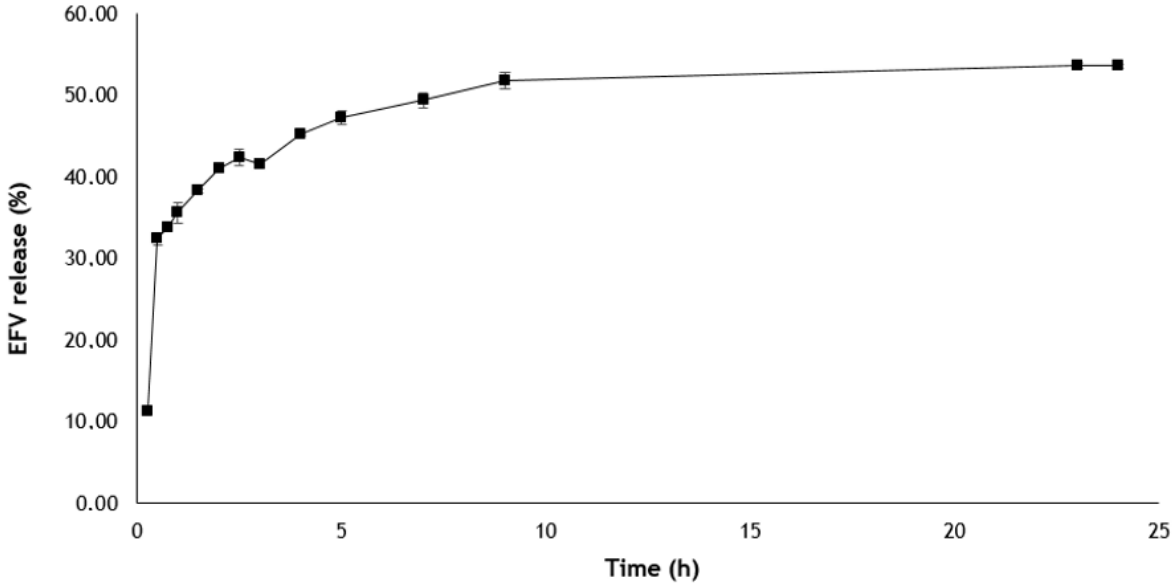

Figure 4.9 – *In vitro* release profile of EFV from microfluidics-produced PLGA NPs.

4.6 Nanoparticles labeling

Nanoparticles were labeled by 6-C encapsulation in order to further detect them during cellular assays. This encapsulation was done by microfluidics, using the model for the co-flow geometry, as described for EFV-loaded NPs.

The 6-C was detected through fluorescence (ex. 460 nm, em. 510 nm). New calibration curves were set in the beginning of every experiment to verify the feasibility of the detection method. Firstly, a stock solution was prepared, containing 153 µg/mL of 6-C in DMSO and 0.1 % of TWEEN®-80 in PBS (pH = 7.4), in a ratio of 1:12. Then, from the stock solution, a solution of 1 µg/mL of 6-C was prepared by dilution in 0.1 % of TWEEN®-80 in PBS (pH = 7.4). The standard solutions were prepared from this last solution by dilutions in the same medium. The calibration curve comprised a range of 6-C concentrations from 0.002 µg/mL to 0.01 µg/mL, at equally spaced intervals. In Figure 4.10 is possible to find a model for this curve. The obtained calibration curves always presented a value of R^2 between 0.990 and 0.999, which demonstrates the feasibility of the methodology [256].

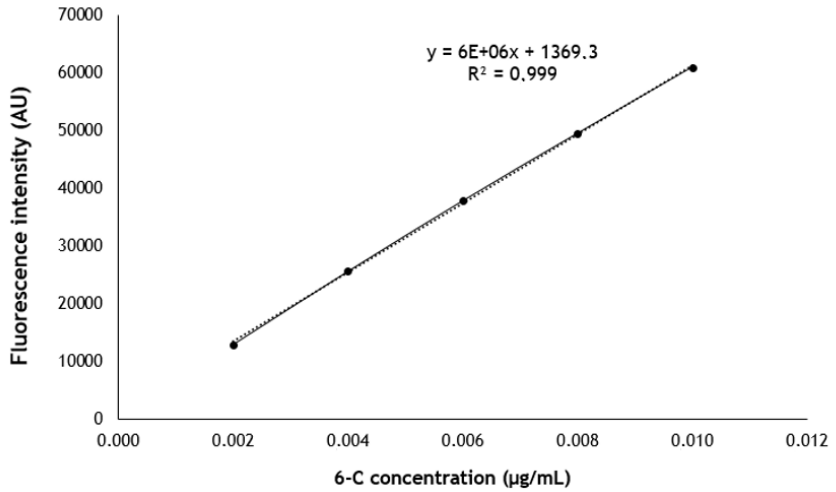

Figure 4.10 – Standard curve calibration for 6-C detection through fluorescence.

The Z-average, PDI, ζ-potential, and AE of 6-C loaded NPs are depicted in Table 4.5. As can be seen, the properties of 6-C loaded NPs were similar to EFV-loaded NPs resulting from the same methodology of production (Table 4.2), and thus fluorescent NPs were appropriate to mimic drug-loaded NPs in cellular assays.

Table 4.5 - 6-C loaded NPs properties. Results are presented as mean ± SD (n = 3).

NPs type	Z-average (nm)	PDI	ζ-Potential (mV)	AE (%)
6-C loaded	89.6 ± 5.5	0.106 ± 0.014	-12.8 ± 0.4	99.9 ± 0.0

Z-average: average size; PDI: polydispersity index; ζ-Potential: zeta-potential; AE: association efficiency; NP: nanoparticle; 6-C: 6-coumarin.

Previously to the release profile, the solubility of 6-C in 0.1 % of TWEEN®-80 in PBS after 24 h was determined to assure the presence of sink conditions. The value obtained for the solubility of 6-C in this medium was 2.88 ng/mL. The results for the *in vitro* release of fluorescent NPs (Figure 4.11) showed that after 24 h, only around 0.2 % of 6-C was released from PLGA NPs, which means that the fluorescence observed on cellular assays where the particles were used potentially corresponded to these nanosystem and not to free fluorescent dye [224]. Therefore, this system was approved to be used in some of the next experiments.

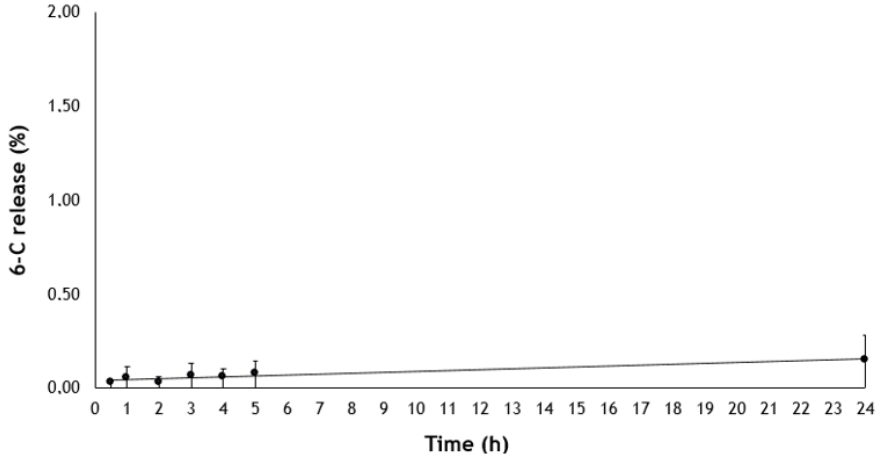

Figure 4.11 – Release profile of 6-C from the nanosystem.

4.7 Nanoparticles functionalization and characterization

Nanoparticles were functionalized with a peptide-binding transferrin receptor in order to target the BBB, avoid drug-related side effects and enhance therapeutic efficacy. The structure of the peptide used in this process is shown in Figure 4.12.

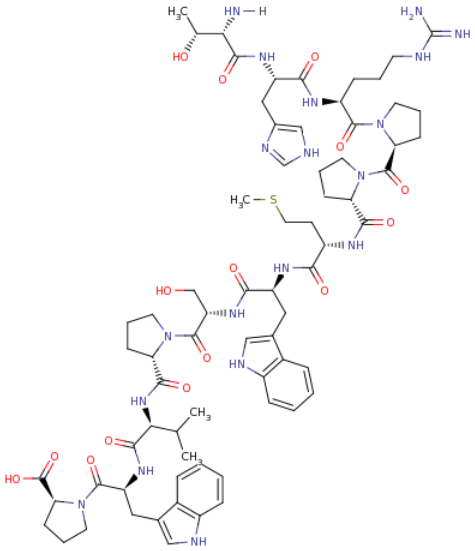

Figure 4.12 – Structure of the 12-amino acids peptide used to functionalized the NPs [257].

The carbodiimide-derived EDC/NHS coupling chemistry was used to attach the peptide to the PLGA of NPs (Figure 4.13). Briefly, EDC reacted with the carboxyl groups (-COOH) of PLGA to form an active O-acylisourea intermediate, which consists on an unstable chemical. When in the presence of the stabilizer NHS, or its water-soluble analog (sulfo-NHS), EDC can couple this organic compound to the carboxyl groups of PLGA, hence establishing an NHS ester that is far more stable than the O-acylisourea intermediate. Thus, the NHS ester was able to react with the amine groups (-NH_2) of the peptide, forming a stable amide linkage between the peptide and PLGA [258].

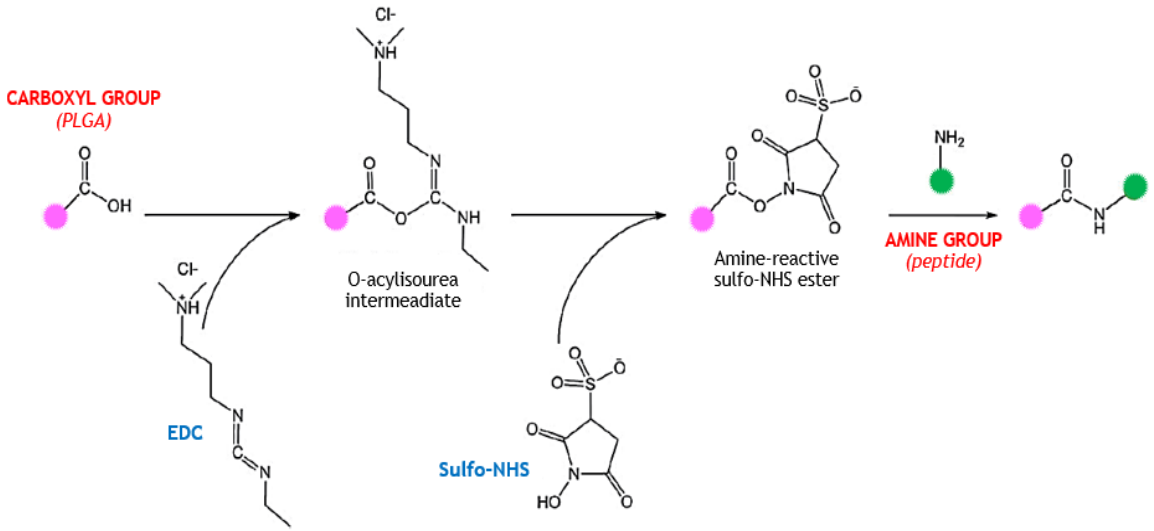

Figure 4.13 - EDC/NHS coupling chemistry. Adapted from [258].

Once the NPs are functionalized, they should be able to reach the brain, in the CNS, mainly by the transferrin receptor-mediated endocytosis pathway (Figure 4.14).

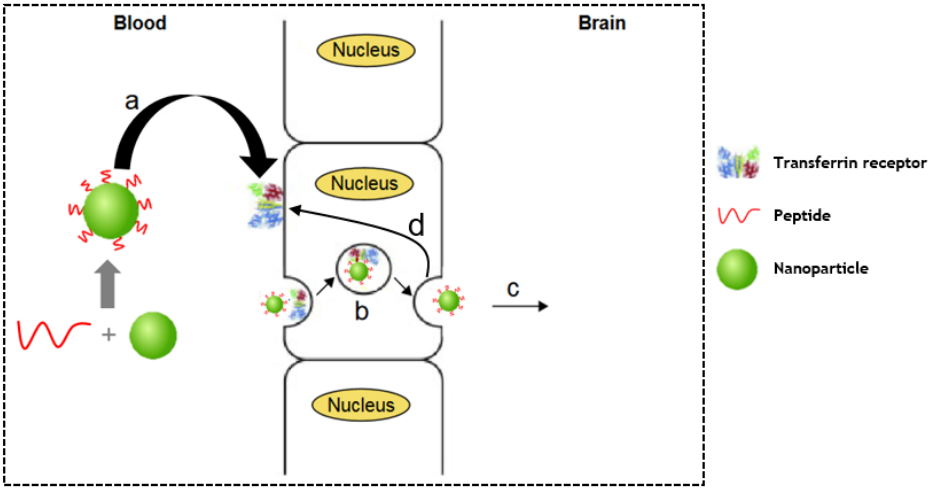

Figure 4.14 – Theoretical mechanism of the passage of functionalized NPs through BBB endothelial cells by the transferrin receptor. a) NPs functionalized with the 12-amino acids peptide should easily recognize the transferrin receptor of the BBB; b) transport of the endocytic vesicle containing NPs through the endothelial cells of the BBB; c) NPs reach the CNS; d) transferrin receptor is recycled back to the cell surface. Adapted from [259].

4.7.1 Average size, polydispersity index and surface charge

After functionalization, NPs were evaluated for Z-average, PDI and ζ-potential. The results are shown in Table 4.6.

Table 4.6 - Functionalized NPs properties. Results are presented as mean ± SD (n = 3).

NPs type	Z-average (nm)	PDI	ζ-Potential (mV)
Functionalized empty	73.4 ± 1.7	0.155 ± 0.018	-15.4 ± 1.6
Functionalized EFV-loaded	73.3 ± 1.7	0.177 ± 0.012	-16.3 ± 1.2
Functionalized 6-C loaded	90.2 ± 2.0	0.186 ± 0.013	-13.0 ± 1.8

Z-average: average size; PDI: polydispersity index; ζ-Potential: zeta-potential; EFV: efavirenz; 6-C: 6-coumarin.

In comparison to the properties of the non-functionalized NPs (represented in Table 4.3 and 4.6 for empty or EFV-loaded and 6-C NPs, respectively), only the PDI demonstrated statistically significant differences. However, previous studies already described the increase in PDI as an effect of the functionalization process [209, 224, 260]. Average size and surface charge did not change significantly.

4.7.2 Bradford assay

Bradford assay was used to indirectly quantify the amount of peptide associated with NPs by measuring the free peptide in the supernatant after each functionalization reaction.

Simultaneously, standards with BSA and 12-amino acids peptide (used to functionalize the NPs) were prepared, and thus two calibration curves were obtained (Figure 4.15). The calculated protein concentration in the supernatants was 0 µg/mL using the data from both calibration curves, and therefore the calculated AE of the peptide to the NPs was 100 %. Still, these results should be carefully interpreted. On the first hand, since the amount of peptide added was very low in comparison to the amount of –COOH activated groups available, this value of AE of the peptide

could be acceptable due to the existence of spatial accessibility to occur the linkage between them. On the other hand, small peptides may present a lack of reactivy in the Bradford assay, and thus this method may not be the most sensitive one to detect them [261].

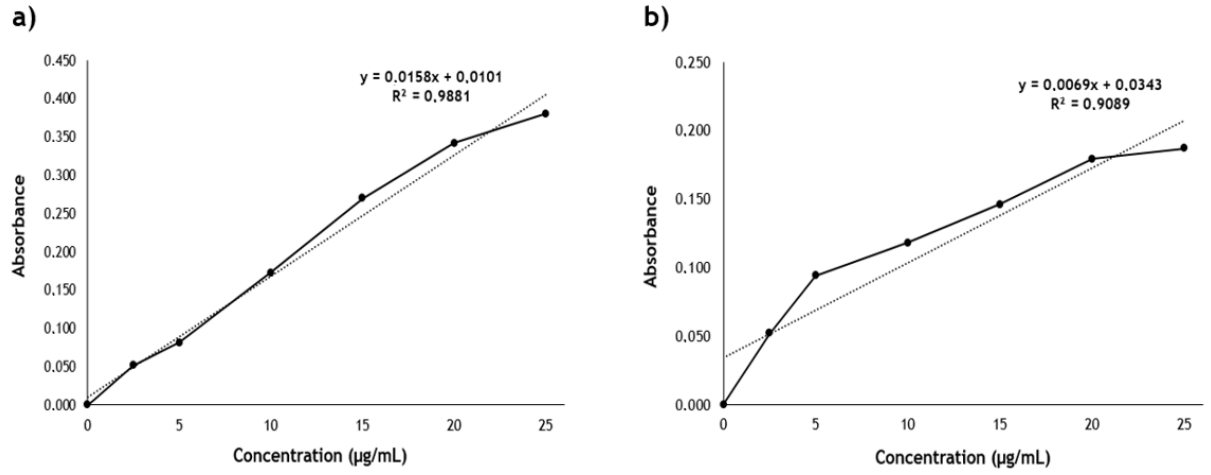

Figure 4.15 – Peptide concentration measurement by Bradford Assay. a) Standard curve of BSA concentration *versus* absorbance at 595 nm; b) standard curve of 12-amino acids peptide concentration *versus* absorbance at 595 nm.

4.7.3 Nuclear magnetic resonance analysis

Samples of commercial PLGA (used in the production process of NPs), functionalized and non-functionalized empty PLGA NPs were dissolved in DMSO in order to verify the presence of their structural components by ^{1}H NMR.

The functionalized and non-functionalized PLGA NPs ^{1}H-NMR spectra were compared with the spectra obtained from the commercial PLGA (Figure 4.16a). It was possible to observe that both nanoformulations presented characteristics peaks at 1.4 (3H), 4.8 (2H) and 5.2 (1H) ppm related to the -CH_3, -CH_2, and -CH protons of PLGA, respectively [262]. In addition, an intense peak related with TWEEN®-80 used in NPs preparation appeared at 3.6 ppm [263]. Since the amount of peptide used on functionalized samples was very small compared to the polymer, it was hard to obtain spectra with enough sensitivity to significantly detect peptide peaks on the samples functionalized – reason why detected differences were all small peaks. Besides that, a close observation of the functionalized PLGA NPs spectra (Figure 4.16b and 4.16c) allowed the confirmation of the presence of small peaks at -0.008 and -0.017 ppm which are described in the literature as traces of the presence of the peptide [224].

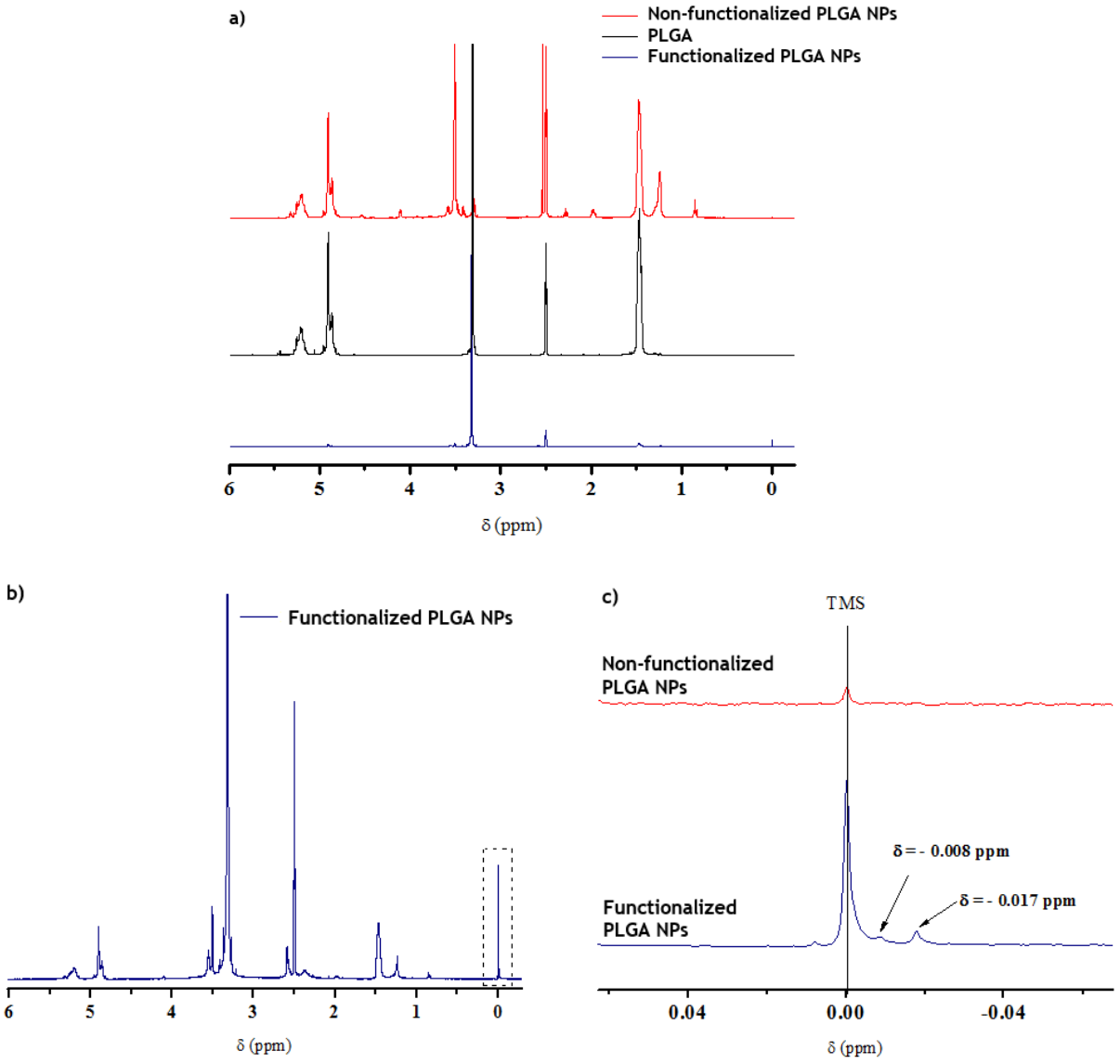

Figure 4.16 - ^{1}H NMR analysis of samples. a) ^{1}H NMR spectra (DMSO-d_6) of commercial PLGA, functionalized and non-functionalized PLGA NPs at 400 MHz; b) spectra with magnification of functionalized PLGA NPs structural data; c) both nanoparticulate systems near to 0.00 ppm. Peak at 3.3 ppm is related with water presence in samples.

Both Bradford and ^{1}H NMR analysis resulted in outcomes which proved the presence of the 12-amino acids peptide in functionalized PLGA NPs samples and the potential bioconjugation of this peptide to the nanosystem.

4.8 Nanoparticles-associated metabolic viability assay

In vitro cell viability determination after contact with NPs resulting from nanoprecipitation technique performed by microfluidics was assessed through a MTT assay in the hCMEC/D3 and ND7/23 cell lines (Figure 4.18a and 4.18b, respectively). The hCMEC/D3 cell line was chosen since brain endothelial cells represent the major cellular component of the BBB and the ND7/23 cells were used as a model of a sensorial neuron cell line of brain parenchyma.

4.8.1 ND7/23 cell line: assessment of the optimal cellular density

In order to evaluate the best cellular density of the ND7/23 cell line for the MTT test, cells were seeded in concentrations of 0.001, 0.005, 0.010, 0.015, 0.020, 0.040, 0.060, 0.080, and 0.100 × 10^6 cells/mL. Then, cells were incubated with supplemented DMEM during 24 h.

After incubation with medium, the concentrations ranging from 0.040 to 0.100 × 10^6 cells/mL were immediately excluded, since they originated an excessive production of formazan crystals. The other concentrations were plotted in function of the average absorbance (Figure 4.17).

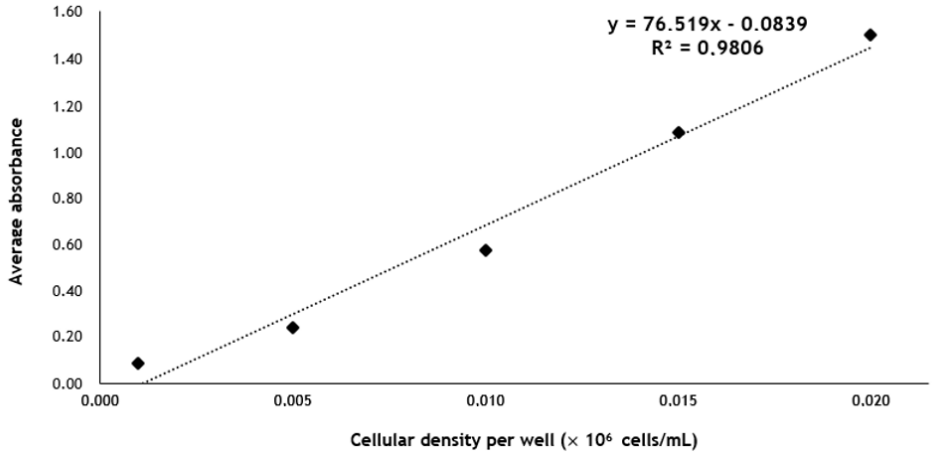

Figure 4.17 – Plotting of cellular density per well *versus* average absorbance for the ND7/23 cell line.

The best cell number for an MTT test should be the one which yields an average absorbance of the sample that mimics the PC between 0.75 and 1.25. Moreover and ideally, this number of cells should fall within the linear portion of the standard curve [264]. Therefore, the cellular density which fulfilled the requirements was 0.015 × 10^6 cells/mL.

4.8.2 Nanoparticles safety evaluation

A range of concentrations from 0.01 μM to 100 μM of free EFV, empty NPs, functionalized empty NPs, EFV-loaded NPs, and functionalized EFV-loaded NPs were tested on the hCMEC/D3 and ND7/23 cell lines and then the metabolic activity was determined. As can be seen in Equation 3.4, the metabolic activity was estimated in comparison to the PC and NC for each group.

In the context of the pre-clinical testing evaluation of the cytotoxicity of a medical device by *in vitro* techniques, the International Organization for Standardization (ISO) defined in the 10993-5 norm that a material associated with a cell viability, directly correlated with cellular metabolic activity, equal or above 70 % is considered non-toxic [265]. In this work, metabolic activity of brain endothelial cells and neuron cells was found to be always above 90 % and 70 %, respectively, when in contact with all NPs at all evaluated concentrations. Therefore, NPs formulations should be considered non-toxic, and potentially safe. As expected, PC and NC for each group assumed metabolic activities of 100 and 0 %, respectively.

For both cell lines, the cellular metabolic activity in the presence of free EFV concentrations of 0.01 μM, 0.1 μM, 1 μM, and 10 μM did not present significant differences between them. For the hCMEC/D3 cell line, the highest concentration of free EFV (100 μM) was significantly different than the others ($^{***}p < 0.001$ for 0.01 μM; $^{**}p < 0.01$ for 0.1 μM; $^{*}p < 0.05$ for 1 and 10 μM). In the case of the ND7/23 cell line, the free EFV concentration of 100 μM was also significantly different than the ones corresponding to 0.1 μM ($^{**}p < 0.01$) and 0.01 μM ($^{*}p < 0.05$). The concentration of 100 μM

demonstrated to cause severe damages to both cell types, resulting in the total absence of metabolic activity. According to the obtained results, the maximum concentration limit for the safe use of the free drug form in the hCMEC/D3 and ND7/23 cell line is probably defined between 10 μM - 100 μM, and 1 μM – 0.1 μM, respectively.

Empty NPs concentrations did not present significant differences between them. The considerable cellular metabolic activity associated with this NPs group (> 90 %) for both cell types, which is similar to the PC, reinforces the apparent low contribution of NPs matrix to the emergence of loaded NPs cellular cytotoxicity phenomena.

Functionalized empty NPs and functionalized EFV-loaded NPs demonstrated to have cytotoxic profiles similar to empty NPs and EFV-loaded NPs, respectively, indicating that the functionalization process with a peptide did not influence the safety of the nanosystems.

Considering EFV-loaded NPs concentrations, no relevant differences were observed between 0.01 and 100 μM in terms of cellular metabolic activity. However, a significant metabolic activity difference can be observed when comparing equal concentrations between this group and the free EFV one, except for the smaller and the two smaller concentrations for endothelial and neuron cells, respectively, as can be seen in Figure 4.18; this difference is particularly accentuated for the concentration of 100 μM (*** $p < 0.001$). The EFV-loaded NPs provided a higher cellular metabolic activity than the free drug, and, therefore, it is possible to state that the cellular cytotoxicity associated with free EFV can be diminished by encapsulating the drug in NPs, demonstrating that these nanocarriers have a protective role for EFV administration in the selected hCMEC/D3 and ND7/23 cell lines. Regarding the targeting ability of the nanosystems, to reach the same biological effect, it would be possible to use a lower therapeutic concentration of EFV in NPs compared to the free drug, and this can reduce EFV-associated side effects and unexpected adverse reactions; still, more detailed release kinetics studies are needed to corroborate this conclusion.

In general, it was possible to denote that the neuron cell line was prone to present smaller values of cellular metabolic activity in comparison to the endothelial cell line. This may be mainly due to one of the principal EFV metabolites, namely, 8-hydroxy-efavirenz, which was already associated with cytotoxicity to neuron cultures [266]. Some mechanisms pointed out as capable of cause this neurotoxicity are modifications in the calcium homeostasis and cannabinoid system, stimulation of the release of brain pro-inflammatory cytokines, and mitochondrial damages. However, once again, this reduction in the cellular metabolic activity was attenuated by the encapsulation of EFV in NPs, which potentially minimized the toxic effect of the drug in the neuron cell line.

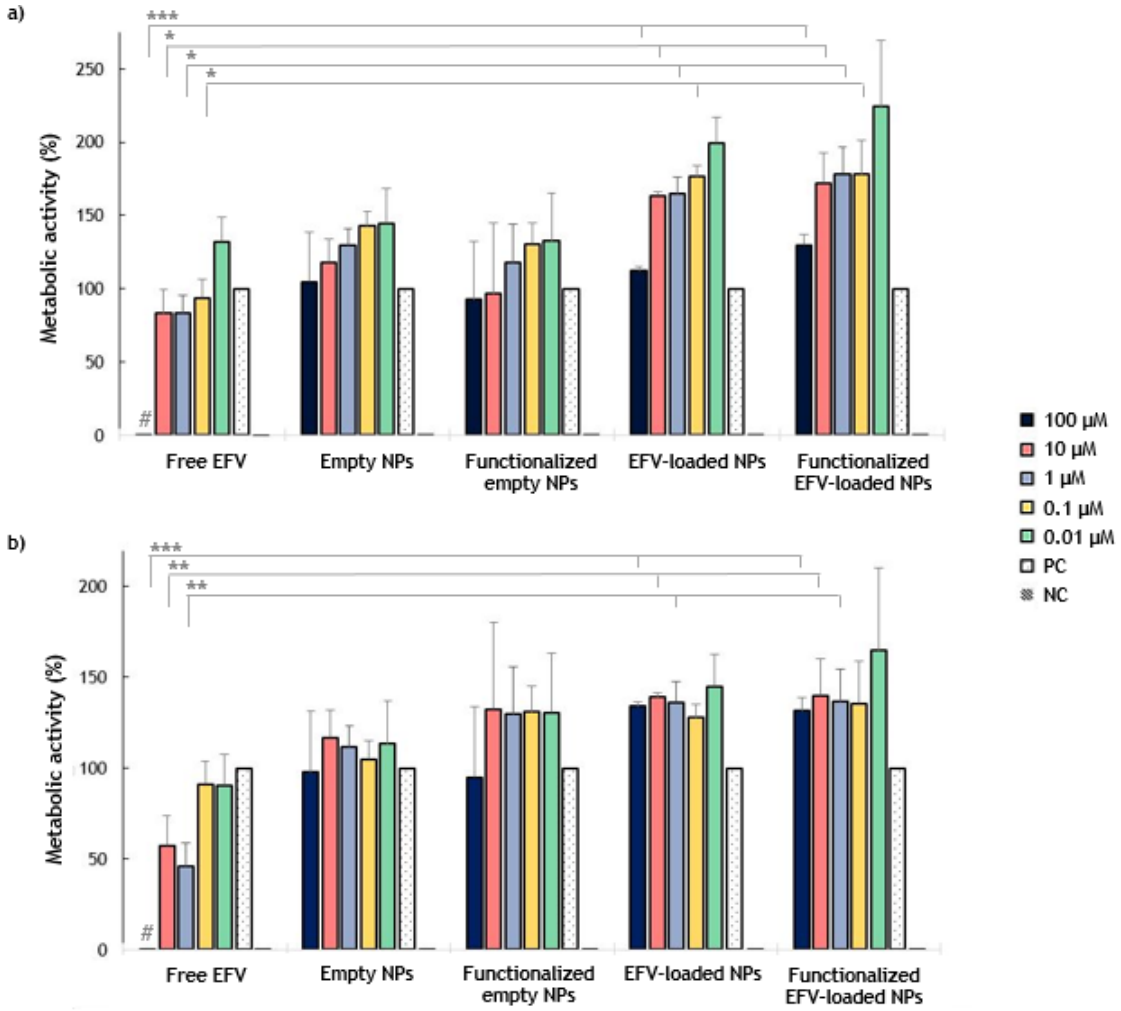

Figure 4.18 – Metabolic activity of hCMEC/D3 (a) and ND7/23 (b) cells when incubated with different concentrations of free EFV, empty NPs, functionalized empty NPs, EFV-loaded NPs, and functionalized EFV-loaded NPs, during 24 h. ($^{\#}$) denotes a significant difference between free EFV 100 µM and the other concentrations in the same group, as described above. (*,**,***) denotes a significant difference *(* $p < 0.05$, ** $p < 0.01$, and *** $p < 0.001$*, respectively) when comparing equal concentrations between free EFV and EFV-loaded or functionalized EFV-loaded NPs group.

4.9 Nanoparticles hemocompatibility assay

The hemolysis test is useful to investigate the safety of parenteral-administered formulations, providing an estimation of the blood compatibility of materials. Erythrocytes are the most abundant cells in the bloodstream, and they may experience deformation or membrane damages derived from intravenous-administered pharmaceutical formulations [226]. Herein, the aim was to target NPs to the BBB after intravenous administration, in order to deliver EFV to the brain, in CNS. Thus, it is of extreme importance to test whether the NPs demonstrate hemolytic effect, and their behavior compared to the free drug, as well.

Hemolysis is defined as the disruption or destruction of red blood cells, promoting the release of the iron-containing protein hemoglobin into the surrounding fluid. These cells may directly interact with biomaterials, or indirectly interact with their extracts [267]. *In vivo*, hemolysis is associated with pain during the release of hemoglobin, and pathological situations as anemia, vascular irritation, acute renal failure, or even death [268].

In this work, the free drug and all types of NPs formulations (empty, functionalized empty, EFV-loaded, and functionalized EFV loaded) were directly incubated with erythrocytes in PBS in concentrations ranging from 0.005 μM to 50 μM. The results for hemolysis are shown in Figure 4.19. Besides the incubation with the free drug and NPs samples, the cells were also incubated with only PBS (NC) and 1 % of Triton X-100 in PBS (PC).

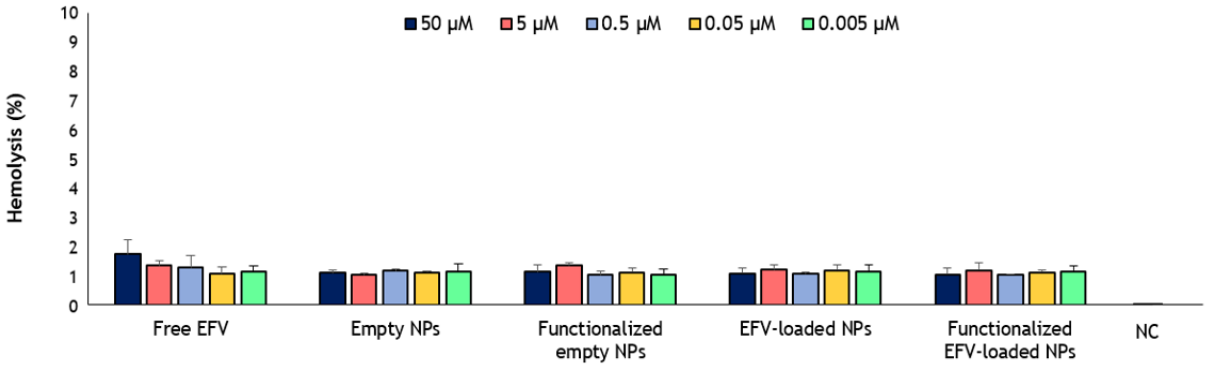

Figure 4.19 – Percentage of hemolysis associated with the free drug, empty NPs, functionalized empty NPs, drug-loaded NPs, and functionalized drug-loaded NPs.

As expected, the percentage of hemolysis calculated for the NC and PC was 0 % and 100 %, respectively. These percentages are correlated with samples hemoglobin concentration of 0.1 mg/dL for the NC, and 209.5 mg/dL for the PC. The percentage of hemolysis for all samples at all analyzed concentrations was always below 2 % (hemoglobin concentrations between 2.1 and 3.7 mg/dL) and no significant differences were found between the different groups. This means that neither the free drug, nor empty NPs, nor drug-loaded NPs can be considered dangerous for red blood cells. Herein, functionalized NPs demonstrated to have a hemolytic profile similar to the non-functionalized NPs, and thus the functionalization process did not affect the hemocompatibility of the nanoformulations. The same was observed for the loaded NPs.

The osmolarity of these formulations was also measured (considering that PBS and blood hold similar osmolarities), in order to understand the relation between their osmotic concentration and the osmotic concentration of blood. All formulations presented osmolarity values within the range for blood osmolarity, which is 285-300 mOsm/L [269], and thus osmolarity-related hemolysis was not expected to occur.

In accordance to a guidance for *in vitro* hemolysis described by representatives of the Johnson & Johnson and Novartis Pharmaceuticals Corporation [268], hemolysis percentages below 10 % are related with nonhemolytic formulations, while hemolysis percentages above 25 % are related with hemolytic formulations. Thus, the nanosystems were considered nonhemolytic.

Besides the quantitative test, the morphology of erythrocytes after interaction with NPs was also evaluated by SEM imaging (Figure 4.20). Since the quantitative test was not enough to conclude about the hemocompatibility of the formulations [226], this qualitative test worked as a proof of concept. Herein, only the maximum concentration of empty NPs and EFV-loaded NPs, 50 μM, was tested. The NPs demonstrated to have an impact on red blood cells similar to the NC and between them. So, no considerable morphological changes in the cells were observed.

All these findings supported the theory that the NPs formulations are hemocompatible, and therefore could be safe for intravenous administration.

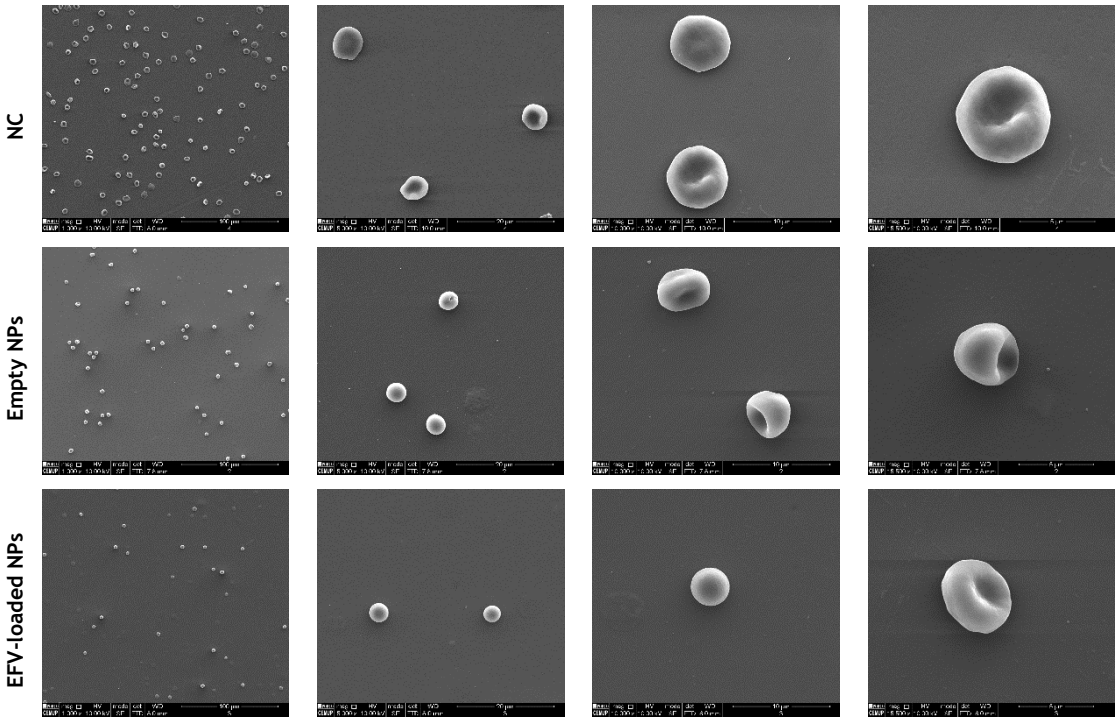

Figure 4.20 - SEM images of red blood cells morphology after interaction with PBS (NC), and 50 μM of empty NPs and EFV-loaded NPs in PBS, during 3 h. From left to right, each column of images corresponds to a different magnification, namely, 1000, 5000, 10000, and 15500 times. No relevant morphological differences were found between the three groups.

4.10 Evaluation of cell-nanoparticle interaction

The interaction between non-functionalized and functionalized NPs with human BBB endothelial cells was quantitatively studied over time through flow cytometry.

Figure 4.21 demonstrates the gating strategy adopted to perform the analysis. On the left panel is possible to observe the viable cell population on a forward scatter area (FSC-A) vs. sideward scatter area (SSC-A) dot plot. On the right panel doublets and aggregates were identified, and excluded, and is possible to observe the gated cells on a FSC-A vs. forward scatter height (FSC-H) dot plot.

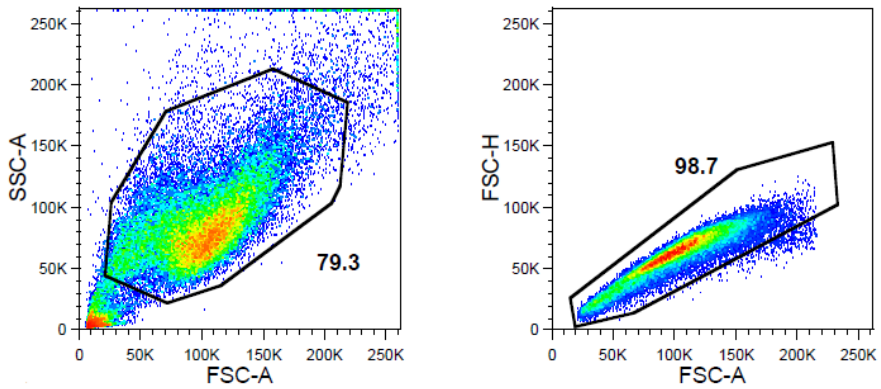

Figure 4.21 - Gating strategy applied in FACS analysis.

The results for the mean fluorescence intensity (MFI) for both groups and time points (Figure 4.22) demonstrated the absence of significant differences between non-functionalized and functionalized NPs in respect to their interaction with BBB endothelial cells. However, it was possible to notice a trend in the MFI evolution, with higher values attributed to the functionalized NPs. This data suggested that the functionalization process applied was not sufficiently effective. Besides the presence of the peptide associated with the NPs, as proved by the previously mentioned Bradford test and ^{1}H NMR spectroscopic analysis, this type of functionalization was not site-oriented. Thus, there were different possibilities for the linkage due to the existence of several carboxyl and amine groups at the PLGA and peptide, respectively [224]. This may affect the structural and spatial availability of the peptide for the binding process to the transferrin receptor, hence avoiding the increase in cells-NPs interaction. Moreover, since the 12-amino acids peptide presented positive charge at the pH in which the functionalization process was carried out (isoelectric point of the peptide around 10.5; functionalization process occurred at pH = 5.5) and the surface charge of NPs was negative (ζ-potential around -14 mV), the peptide may not be covalently linked to NPs, but only adsorbed to the surface based on electrostatic interactions. This justifies the results obtained for Bradford test and ^{1}H NMR spectroscopic analysis, which confirmed the presence of the peptide.

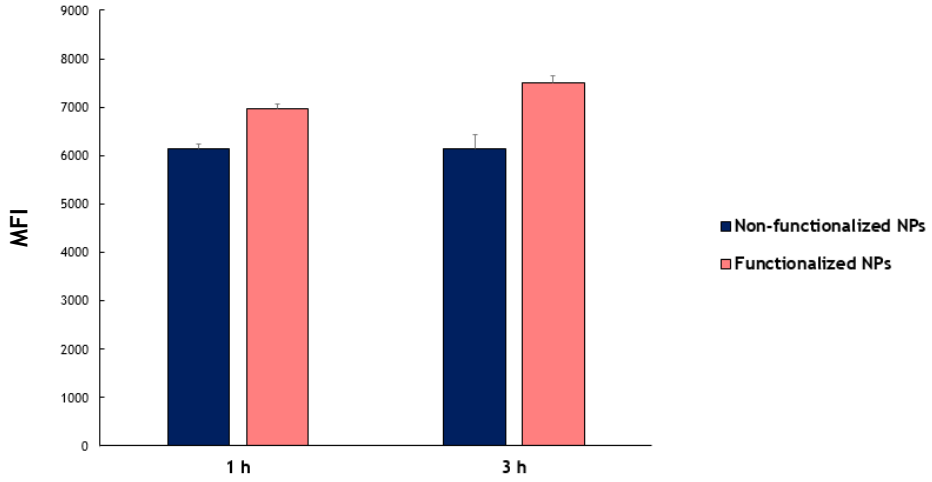

Figure 4.22 - MFI results for non-functionalized and functionalized NPs after 1 h and 3 h of incubation with human BBB endothelial cells.

Still, an attempt based on a site-specific immobilization of the peptide on NPs surface could be introduced in the methodology to improve the efficacy of the functionalization process. Herein, it would be reasonable to use a peptide with only one amino group available to bind the PLGA of the NPs. Thus, the remaining amino groups of the peptide would be available to bind the transferrin receptor.

4.11 Permeability study

Simultaneously to the evaluation of cell-nanoparticle interaction, a permeability assay was conducted through a cell-based BBB *in vitro* model based on a monolayer of hCMEC/D3 cells previously developed [227, 228]. This model demonstrated to be suitable to predict drug passage across the BBB. The monolayer grew in a Transwell® system using cell culture inserts, containing a permeable membrane on the bottom. The test samples were added to the apical compartment, and

the amount of drug that was able to permeate through the insert membrane was detected on the medium of the basolateral compartment. The scheme of this setup is demonstrated in Figure 4.23.

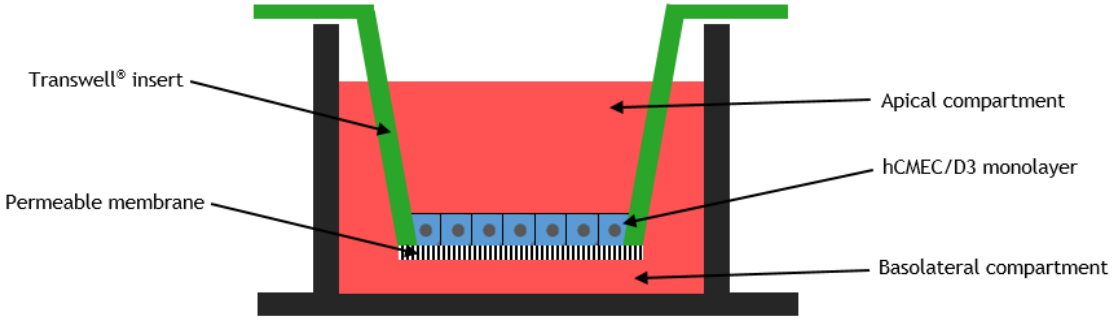

Figure 4.23 - Scheme of the cell-based BBB *in vitro* model used to perform the permeability study.

The TEER is often used as a measure of the tightness and integrity of cell monolayers. It is considered the measurement of the resistance of the monolayer in relation to the flow of charged ions through it. The increase in TEER values is associated with more energy spent to move an ion across the cell layer, and is accepted as an indication of the closing of the tight junctions located between cells [270-272]. During the 8 days needed to develop the BBB *in vitro* model, TEER was monitored. As expected, and due to cells replication, a gradual increase in TEER values was observed (Figure 4.24). In the end, TEER value was within the range 40-70 $\Omega.cm^2$, which is acceptable for this type of BBB *in vitro* models consisting on a hCMEC/D3 cell monolayer [273, 274].

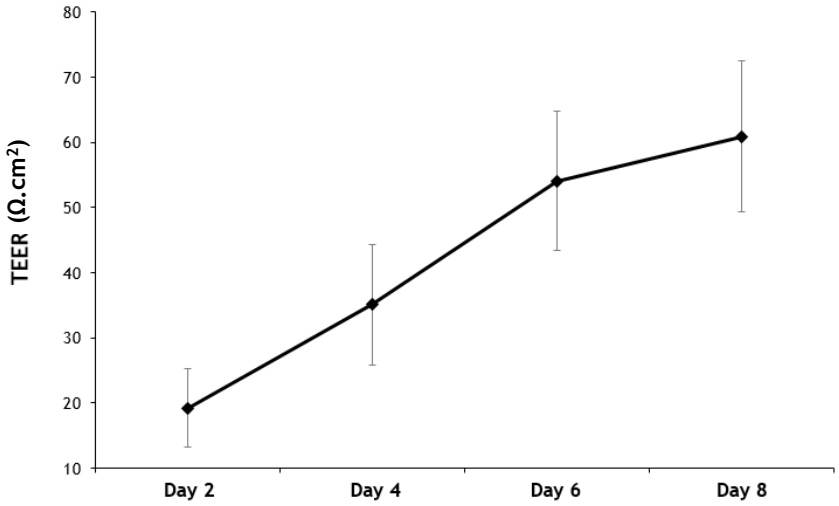

Figure 4.24 - Evolution of TEER during the 8 days necessary to develop the BBB in vitro model.

Confocal microscopy was used to evaluate the morphological characteristics of BBB endothelial cells of the monolayer at the day 8 of the *in vitro* model. Moreover, microscopy data was useful to understand whether the model was indeed constituted by a cellular monolayer, or a superposition of layers. Images are represented in Figure 4.25.

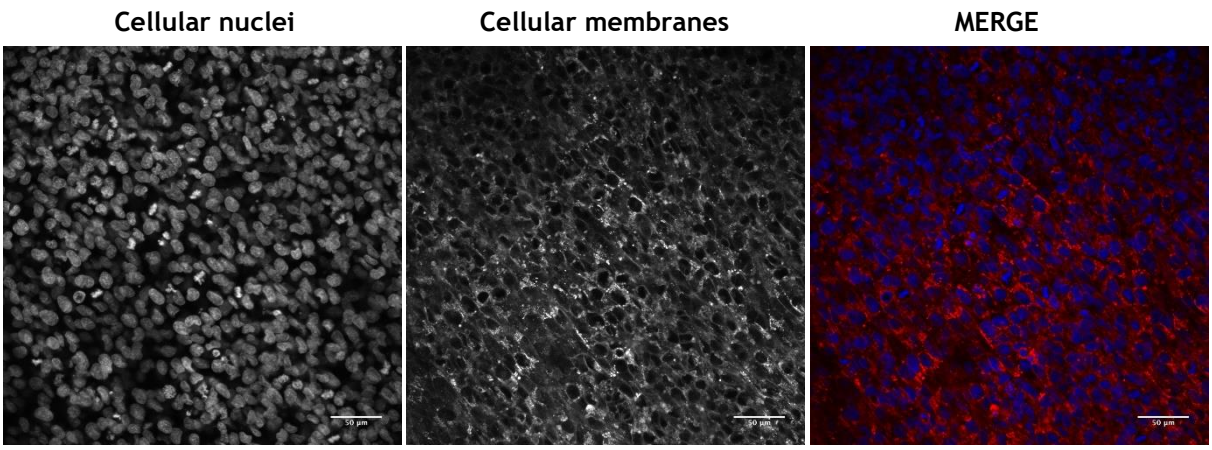

Figure 4.25 - Evaluation of the BBB *in vitro* model integrity by confocal microscopy. DAPI and Alexa Fluor® 594 WGA were used to stain cellular nuclei in blue (left panel) and membranes in red (middle panel), respectively. Then, the images were superposed (right panel). Scale bars of 50 μm were represented.

It was concluded that, in fact, the BBB *in vitro* model consisted on a monolayer of hCMEC/D3 cells. It was possible to observe cells with a prolonged morphology and growing in a parallel direction, resulting in a confluent membrane.

When the BBB was established (8th day), EFV permeability was determined either as a free drug or loaded in both non-functionalized and functionalized NPs, in order to understand to what extent these nanosystems could enhance the bioavailability of EFV across this biological barrier. Moreover, it is important to mention that this assay was conducted simultaneously to the evaluation of cell-nanoparticle interaction, and thus the outcomes of that experiment were not known before start this permeability study. The results were expressed in percentage of permeability (Figure 4.26) and Papp (Figure 4.27). The TEER values monitored during the permeability assay (Figure 4.26), showed no significant deviations from the range 40-70 Ω.cm^2, which proved the membrane integrity and the reliability of the model to proceed with this experiment. In relation to the results, no significant differences were observed for percentage of permeability and Papp of free EFV, non-functionalized EFV-loaded NPs, and functionalized EFV-loaded NPs. The amount of drug detected in the apical compartment and cell lysates after the assay were very similar for all samples, as well. This was in accordance with the outcomes of the evaluation of cell-nanoparticle interaction, whose data suggested that the functionalization process applied to EFV-loaded NPs was not sufficiently effective. However, once again, it was possible to notice a general trend in the permeability across the BBB model consisting on functionalized EFV NPs > non-functionalized EFV NPS > free EFV.

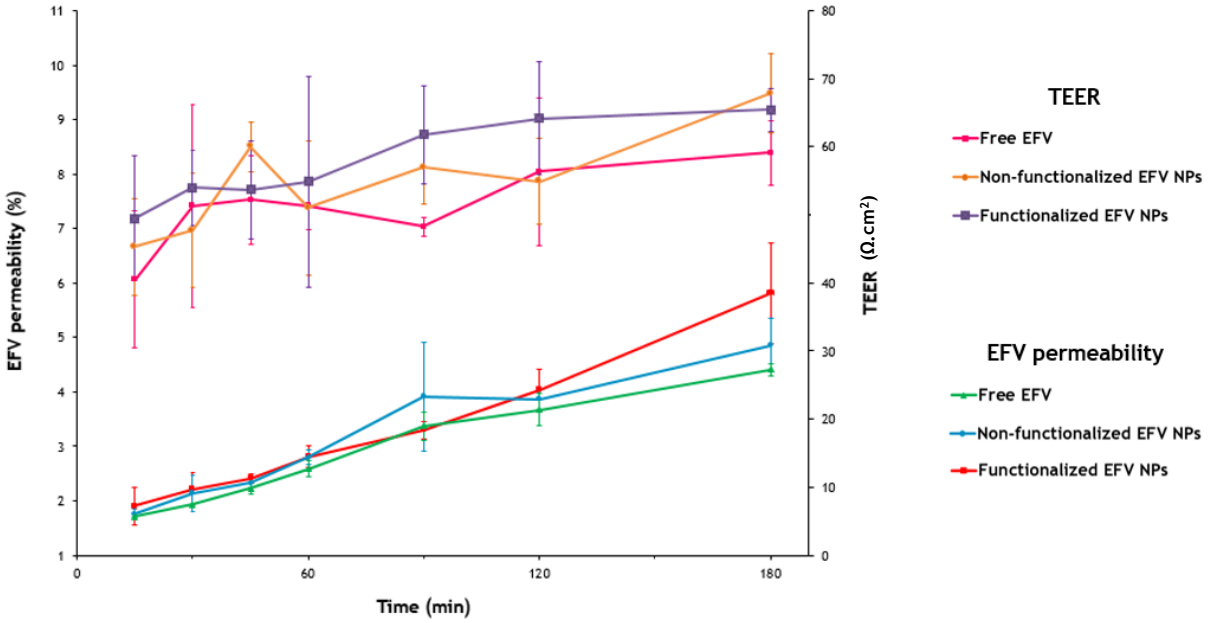

Figure 4.26 - TEER and percentage of EFV permeability evolution during the permeability study.

As mentioned in the previous section, a possible solution to increase the permeability of EFV NPs would involve a site-oriented functionalization of the nanoparticulate systems with a transferrin receptor-binding peptide. When an effective functionalization is achieved, an improved interaction between NPs and BBB endothelial cells is expected, as well as an increase in NPs permeability across endothelial cells monolayer [224, 228].

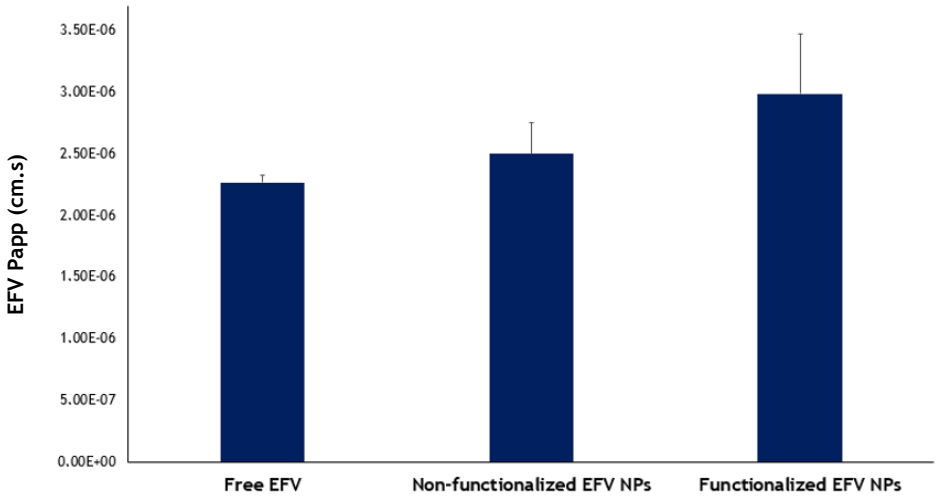

Figure 4.27 - Papp results for the EFV permeability study.

Finally, it is important to mention that, although the results for the functionalized NPs interaction and permeability across BBB endothelial cells were less positive and even unexpected, these two studies were crucial to understand in which aspects is necessary to improve the nanosystem. Only in this way it is possible to reach a final formulation with suitable properties to move forward to a potential commercial application.

Chapter 5

Conclusion

5.1 Work conclusions

In the present work, EFV-loaded PLGA NPs were developed using the nanoprecipitation technique. This technique was performed by the conventional methodology, including the regular procedure and a modified version, and microfluidics, using the co-flow and flow-focusing geometries. A dispersed phase, containing PLGA and EFV dissolved in DMSO, and a continuous phase, containing a solution of TWEEN®-80, were used. Additionally, an optimization of the flow rates of the two phases inside the microfluidic chip was conducted, in order to find the best arrangement in terms of NPs final properties.

The physico-chemical properties of NPs obtained for the microfluidic method were compared with the ones obtained for the conventional process. According to the obtained results, performing the nanoprecipitation technique by microfluidics using the co-flow geometry was indeed advantageous. The obtained particles presented a smaller size compared to the ones formed by the conventional method (around 70 nm), comparable features to the conventional procedure regarding PDI (around 0.1), and less negative surface charge (around -14 mV). Furthermore, EFV-loaded NPs resulting from microfluidics-assisted nanoprecipitation technique demonstrated a remarkable increase in AE (around 80 %) and DL (around 10 %) compared to the conventionally-performed method, which are key aspects to achieve the desired drug delivery nanosystem therapeutic effect. Morphological analysis proved the round-shaped profile of the NPs, and chemical screening reinforced the increase in the amount of EFV associated to the NPs when they are produced by microfluidics, as well as the residual quantity of DMSO presented in the nanoformulation. Moreover, the *in vitro* release assay demonstrated that these PLGA NPs produced through microfluidics were able to exhibit a sustained release of EFV over time from their matrix.

By performing a scaling experiment of ten times regarding the final volume of NPs batch, the robustness of the microfluidic method was successfully demonstrated. It was possible to decrease and increase ten times the final volume of NPs batch without observing changes in the final properties of particles. This was a great achievement, especially for the scale-up assay, since it symbolized a preliminary step towards the application of the microfluidic technology to produce drug-loaded NPs in industrial dimensions. Besides the formulation parameters, it is important to

state the inherent advantages of microfluidics in comparison to the conventional methodology. The microfluidic method is far more fast, user-friendly and easy to handle.

The nanosystem resulting from the nanoprecipitation technique executed by microfluidics using the co-flow geometry was tested in *in vitro* cellular assays. The NPs proved to be safe to be used with brain endothelial cells (hCMEC/D3 cell line), the major BBB cellular component, and neuron cells (ND7/23 cell line), a cellular population representative of the brain parenchyma environment. Herein, the effectiveness of the nanoparticulate system to avoid cytotoxicity in relation to the free drug was proved. Moreover, NPs proved to be nonhemolytic, demonstrating an associated percentage of hemolysis of only around 1-2 % and absence of changes in the normal morphology of red blood cells. This was important to support the intravenous administration of the nanosystem.

Then, NPs were functionalized with a transferrin receptor-binding peptide using the carbodiimide coupling chemistry. Since this receptor is overexpressed at the BBB, the functionalization strategy was expected to be associated with an increase in the interaction of NPs with BBB endothelial cells (hCMEC/D3 cell line), and a consequent increase in the permeability of the nanosystem through this biological barrier. For the permeability study, the integrity and presence of a monolayer in the BBB *in vitro* model used, was confirmed. For both cells-NPs and permeability studies, no significant differences were observed between non-functionalized and functionalized NPs. However, it was possible to observe a trend, since higher values of interaction and permeability through hCMEC/D3 cells were attributed to the functionalized NPs. This demonstrated that, besides the proved bioconjugation of the peptide to the NPs, the non-oriented functionalization was not a good strategy to be adopted, since it may affect the spatial bioavailability of the peptide to bind to the transferrin receptor.

In conclusion, and attending the results obtained so far, the work inherent to this dissertation allowed the successful microfluidics-based development of a PLGA nanosystem with suitable properties to encapsulate EFV and to be possibly administered by the intravenous route, in order to target the BBB. This technology proved to bring advantages in the loading of this ARV drug in NPs with tunable and favorable biological properties.

5.2 Future work

Besides all the work performed in the scope of this dissertation, there is always room for improvement and different attempts could be introduced to improve the nanosystem under development.

First and foremost, the issue related to the functionalization process of NPs and, consequently, its permeability trough the BBB *in vitro* model, is prone to be improved. Herein, a site-oriented functionalization would be a priority. It could be possible to use a peptide with the above mentioned structure but adding an extra cysteine on the carboxyl termination, whose sulfhydryl group would be the only connection point with the carboxyl groups of the PLGA, by using a specific linker. In this way, the remaining amino acids of the peptide would be available to bind the transferrin receptor. Another alternative would be to use the initial peptide but somehow blocked in order to have only one amine group available to react with the PLGA.

The nanoparticulate system developed by microfluidics could also be evaluated for its antiviral activity, comparing the efficiency of the EFV-loaded NPs and the free EFV in the interference with HIV replication in the viral reservoir in study, the brain.

Another alternative would be to study the versatility and scaling opportunity of the microfluidic method, by encapsulating other ARV model drugs. Besides this, the microfluidic method could be

used to produce nanosystems encapsulating drugs used in the therapy of other pathologies, such as anticancer drugs. Moreover, it would be important to test the behavior of the system during the production of nanosystems with different polymeric matrices, as well as the final properties of the obtained NPs. The production of NPs with a skeleton based on a diblock copolymer of PLGA and polyethylene glycol would be a good attempt, emphasizing the benefits of polyethylene glycol in a possible intravenous administration. In relation to this, besides the evaluation of NPs hemocompatibility, it would be important to perform other safety studies. Herein, it would be pertinent to accomplish protein adsorption, coagulation, and activation of the complement system studies.

Regarding the microfluidic chip, the production of NPs using a different platform, or even a microfluidizer, could be tried. Moreover, the manufacturing of PLGA NPs to encapsulate EFV using droplet microfluidics, based on emulsion techniques, could be explored.

Finally, the *in vivo* study for the assessment of biodistribution, safety and therapeutic efficiency of the nanosystem developed by the microfluidic tool would be essential to prosecute for a clinical application of the product.

References

[1] N. J. Abbott, L. Ronnback, and E. Hansson, "Astrocyte-endothelial interactions at the blood-brain barrier," *Nature Reviews Neuroscience,* vol. 7, pp. 41-53, 2006.

[2] S. A. Pathan, Z. Iqbal, S. M. Zaidi, S. Talegaonkar, D. Vohra, G. K. Jain, *et al.*, "CNS drug delivery systems: novel approaches," *Recent Patents on Drug Delivery & Formulation,* vol. 3, pp. 71-89, 2009.

[3] J. M. Koziara, P. R. Lockman, D. D. Allen, and R. J. Mumper, "In situ blood–brain barrier transport of nanoparticles," *Pharmaceutical Research,* vol. 20, pp. 1772-1778, 2003.

[4] E. M. Maiese, P. T. Johnson, T. Bancroft, A. Goolsby Hunter, and A. W. Wu, "Quality of life of HIV-infected patients who switch antiretroviral medication due to side effects or other reasons," *Current Medical Research and Opinion,* vol. 32, pp. 2039-2046, 2016.

[5] V. Valcour, P. Sithinamsuwan, S. Letendre, and B. Ances, "Pathogenesis of HIV in the central nervous system," *Current HIV/AIDS Reports,* vol. 8, pp. 54-61, 2011.

[6] E. Vazquez, "Sustiva (efavirenz) is approved," *Positively Aware,* vol. 9, p. 17, Nov-Dec 1998.

[7] S. Sierra, B. Kupfer, and R. Kaiser, "Basics of the virology of HIV-1 and its replication," *Journal of Clinical Virology,* vol. 34, pp. 233-244, 2005.

[8] S. G. Sarafianos, B. Marchand, K. Das, D. M. Himmel, M. A. Parniak, S. H. Hughes, *et al.*, "Structure and function of HIV-1 reverse transcriptase: molecular mechanisms of polymerization and inhibition," *Journal of Molecular Biology,* vol. 385, pp. 693-713, 2009.

[9] D. D. Richman, "HIV chemotherapy," *Nature,* vol. 410, pp. 995-1001, 2001.

[10] S. Desgouilles, C. Vauthier, D. Bazile, J. Vacus, J.-L. Grossiord, M. Veillard, *et al.*, "The design of nanoparticles obtained by solvent evaporation: a comprehensive study," *Langmuir,* vol. 19, pp. 9504-9510, 2003.

[11] I. U. Khan, C. A. Serra, N. Anton, and T. Vandamme, "Microfluidics: a focus on improved cancer targeted drug delivery systems," *Journal of Controlled Release,* vol. 172, pp. 1065-1074, 2013.

[12] K. K. Jain, "Drug delivery systems - an overview," *Methods in Molecular Biology,* vol. 437, pp. 1-50, 2008.

[13] S. S. Suri, H. Fenniri, and B. Singh, "Nanotechnology-based drug delivery systems," *Journal of Occupational Medicine and Toxicology,* vol. 2, p. 16, 2007.

[14] C. Saraiva, C. Praça, R. Ferreira, T. Santos, L. Ferreira, and L. Bernardino, "Nanoparticle-mediated brain drug delivery: Overcoming blood-brain barrier to treat neurodegenerative diseases," *Journal of Controlled Release,* vol. 235, pp. 34-47, 2016.

[15] S. Wohlfart, S. Gelperina, and J. Kreuter, "Transport of drugs across the blood–brain barrier by nanoparticles," *Journal of Controlled Release,* vol. 161, pp. 264-273, 2012.

[16] M. J. Gomes, J. Neves, and B. Sarmento, "Nanoparticle-based drug delivery to improve the efficacy of antiretroviral therapy in the central nervous system," *International Journal of Nanomedicine,* vol. 9, pp. 1757-1769, 2014.

[17] V. Mishra, S. Mahor, A. Rawat, P. N. Gupta, P. Dubey, K. Khatri, *et al.*, "Targeted brain delivery of AZT via transferrin anchored pegylated albumin nanoparticles," *Journal of Drug Targeting,* vol. 14, pp. 45-53, 2006.

[18] R. Singh and J. W. Lillard, "Nanoparticle-based targeted drug delivery," *Experimental and Molecular Pathology,* vol. 86, pp. 215-223, 2009.
[19] J. Safari and Z. Zarnegar, "Advanced drug delivery systems: Nanotechnology of health design A review," *Journal of Saudi Chemical Society,* vol. 18, pp. 85-99, 2014.
[20] M. Singh, S. Singh, S. Prasad, and I. Gambhir, "Nanotechnology in medicine and antibacterial effect of silver nanoparticles," *Digest Journal of Nanomaterials and Biostructures,* vol. 3, pp. 115-122, 2008.
[21] M. Z. Ahmad, S. Akhter, G. K. Jain, M. Rahman, S. A. Pathan, F. J. Ahmad*, et al.*, "Metallic nanoparticles: technology overview & drug delivery applications in oncology," *Expert Opinion on Drug Delivery,* vol. 7, pp. 927-942, 2010.
[22] K. Cho, X. Wang, S. Nie, and D. M. Shin, "Therapeutic nanoparticles for drug delivery in cancer," *Clinical Cancer Research,* vol. 14, pp. 1310-1316, 2008.
[23] F. Danhier, E. Ansorena, J. M. Silva, R. Coco, A. Le Breton, and V. Préat, "PLGA-based nanoparticles: an overview of biomedical applications," *Journal of Controlled Release,* vol. 161, pp. 505-522, 2012.
[24] A. Zattoni, B. Roda, F. Borghi, V. Marassi, and P. Reschiglian, "Flow field-flow fractionation for the analysis of nanoparticles used in drug delivery," *Journal of Pharmaceutical and Biomedical Analysis,* vol. 87, pp. 53-61, 2014.
[25] S. Garg, G. Heuck, S. Ip, and E. Ramsay, "Microfluidics: a transformational tool for nanomedicine development and production," *Journal of Drug Targeting,* vol. 24, pp. 821-835, Nov 2016.
[26] G. A. Silva, "Nanotechnology approaches to crossing the blood-brain barrier and drug delivery to the CNS," *BMC Neuroscience,* vol. 9, pp. S3-S4, 2008.
[27] N. J. Abbott, "Blood–brain barrier structure and function and the challenges for CNS drug delivery," *Journal of Inherited Metabolic Disease,* vol. 36, pp. 437-449, 2013.
[28] M. Brunner, O. Langer, R. Sunder-Plassmann, G. Dobrozemsky, U. Müller, W. Wadsak*, et al.*, "Influence of functional haplotypes in the drug transporter gene ABCB1 on central nervous system drug distribution in humans," *Clinical Pharmacology & Therapeutics,* vol. 78, pp. 182-190, 2005.
[29] Y.-K. Choi and K.-W. Kim, "Blood-neural barrier: its diversity and coordinated cell-to-cell communication," *BMB Reports,* vol. 41, pp. 345-352, 2008.
[30] N. R. Saunders, C. J. Ek, M. D. Habgood, and K. M. Dziegielewska, "Barriers in the brain: a renaissance?," *Trends in Neurosciences,* vol. 31, pp. 279-286, 2008.
[31] D. J. Begley, "Delivery of therapeutic agents to the central nervous system: the problems and the possibilities," *Pharmacology & Therapeutics,* vol. 104, pp. 29-45, 2004.
[32] P. Esposito, S. Jacobson, R. Connolly, D. Gheorghe, and T. C. Theoharides, "Non-invasive assessment of blood–brain barrier (BBB) permeability using a gamma camera to detect 99 technetium-gluceptate extravasation in rat brain," *Brain Research Protocols,* vol. 8, pp. 143-149, 2001.
[33] W. M. Pardridge, "The blood-brain barrier: bottleneck in brain drug development," *Neurotherapeutics,* vol. 2, pp. 3-14, 2005.
[34] C. Ghosh, V. Puvenna, J. Gonzalez-Martinez, D. Janigro, and N. Marchi, "Blood-brain barrier P450 enzymes and multidrug transporters in drug resistance: a synergistic role in neurological diseases," *Current Drug Metabolism,* vol. 12, pp. 742-749, 2011.
[35] J. H. McCarty, "Cell biology of the neurovascular unit: implications for drug delivery across the blood-brain barrier," *Assay and Drug Development Technologies,* vol. 3, pp. 89-95, 2005.
[36] R. Paolinelli, M. Corada, L. Ferrarini, K. Devraj, C. Artus, C. J. Czupalla*, et al.*, "Wnt activation of immortalized brain endothelial cells as a tool for generating a standardized model of the blood brain barrier in vitro," *PLoS One,* vol. 8, p. e70233, 2013.
[37] S. M. Stamatovic, R. F. Keep, and A. V. Andjelkovic, "Brain endothelial cell-cell junctions: how to "open" the blood brain barrier," *Current Neuropharmacology,* vol. 6, pp. 179-192, 2008.
[38] F. Arshad, L. Wang, C. Sy, S. Avraham, and H. K. Avraham, "Blood-brain barrier integrity and breast cancer metastasis to the brain," *Pathology Research International,* vol. 2011, p. 920509, 2010.
[39] S. Tietz and B. Engelhardt, "Brain barriers: crosstalk between complex tight junctions and adherens junctions," *The Journal of Cell Biology,* vol. 209, pp. 493-506, 2015.

[40] D. A. Goodenough, J. A. Goliger, and D. L. Paul, "Connexins, connexons, and intercellular communication," *Annual Review of Biochemistry,* vol. 65, pp. 475-502, 1996.
[41] S. F. Rodrigues and D. N. Granger, "Blood cells and endothelial barrier function," *Tissue Barriers,* vol. 3, p. E978720, 2015.
[42] J. R. Gee and J. N. Keller, "Astrocytes: regulation of brain homeostasis via apolipoprotein E," *The International Journal of Biochemistry & Cell Biology,* vol. 37, pp. 1145-1150, 2005.
[43] H. Mi, H. Haeberle, and B. A. Barres, "Induction of astrocyte differentiation by endothelial cells," *The Journal of Neuroscience,* vol. 21, pp. 1538-1547, 2001.
[44] R. Cabezas, M. Ávila, J. Gonzalez, R. S. El-Bachá, E. Báez, L. M. García-Segura*, et al.*, "Astrocytic modulation of blood brain barrier: perspectives on Parkinson's disease," *Frontiers in Cellular Neuroscience,* vol. 8, 2015.
[45] K. M. Baeten and K. Akassoglou, "Extracellular matrix and matrix receptors in blood–brain barrier formation and stroke," *Developmental Neurobiology,* vol. 71, pp. 1018-1039, 2011.
[46] S. Sarkar and L. Schmued, "In vivo administration of fluorescent dextrans for the specific and sensitive localization of brain vascular pericytes and their characterization in normal and neurotoxin exposed brains," *Neurotoxicology,* vol. 33, pp. 436-443, 2012.
[47] J. Correale and A. Villa, "Cellular elements of the blood-brain barrier," *Neurochemical Research,* vol. 34, pp. 2067-2077, 2009.
[48] W. F. Hickey, K. Vass, and H. Lassmann, "Bone marrow-derived elements in the central nervous system: an immunohistochemical and ultrastructural survey of rat chimeras," *Journal of Neuropathology & Experimental Neurology,* vol. 51, pp. 246-56, 1992.
[49] B. Obermeier, R. Daneman, and R. M. Ransohoff, "Development, maintenance and disruption of the blood-brain barrier," *Nature Medicine,* vol. 19, pp. 1584-1596, 2013.
[50] A. Bignami, M. Hosley, and D. Dahl, "Hyaluronic acid and hyaluronic acid-binding proteins in brain extracellular matrix," *Anatomy and Embryology,* vol. 188, pp. 419-433, 1993.
[51] L. W. Lau, R. Cua, M. B. Keough, S. Haylock-Jacobs, and V. W. Yong, "Pathophysiology of the brain extracellular matrix: a new target for remyelination," *Nature Reviews Neuroscience,* vol. 14, pp. 722-729, 2013.
[52] Francis, Karen, J. v. Beek, C. Canova, J. W. Neal, and P. Gasque, "The Blood-brain Barrier," Photograph, Ed., ed: Cambridge University Press, 2003.
[53] J. E. Hazleton, J. W. Berman, and E. A. Eugenin, "Novel mechanisms of central nervous system damage in HIV infection," *HIV/AIDS - Research and Palliative Care,* vol. 2, pp. 39-49, 2010.
[54] E. CM de Lange, "The physiological characteristics and transcytosis mechanisms of the blood-brain barrier (BBB)," *Current Pharmaceutical Biotechnology,* vol. 13, pp. 2319-2327, 2012.
[55] W. M. Pardridge, "Blood–brain barrier delivery," *Drug Discovery Today,* vol. 12, pp. 54-61, 2007.
[56] W. M. Pardridge, "The blood-brain barrier and neurotherapeutics," *Neurotherapeutics,* vol. 2, pp. 1-2, 2005.
[57] W. M. Pardridge, "Drug and gene targeting to the brain with molecular Trojan horses," *Nature Reviews Drug Discovery,* vol. 1, pp. 131-139, 2002.
[58] B. Pavan, A. Dalpiaz, N. Ciliberti, C. Biondi, S. Manfredini, and S. Vertuani, "Progress in drug delivery to the central nervous system by the prodrug approach," *Molecules,* vol. 13, pp. 1035-1065, 2008.
[59] I. B. Sivaev and V. V. Bregadze, "Polyhedral boranes for medical applications: current status and perspectives," *European Journal of Inorganic Chemistry,* vol. 2009, pp. 1433-1450, 2009.
[60] D. Nathanson and P. S. Mischel, "Charting the course across the blood-brain barrier," *The Journal of Clinical Investigation,* vol. 121, pp. 31-33, 2011.
[61] Y. Zhang and W. M. Pardridge, "Rapid transferrin efflux from brain to blood across the blood–brain barrier," *Journal of Neurochemistry,* vol. 76, pp. 1597-1600, 2001.
[62] Y. Zhang and W. M. Pardridge, "Mediated efflux of IgG molecules from brain to blood across the blood–brain barrier," *Journal of Neuroimmunology,* vol. 114, pp. 168-172, 2001.
[63] W. M. Pardridge, "Blood–brain barrier endogenous transporters as therapeutic targets: a new model for small molecule CNS drug discovery," *Expert Opinion on Therapeutic Targets,* vol. 19, pp. 1059-1072, 2015.

[64] S. Letendre, "Central nervous system complications in HIV disease: HIV-associated neurocognitive disorder," *Topics in Antiviral Medicine,* vol. 19, pp. 137-142, 2011.
[65] D. J. Mc Carthy, M. Malhotra, A. M. O'Mahony, J. F. Cryan, and C. M. O'Driscoll, "Nanoparticles and the blood-brain barrier: advancing from in-vitro models towards therapeutic significance," *Pharmaceutical Research,* vol. 32, pp. 1161-1185, 2015.
[66] A. Tóth, S. Veszelka, S. Nakagawa, M. Niwa, and M. A Deli, "Patented in vitro blood-brain barrier models in CNS drug discovery," *Recent Patents on CNS Drug Discovery,* vol. 6, pp. 107-118, 2011.
[67] M. J. Gomes, J. Dreier, J. Brewer, S. Martins, M. Brandl, and B. Sarmento, "A new approach for a blood-brain barrier model based on phospholipid vesicles: Membrane development and siRNA-loaded nanoparticles permeability," *Journal of Membrane Science,* vol. 503, pp. 8-15, 2016.
[68] S. T. Buckley, S. M. Fischer, G. Fricker, and M. Brandl, "In vitro models to evaluate the permeability of poorly soluble drug entities: challenges and perspectives," *European Journal of Pharmaceutical Sciences,* vol. 45, pp. 235-250, 2012.
[69] A. Patabendige, "The value of in vitro models of the blood–brain barrier and their uses," *Alternatives to Laboratory Animals,* vol. 40, pp. 335-338, 2012.
[70] UNAIDS, "Global AIDS update: 2016," 2016.
[71] R. K. Vadlapatla, M. Patel, D. K. Paturi, D. Pal, and A. K. Mitra, "Clinically relevant drug–drug interactions between antiretrovirals and antifungals," *Expert Opinion on Drug Metabolism & Toxicology,* vol. 10, pp. 561-580, 2014.
[72] A. Ngo, E. Ratliff, S. McCurdy, M. Ross, C. Markham, and H. Pham, "Health-seeking behaviour for sexually transmitted infections and HIV testing among female sex workers in Vietnam," *AIDS Care,* vol. 19, pp. 878-887, 2007.
[73] T. V. Fontes, F. Vidal, and L. S. Gonçalves, "Endodontic infection in HIV-infected individuals: an overview," *ENDO,* vol. 9, pp. 15-23, 2015.
[74] K. Vidyavijayan, S. Hassan, L. Precilla, S. Swaminathan, and L. Hanna, "Comparative codon usage analysis of HIV-1 and HIV-2 genomes," *BMC Infectious Diseases,* vol. 14, p. E2, 2014.
[75] K. M. De Cock, G. Adjorlolo, E. Ekpini, T. Sibailly, J. Kouadio, M. Maran, *et al.*, "Epidemiology and transmission of HIV-2: why there is no HIV-2 pandemic," *Journal of the American Medical Association,* vol. 270, pp. 2083-2086, 1993.
[76] L. Morison, "The global epidemiology of HIV/AIDS," *British Medical Bulletin,* vol. 58, pp. 7-18, 2001.
[77] B. Tchounga, D. K. Ekouevi, E. Balestre, and F. Dabis, "Mortality and survival patterns of people living with HIV-2," *Current Opinion in HIV and AIDS,* vol. 11, pp. 537–544, 2016.
[78] J. M. Rawson, S. R. Landman, C. S. Reilly, and L. M. Mansky, "HIV-1 and HIV-2 exhibit similar mutation frequencies and spectra in the absence of G-to-A hypermutation," *Retrovirology,* vol. 12, pp. 12-60, 2015.
[79] M. Ghafouri, S. Amini, K. Khalili, and B. E. Sawaya, "HIV-1 associated dementia: symptoms and causes," *Retrovirology,* vol. 3, p. 28, 2006.
[80] H. Jonckheere, J. Anné, and E. De Clercq, "The HIV-1 reverse transcription (RT) process as target for RT inhibitors," *Medicinal Research Reviews,* vol. 20, pp. 129-154, 2000.
[81] K. Strebel, J. Luban, and K.-T. Jeang, "Human cellular restriction factors that target HIV-1 replication," *BMC Medicine,* vol. 7, p. 48, 2009.
[82] K. Das and E. Arnold, "HIV-1 reverse transcriptase and antiviral drug resistance. Part 1," *Current Opinion in Virology,* vol. 3, pp. 111-118, 2013.
[83] A. Calistri, D. Munegato, I. Carli, C. Parolin, and G. Palù, "The ubiquitin-conjugating system: Multiple roles in viral replication and infection," *Cells,* vol. 3, pp. 386-417, 2014.
[84] (December 29, 2016). *http://www.learner.org*.
[85] J. E. Clements and M. C. Zink, "Molecular biology and pathogenesis of animal lentivirus infections," *Clinical Microbiology Reviews,* vol. 9, pp. 100-117, 1996.
[86] M. K. Das and T. Chakraborty, "Progress in Brain Delivery of Anti-HIV Drugs," 2015.
[87] F. Gonzalez-Scarano and J. Martin-Garcia, "The neuropathogenesis of AIDS," *Nature Reviews Immunology,* vol. 5, pp. 69-81, 2005.
[88] M. Strazza, V. Pirrone, B. Wigdahl, and M. R. Nonnemacher, "Breaking down the barrier: the effects of HIV-1 on the blood–brain barrier," *Brain Research,* vol. 1399, pp. 96-115, 2011.

[89] A. V. Albright, S. S. Soldan, and F. González-Scarano, "Pathogenesis of human immunodeficiency virus-induced neurological disease," *Journal of Neurovirology,* vol. 9, pp. 222-227, 2003.
[90] A. Nath, "Eradication of human immunodeficiency virus from brain reservoirs," *Journal of Neurovirology,* vol. 21, pp. 227-234, 2015.
[91] V. R. Rao, A. P. Ruiz, and V. R. Prasad, "Viral and cellular factors underlying neuropathogenesis in HIV associated neurocognitive disorders (HAND)," *AIDS Research and Therapy,* vol. 11, p. 13, 2014.
[92] L. R. Sharer, E.-S. Cho, and L. G. Epstein, "Multinucleated giant cells and HTLV-III in AIDS encephalopathy," *Human Pathology,* vol. 16, p. 760, 1985.
[93] S. F. An, B. Giometto, M. Groves, R. F. Miller, A. A. Beckett, F. Gray, *et al.*, "Axonal damage revealed by accumulation of ß-APP in HIV-positive individuals without AIDS," *Journal of Neuropathology & Experimental Neurology,* vol. 56, pp. 1262-1268, 1997.
[94] H. Liu and L. Li, "A class age-structured HIV/AIDS model with impulsive drug-treatment strategy," *Discrete Dynamics in Nature and Society,* vol. 2010, 2010.
[95] P. Yeni, "Update on HAART in HIV," *Journal of Hepatology,* vol. 44, pp. S100-S103, 2006.
[96] H. Hatano, E. L. Delwart, P. J. Norris, T.-H. Lee, T. B. Neilands, C. F. Kelley, *et al.*, "Evidence of persistent low-level viremia in long-term HAART-suppressed, HIV-infected individuals," *AIDS* vol. 24, pp. 2535-2539, 2010.
[97] V. A. Braz, M. D. Barkley, R. A. Jockusch, and P. L. Wintrode, "Efavirenz binding site in HIV-1 reverse transcriptase monomers," *Biochemistry,* vol. 49, pp. 10565-10573, 2010.
[98] J. Velasco-Hernandez, H. B. Gershengorn, and S. Blower, "Could widespread use of combination antiretroviral therapy eradicate HIV epidemics?," *The Lancet Infectious Diseases,* vol. 2, pp. 487-493, 2002.
[99] E. Wong, N. Trustman, and A. Yalong, "HIV pharmacotherapy: A review of integrase inhibitors," *Journal of the American Academy of Physician Assistants,* vol. 29, pp. 36-40, 2016.
[100] D. J. McColl and X. Chen, "Strand transfer inhibitors of HIV-1 integrase: bringing IN a new era of antiretroviral therapy," *Antiviral Research,* vol. 85, pp. 101-118, 2010.
[101] P. Cotelle, "Patented HIV-1 integrase inhibitors (1998-2005)," *Recent Patents on Anti-Infective Drug Discovery,* vol. 1, pp. 1-15, 2006.
[102] I. Malet, B. Roquebert, C. Dalban, M. Wirden, B. Amellal, R. Agher, *et al.*, "Association of Gag cleavage sites to protease mutations and to virological response in HIV-1 treated patients," *Journal of Infection,* vol. 54, pp. 367-374, 2007.
[103] J. C. Tilton and R. W. Doms, "Entry inhibitors in the treatment of HIV-1 infection," *Antiviral Research,* vol. 85, pp. 91-100, 2010.
[104] WHO, "Consolidated guidelines on the use of antroviral drugs for treating and preventing HIV infection " 2016.
[105] (January 7, 2017). *https://pubchem.ncbi.nlm.nih.gov/compound/efavirenz*.
[106] I. Usach, V. Melis, and J.-E. Peris, "Non-nucleoside reverse transcriptase inhibitors: a review on pharmacokinetics, pharmacodynamics, safety and tolerability," *Journal of the International AIDS Society,* vol. 16, pp. 1-14, 2013.
[107] N. Apostolova, H. A. Funes, A. Blas-Garcia, M. J. Galindo, A. Alvarez, and J. V. Esplugues, "Efavirenz and the CNS: what we already know and questions that need to be answered," *Journal of Antimicrobial Chemotherapy,* vol. 70, pp. 2693-2708, 2015.
[108] S. Sathigari, G. Chadha, Y. P. Lee, N. Wright, D. L. Parsons, V. K. Rangari, *et al.*, "Physicochemical characterization of efavirenz–cyclodextrin inclusion complexes," *American Association of Pharmaceutical Scientists PharmSciTech,* vol. 10, pp. 81-87, 2009.
[109] S. Taneja, S. Shilpi, and K. Khatri, "Formulation and optimization of efavirenz nanosuspensions using the precipitation-ultrasonication technique for solubility enhancement," *Artificial Cells, Nanomedicine, and Biotechnology,* vol. 44, pp. 978-984, 2016.
[110] A. Mutlib, H. Chen, G. Nemeth, J. Markwalder, S. Seitz, L. Gan, *et al.*, "Identification and characterization of efavirenz metabolites by liquid chromatography/mass spectrometry and high field NMR: species differences in the metabolism of efavirenz," *Drug Metabolism and Disposition,* vol. 27, pp. 1319-1333, 1999.
[111] A. Mutlib, H. Chen, G. Nemeth, L.-S. Gan, and D. Christ, "Liquid chromatography/mass spectrometry and high-field nuclear magnetic resonance characterization of novel mixed

diconjugates of the non-nucleoside human immunodeficiency virus-1 reverse transcriptase inhibitor, efavirenz," *Drug Metabolism and Disposition,* vol. 27, pp. 1045-1056, 1999.

[112] P. F. Smith, R. DiCenzo, and G. D. Morse, "Clinical pharmacokinetics of non-nucleoside reverse transcriptase inhibitors," *Clinical Pharmacokinetics,* vol. 40, pp. 893-905, 2001.

[113] W. M. Pardridge, "Drug transport in brain via the cerebrospinal fluid," *Fluids and Barriers of the CNS,* vol. 8, p. 7, 2011.

[114] S. L. Letendre, R. J. Ellis, I. Everall, B. Ances, A. Bharti, and J. A. McCutchan, "Neurologic complications of HIV disease and their treatment," *Topics in HIV Medicine,* vol. 17, pp. 46-56, 2009.

[115] S. Letendre, C. FitzSimons, R. Ellis, D. Clifford, A. Collier, B. Gelman, *et al.*, "Correlates of CSF viral loads in 1221 volunteers of the CHARTER cohort," in *17th Conference on Retroviruses and Opportunistic infections*, 2010.

[116] N. Ciccarelli, M. Fabbiani, M. Colafigli, E. M. Trecarichi, M. C. Silveri, R. Cauda, *et al.*, "Revised central nervous system neuropenetration-effectiveness score is associated with cognitive disorders in HIV-infected patients with controlled plasma viraemia," *Antiviral Therapy,* vol. 18, pp. 153-160, 2013.

[117] A. Calcagno, "Antiretroviral Drug Penetration into the CNS Compartment," pp. 1-7, 2015.

[118] E. Stormer, L. L. von Moltke, M. D. Perloff, and D. J. Greenblatt, "Differential modulation of P-glycoprotein expression and activity by non-nucleoside HIV-1 reverse transcriptase inhibitors in cell culture," *Pharmaceutical Research,* vol. 19, pp. 1038-45, 2002.

[119] P. Curley, R. K. Rajoli, D. M. Moss, N. J. Liptrott, S. Letendre, A. Owen, *et al.*, "Efavirenz Is Predicted To Accumulate in Brain Tissue: an In Silico, In Vitro, and In Vivo Investigation," *Antimicrobial Agents and Chemotherapy,* vol. 61, pp. E1841-E1816, 2017.

[120] M. Blum, S. Liao, S. Good, and P. De Miranda, "Pharmacokinetics and bioavailability of zidovudine in humans," *The American Journal of Medicine,* vol. 85, pp. 189-194, 1988.

[121] M. J. Shelton, A. M. O'Donnell, and G. D. Morse, "Didanosine," *Annals of Pharmacotherapy,* vol. 26, pp. 660-670, 1992.

[122] S. J. Haworth, B. Christofalo, R. D. Anderson, and L. M. Dunkle, "A single-dose study to assess the penetration of stavudine into human cerebrospinal fluid in adults," *Journal of Acquired Immune Deficiency Syndromes,* vol. 17, pp. 235-238, 1998.

[123] A. Antinori, C. F. Perno, M. L. Giancola, F. Forbici, G. Ippolito, R. M. Hoetelmans, *et al.*, "Efficacy of cerebrospinal fluid (CSF)–penetrating antiretroviral drugs against HIV in the neurological compartment: different patterns of phenotypic resistance in CSF and plasma," *Clinical Infectious Diseases,* vol. 41, pp. 1787-1793, 2005.

[124] R. van Leeuwen, C. Katlama, V. Kitchen, C. A. Boucher, R. Tubiana, M. McBride, *et al.*, "Evaluation of safety and efficacy of 3TC (lamivudine) in patients with asymptomatic or mildly symptomatic human immunodeficiency virus infection: a phase I/II study," *Journal of Infectious Diseases,* vol. 171, pp. 1166-1171, 1995.

[125] P. G. Clay, "The abacavir hypersensitivity reaction: a review," *Clinical Therapeutics,* vol. 24, pp. 1502-1514, 2002.

[126] A. Calcagno, S. Bonora, M. Simiele, R. Rostagno, M. C. Tettoni, M. Bonasso, *et al.*, "Tenofovir and emtricitabine cerebrospinal fluid-to-plasma ratios correlate to the extent of blood-brainbarrier damage," *AIDS,* vol. 25, pp. 1437-1439, 2011.

[127] B. M. Best, S. L. Letendre, P. Koopmans, S. S. Rossi, D. B. Clifford, A. C. Collier, *et al.*, "Low CSF concentrations of the nucleotide HIV reverse transcriptase inhibitor, tenofovir," *Journal of Acquired Immune Deficiency Syndromes* vol. 59, pp. 376-381, 2012.

[128] J. Tiraboschi, J. Niubo, A. Vila, S. Perez-Pujol, and D. Podzamczer, "Etravirine concentrations in CSF in HIV-infected patients," *Journal of Antimicrobial Chemotherapy,* vol. 67, pp. 1446-1448, 2012.

[129] A. Yilmaz, M. Gisslen, S. Spudich, E. Lee, A. Jayewardene, F. Aweeka, *et al.*, "Raltegravir cerebrospinal fluid concentrations in HIV-1 infection," *PLoS One,* vol. 4, p. E6877, 2009.

[130] S. Letendre, A. Mills, K. Tashima, D. Thomas, S. Min, S. Chen, *et al.*, "Distribution and antiviral activity in cerebrospinal fluid (CSF) of the integrase inhibitor, dolutegravir (DTG)," in *20th Conference on Retroviruses and Opportunistic Infections*, 2013.

[131] S. Vella and M. Floridia, "Saquinavir - clinical pharmacology and efficacy," *Clinical Pharmacokinetics,* vol. 34, pp. 189-201, 1998.

[132] S. Kravcik, K. Gallicano, V. Roth, S. Cassol, N. Hawley-Foss, A. Badley, *et al.*, "Cerebrospinal fluid HIV RNA and drug levels with combination ritonavir and saquinavir," *Journal of Acquired Immune Deficiency Syndromes,* vol. 21, pp. 371-375, 1999.

[133] B. M. Best, S. L. Letendre, E. Brigid, D. B. Clifford, A. C. Collier, B. B. Gelman, *et al.*, "Low atazanavir concentrations in cerebrospinal fluid," *AIDS* vol. 23, pp. 83-87, 2009.

[134] D. Croteau, S. Letendre, B. M. Best, S. S. Rossi, R. J. Ellis, D. B. Clifford, *et al.*, "Therapeutic amprenavir concentrations in cerebrospinal fluid," *Antimicrobial Agents and Chemotherapy,* vol. 56, pp. 1985-1989, 2012.

[135] A. Yilmaz, A. Izadkhashti, R. W. Price, P. W. Mallon, M. De Meulder, P. Timmerman, *et al.*, "Darunavir concentrations in cerebrospinal fluid and blood in HIV-1–infected individuals," *AIDS Research and Human Retroviruses,* vol. 25, pp. 457-461, 2009.

[136] R. W. Price, R. Parham, J. Lu, S. A. Wring, B. Baker, J. Sailstad, *et al.*, "Enfuvirtide cerebrospinal fluid (CSF) pharmacokinetics and potential use in defining CSF HIV-1 origin," *Antiviral Therapy,* vol. 13, pp. 369-374, 2008.

[137] D. Croteau, B. M. Best, S. Letendre, S. S. Rossi, R. J. Ellis, D. B. Clifford, *et al.*, "Lower than expected maraviroc concentrations in cerebrospinal fluid exceed the wild-type CCR5-tropic HIV-1 50% inhibitory concentration," *AIDS,* vol. 26, pp. 890-893, 2012.

[138] D. F. Williams, *The Williams dictionary of biomaterials*: Liverpool University Press, 1999.

[139] A. Gautam and F. C. Van Veggel, "Synthesis of nanoparticles, their biocompatibility, and toxicity behavior for biomedical applications," *Journal of Materials Chemistry B,* vol. 1, pp. 5186-5200, 2013.

[140] A. Asti and L. Gioglio, "Natural and synthetic biodegradable polymers: different scaffolds for cell expansion and tissue formation," *International Journal of Artificial Organs,* vol. 37, pp. 187-205, 2014.

[141] K. S. Finnie, D. J. Waller, F. L. Perret, A. M. Krause-Heuer, H. Q. Lin, J. V. Hanna, *et al.*, "Biodegradability of sol–gel silica microparticles for drug delivery," *Journal of Sol-gel Science and Technology,* vol. 49, pp. 12-18, 2009.

[142] J. Roul, R. Mohapatra, and S. K. Sahoo, "Preparation, characterization and drug delivery behaviour of novel biopolymer/hydroxyapatite nanocomposite beads," *Asian Journal of Biomedical and Pharmaceutical Sciences,* vol. 3, pp. 33-38, 2013.

[143] S. Ramakrishna, J. Mayer, E. Wintermantel, and K. W. Leong, "Biomedical applications of polymer-composite materials: a review," *Composites Science and Technology,* vol. 61, pp. 1189-1224, 2001.

[144] V. B. Damodaran, D. Bhatnagar, and N. S. Murthy, "Biomedical Polymers: Synthesis and Processing," ed: Springer, 2016.

[145] S. G. Sukaryo, A. Purnama, and H. Hermawan, "Structure and Properties of Biomaterials," in *Biomaterials and Medical Devices*, ed: Springer, 2016, pp. 1-22.

[146] A. Halliday and M. Cook, "Polymer-based drug delivery devices for neurological disorders," *CNS & Neurological Disorders - Drug Targets* vol. 8, pp. 205-221, 2009.

[147] C. P. Reis, R. J. Neufeld, A. J. Ribeiro, and F. Veiga, "Nanoencapsulation I. Methods for preparation of drug-loaded polymeric nanoparticles," *Nanomedicine: Nanotechnology, Biology and Medicine,* vol. 2, pp. 8-21, 2006.

[148] E. M. Pridgen, R. Langer, and O. C. Farokhzad, "Biodegradable, polymeric nanoparticle delivery systems for cancer therapy," *Nanomedicine* vol. 2, pp. 669-680, 2007.

[149] S. Sharma, A. Parmar, S. Kori, and R. Sandhir, "PLGA-based nanoparticles: a new paradigm in biomedical applications," *Trends in Analytical Chemistry,* vol. 80, pp. 30-40, 2015.

[150] K. Letchford and H. Burt, "A review of the formation and classification of amphiphilic block copolymer nanoparticulate structures: micelles, nanospheres, nanocapsules and polymersomes," *European Journal of Pharmaceutics and Biopharmaceutics,* vol. 65, pp. 259-269, 2007.

[151] W. Abdelwahed, G. Degobert, S. Stainmesse, and H. Fessi, "Freeze-drying of nanoparticles: formulation, process and storage considerations," *Advanced Drug Delivery Reviews,* vol. 58, pp. 1688-1713, 2006.

[152] H. K. Makadia and S. J. Siegel, "Poly lactic-co-glycolic acid (PLGA) as biodegradable controlled drug delivery carrier," *Polymers,* vol. 3, pp. 1377-1397, 2011.

[153] H. Jeffery, S. Davis, and D. O'hagan, "The preparation and characterisation of poly(lactide-co-glycolide) microparticles. I: Oil-in-water emulsion solvent evaporation," *International Journal of Pharmaceutics,* vol. 77, pp. 169-175, 1991.

[154] K. Avgoustakis, "Pegylated poly(lactide) and poly(lactide-co-glycolide) nanoparticles: preparation, properties and possible applications in drug delivery," *Current Drug Delivery,* vol. 1, pp. 321-333, 2004.
[155] (January 8, 2017). *http://www.medscape.com*.
[156] P. Fonte, F. Araújo, C. Silva, C. Pereira, S. Reis, H. A. Santos, *et al.*, "Polymer-based nanoparticles for oral insulin delivery: revisited approaches," *Biotechnology Advances,* vol. 33, pp. 1342-1354, 2015.
[157] I. Vroman and L. Tighzert, "Biodegradable polymers," *Materials,* vol. 2, pp. 307-344, 2009.
[158] P. Qu, Y. Gao, G. Wu, and L. Zhang, "Nanocomposites of poly(lactic acid) reinforced with cellulose nanofibrils," *BioResources,* vol. 5, pp. 1811-1823, 2010.
[159] L. Lim, R. Auras, and M. Rubino, "Processing technologies for poly(lactic acid)," *Progress in Polymer Science,* vol. 33, pp. 820-852, 2008.
[160] F. Luderer, M. Löbler, H. W. Rohm, C. Gocke, K. Kunna, K. Köck, *et al.*, "Biodegradable sirolimus-loaded poly(lactide) nanoparticles as drug delivery system for the prevention of in-stent restenosis in coronary stent application," *Journal of Biomaterials Applications,* vol. 25, pp. 851-875, 2011.
[161] M. Li, O. Rouaud, and D. Poncelet, "Microencapsulation by solvent evaporation: state of the art for process engineering approaches," *International Journal of Pharmaceutics,* vol. 363, pp. 26-39, 2008.
[162] T. Betancourt, B. Brown, and L. Brannon-Peppas, "Doxorubicin-loaded PLGA nanoparticles by nanoprecipitation: preparation, characterization and in vitro evaluation," *Nanomedicine* vol. 2, pp. 219-232, 2007.
[163] K. S. Yadav and K. K. Sawant, "Modified nanoprecipitation method for preparation of cytarabine-loaded PLGA nanoparticles," *American Association of Pharmaceutical Scientists PharmSciTech,* vol. 11, pp. 1456-1465, 2010.
[164] A. Alshamsan, "Nanoprecipitation is more efficient than emulsion solvent evaporation method to encapsulate cucurbitacin I in PLGA nanoparticles," *Saudi Pharmaceutical Journal,* vol. 22, pp. 219-222, 2014.
[165] A. Perez, R. Hernández, D. Velasco, D. Voicu, and C. Mijangos, "Poly(lactic-co-glycolic acid) particles prepared by microfluidics and conventional methods. Modulated particle size and rheology," *Journal of Colloid and Interface Science,* vol. 441, pp. 90-97, 2015.
[166] A. Kazimirova, Z. Magdolenova, M. Barancokova, M. Staruchova, K. Volkovova, and M. Dusinska, "Genotoxicity testing of PLGA–PEO nanoparticles in TK6 cells by the comet assay and the cytokinesis-block micronucleus assay," *Mutation Research/Genetic Toxicology and Environmental Mutagenesis,* vol. 748, pp. 42-47, 2012.
[167] P. Gentile, V. Chiono, I. Carmagnola, and P. V. Hatton, "An overview of poly(lactic-co-glycolic) acid (PLGA)-based biomaterials for bone tissue engineering," *International Journal of Molecular Sciences,* vol. 15, pp. 3640-3659, 2014.
[168] J.-M. Lü, X. Wang, C. Marin-Muller, H. Wang, P. H. Lin, Q. Yao, *et al.*, "Current advances in research and clinical applications of PLGA-based nanotechnology," *Expert Review of Molecular Diagnostics,* vol. 9, pp. 325-341, 2009.
[169] K. K. Vangara, J. L. Liu, and S. Palakurthi, "Hyaluronic acid-decorated PLGA-PEG nanoparticles for targeted delivery of SN-38 to ovarian cancer," *Anticancer Research,* vol. 33, pp. 2425-34, 2013.
[170] A. Kumari, S. K. Yadav, and S. C. Yadav, "Biodegradable polymeric nanoparticles based drug delivery systems," *Colloids and Surfaces B: Biointerfaces,* vol. 75, pp. 1-18, 2010.
[171] M. V. Bandulasena, G. T. Vladisavljević, O. G. Odunmbaku, and B. Benyahia, "Continuous synthesis of PVP stabilized biocompatible gold nanoparticles with a controlled size using a 3D glass capillary microfluidic device," *Chemical Engineering Science,* vol. 171, pp. 233-243, 2017.
[172] I. D. Rosca, F. Watari, and M. Uo, "Microparticle formation and its mechanism in single and double emulsion solvent evaporation," *Journal of Controlled Release,* vol. 99, pp. 271-280, 2004.
[173] U. Wais, A. W. Jackson, T. He, and H. Zhang, "Nanoformulation and encapsulation approaches for poorly water-soluble drug nanoparticles," *Nanoscale,* vol. 8, pp. 1746-1769, 2016.

[174] H. Fessi, F. Puisieux, J. P. Devissaguet, N. Ammoury, and S. Benita, "Nanocapsule formation by interfacial polymer deposition following solvent displacement," *International Journal of Pharmaceutics,* vol. 55, pp. R1-R4, 1989.

[175] S. Stainmesse, H. Fessi, J.-P. Devissaguet, F. Puisieux, and C. Theis, "Process for the preparation of dispersible colloidal systems of a substance in the form of nanoparticles," *US Patent 5, 118, 528,* 1992.

[176] U. Bilati, E. Allémann, and E. Doelker, "Development of a nanoprecipitation method intended for the entrapment of hydrophilic drugs into nanoparticles," *European Journal of Pharmaceutical Sciences,* vol. 24, pp. 67-75, 2005.

[177] Y. Tan, K. Xu, L. Li, C. Liu, C. Song, and P. Wang, "Fabrication of size-controlled starch-based nanospheres by nanoprecipitation," *ACS Applied Materials & Interfaces,* vol. 1, pp. 956-959, 2009.

[178] D. T. Birnbaum, J. D. Kosmala, D. B. Henthorn, and L. Brannon-Peppas, "Controlled release of ß-estradiol from PLAGA microparticles:: The effect of organic phase solvent on encapsulation and release," *Journal of Controlled Release,* vol. 65, pp. 375-387, 2000.

[179] K. Bouchemal, S. Briançon, E. Perrier, and H. Fessi, "Nano-emulsion formulation using spontaneous emulsification: solvent, oil and surfactant optimisation," *International Journal of Pharmaceutics,* vol. 280, pp. 241-251, 2004.

[180] A. M. de Oliveira, E. Jäger, A. Jäger, P. Stepánek, and F. C. Giacomelli, "Physicochemical aspects behind the size of biodegradable polymeric nanoparticles: a step forward," *Colloids and Surfaces A: Physicochemical and Engineering Aspects,* vol. 436, pp. 1092-1102, 2013.

[181] L. Wu, J. Zhang, and W. Watanabe, "Physical and chemical stability of drug nanoparticles," *Advanced Drug Delivery Reviews,* vol. 63, pp. 456-469, 2011.

[182] P. Legrand, S. Lesieur, A. Bochot, R. Gref, W. Raatjes, G. Barratt, *et al.*, "Influence of polymer behaviour in organic solution on the production of polylactide nanoparticles by nanoprecipitation," *International Journal of Pharmaceutics,* vol. 344, pp. 33-43, 2007.

[183] J. S. Lee, S. J. Hwang, D. S. Lee, S. C. Kim, and D. J. Kim, "Formation of poly(ethylene glycol)-poly(ε-caprolactone) nanoparticles via nanoprecipitation," *Macromolecular Research,* vol. 17, pp. 72-78, 2009.

[184] J. P. Rao and K. E. Geckeler, "Polymer nanoparticles: preparation techniques and size-control parameters," *Progress in Polymer Science,* vol. 36, pp. 887-913, 2011.

[185] E. Rideal and J. Davies, "Interfacial phenomena," ed: Academic Press, 1963.

[186] G. M. Whitesides, "The origins and the future of microfluidics," *Nature,* vol. 442, pp. 368-373, 2006.

[187] W. C. Tian and E. Finehout, "Microfluidics for biological applications," ed: Springer Science & Business Media, 2009.

[188] X. Yi, R. Kodzius, X. Gong, K. Xiao, and W. Wen, "A simple method of fabricating mask-free microfluidic devices for biological analysis," *Biomicrofluidics,* vol. 4, p. 036503, 2010.

[189] M. J. Jebrail, N. Assem, J. M. Mudrik, M. D. Dryden, K. Lin, A. K. Yudin, *et al.*, "Combinatorial synthesis of peptidomimetics using digital microfluidics," *Journal of Flow Chemistry,* vol. 2, pp. 103-107, 2012.

[190] Y. Ling, J. Rubin, Y. Deng, C. Huang, U. Demirci, J. M. Karp, *et al.*, "A cell-laden microfluidic hydrogel," *Lab on a Chip,* vol. 7, pp. 756-762, 2007.

[191] R. P. Johnson, E. Choi, K. M. Lee, S. J. Yu, H. C. Chang, H. Suh, *et al.*, "Microfluidics assisted fabrication of microspheres by poly(2–hydroxyethyl methacrylate)-block-poly(l-histidine) hybrid materials and their utilization as potential drug encapsulants," *Microfluidics and Nanofluidics,* vol. 14, pp. 257-263, 2013.

[192] X. Kang, C. Luo, Q. Wei, C. Xiong, Q. Chen, Y. Chen, *et al.*, "Mass production of highly monodisperse polymeric nanoparticles by parallel flow focusing system," *Microfluidics and Nanofluidics,* vol. 15, pp. 337-345, 2013.

[193] F. Bally, D. K. Garg, C. A. Serra, Y. Hoarau, N. Anton, C. Brochon, *et al.*, "Improved size-tunable preparation of polymeric nanoparticles by microfluidic nanoprecipitation," *Polymer,* vol. 53, pp. 5045-5051, 2012.

[194] R. Karnik, F. Gu, P. Basto, C. Cannizzaro, L. Dean, W. Kyei-Manu, *et al.*, "Microfluidic platform for controlled synthesis of polymeric nanoparticles," *Nano letters,* vol. 8, pp. 2906-2912, 2008.

[195] H. Xie and J. W. Smith, "Fabrication of PLGA nanoparticles with a fluidic nanoprecipitation system," *Journal of Nanobiotechnology,* vol. 8, p. 18, 2010.

[196] L.-H. Hung, S.-Y. Teh, J. Jester, and A. P. Lee, "PLGA micro/nanosphere synthesis by droplet microfluidic solvent evaporation and extraction approaches," *Lab on a chip,* vol. 10, pp. 1820-1825, 2010.

[197] Q. Feng, J. Sun, and X. Jiang, "Microfluidics-mediated assembly of functional nanoparticles for cancer-related pharmaceutical applications," *Nanoscale,* vol. 8, pp. 12430-12443, 2016.

[198] M. M. Yallapu, B. K. Gupta, M. Jaggi, and S. C. Chauhan, "Fabrication of curcumin encapsulated PLGA nanoparticles for improved therapeutic effects in metastatic cancer cells," *Journal of Colloid and Interface Science,* vol. 351, pp. 19-29, 2010.

[199] R. Riahi, A. Tamayol, S. A. M. Shaegh, A. M. Ghaemmaghami, M. R. Dokmeci, and A. Khademhosseini, "Microfluidics for advanced drug delivery systems," *Current Opinion in Chemical Engineering,* vol. 7, pp. 101-112, 2015.

[200] L. Capretto, D. Carugo, S. Mazzitelli, C. Nastruzzi, and X. Zhang, "Microfluidic and lab-on-a-chip preparation routes for organic nanoparticles and vesicular systems for nanomedicine applications," *Advanced Drug Delivery Reviews,* vol. 65, pp. 1496-1532, 2013.

[201] W. J. Duncanson, T. Lin, A. R. Abate, S. Seiffert, R. K. Shah, and D. A. Weitz, "Microfluidic synthesis of advanced microparticles for encapsulation and controlled release," *Lab on a Chip,* vol. 12, pp. 2135-2145, 2012.

[202] D. Liu, H. Zhang, F. Fontana, J. Hirvonen, and H. A. Santos, "Microfluidic-assisted fabrication of carriers for controlled drug delivery," *Lab on a Chip,* vol. 17, pp. 1856-1883 2017.

[203] H. F. Chan, S. Ma, and K. W. Leong, "Can microfluidics address biomanufacturing challenges in drug/gene/cell therapies?," *Regenerative Biomaterials,* vol. 3, pp. 87–98, 2016.

[204] P. Mitchell, "Microfluidics-downsizing large-scale biology," *Nature Biotechnology,* vol. 19, pp. 717-721, 2001.

[205] G. T. Vladisavljević, N. Khalid, M. A. Neves, T. Kuroiwa, M. Nakajima, K. Uemura*, et al.*, "Industrial lab-on-a-chip: Design, applications and scale-up for drug discovery and delivery," *Advanced Drug Delivery Reviews,* vol. 65, pp. 1626-1663, 2013.

[206] S. L. Anna, N. Bontoux, and H. A. Stone, "Formation of dispersions using “flow focusing” in microchannels," *Applied Physics Letters,* vol. 82, pp. 364-366, 2003.

[207] J. Shan, M. Nuopponen, H. Jiang, T. Viitala, E. Kauppinen, K. Kontturi*, et al.*, "Amphiphilic gold nanoparticles grafted with poly(N-isopropylacrylamide) and polystyrene," *Macromolecules,* vol. 38, pp. 2918-2926, 2005.

[208] C.-X. Zhao, "Multiphase flow microfluidics for the production of single or multiple emulsions for drug delivery," *Advanced Drug Delivery Reviews,* vol. 65, pp. 1420-1446, 2013.

[209] F. Araujo, N. Shrestha, M.-A. Shahbazi, D. Liu, B. Herranz-Blanco, E. M. Mäkilä*, et al.*, "Microfluidic assembly of a multifunctional tailorable composite system designed for site specific combined oral delivery of peptide drugs," *ACS Nano,* vol. 9, pp. 8291-8302, 2015.

[210] C. A. Serra and Z. Chang, "Microfluidic-assisted synthesis of polymer particles," *Chemical Engineering & Technology,* vol. 31, pp. 1099-1115, 2008.

[211] D. Liu, H. Zhang, E. Mäkilä, J. Fan, B. Herranz-Blanco, C.-F. Wang*, et al.*, "Microfluidic assisted one-step fabrication of porous silicon@ acetalated dextran nanocomposites for precisely controlled combination chemotherapy," *Biomaterials,* vol. 39, pp. 249-259, 2015.

[212] D. Liu, S. Cito, Y. Zhang, C. F. Wang, T. M. Sikanen, and H. A. Santos, "A versatile and robust microfluidic platform toward high throughput synthesis of homogeneous nanoparticles with tunable properties," *Advanced Materials,* vol. 27, pp. 2298-2304, 2015.

[213] T. He, Q. Liang, K. Zhang, X. Mu, T. Luo, Y. Wang*, et al.*, "A modified microfluidic chip for fabrication of paclitaxel-loaded poly(l-lactic acid) microspheres," *Microfluidics and Nanofluidics,* vol. 10, pp. 1289-1298, 2011.

[214] T. Watanabe, T. Ono, and Y. Kimura, "Continuous fabrication of monodisperse polylactide microspheres by droplet-to-particle technology using microfluidic emulsification and emulsion–solvent diffusion," *Soft Matter,* vol. 7, pp. 9894-9897, 2011.

[215] S.-Y. Teh, R. Lin, L.-H. Hung, and A. P. Lee, "Droplet microfluidics," *Lab on a Chip,* vol. 8, pp. 198-220, 2008.

[216] A. Utada, E. Lorenceau, D. Link, P. Kaplan, H. Stone, and D. Weitz, "Monodisperse double emulsions generated from a microcapillary device," *Science,* vol. 308, pp. 537-541, 2005.

[217] Z. Nie, S. Xu, M. Seo, P. C. Lewis, and E. Kumacheva, "Polymer particles with various shapes and morphologies produced in continuous microfluidic reactors," *Journal of the American Chemical Society,* vol. 127, pp. 8058-63, 2005.

[218] M. Seo, C. Paquet, Z. Nie, S. Xu, and E. Kumacheva, "Microfluidic consecutive flow-focusing droplet generators," *Soft Matter,* vol. 3, pp. 986-992, 2007.
[219] A. R. Abate, J. Thiele, and D. A. Weitz, "One-step formation of multiple emulsions in microfluidics," *Lab on a Chip,* vol. 11, pp. 253-258, 2011.
[220] D. Liu, H. Zhang, B. Herranz-Blanco, E. Mäkilä, V. P. Lehto, J. Salonen, *et al.*, "Microfluidic Assembly of Monodisperse Multistage pH-Responsive Polymer/Porous Silicon Composites for Precisely Controlled Multi-Drug Delivery," *Small,* vol. 10, pp. 2029-2038, 2014.
[221] L. Y. Chu, J. W. Kim, R. K. Shah, and D. A. Weitz, "Monodisperse Thermoresponsive Microgels with Tunable Volume-Phase Transition Kinetics," *Advanced Functional Materials,* vol. 17, pp. 3499-3504, 2007.
[222] J. das Neves and B. Sarmento, "Precise engineering of dapivirine-loaded nanoparticles for the development of anti-HIV vaginal microbicides," *Acta Biomaterialia,* vol. 18, pp. 77-87, 2015.
[223] C. Cunha-Reis, A. Machado, L. Barreiros, F. Araujo, R. Nunes, V. Seabra, *et al.*, "Nanoparticles-in-film for the combined vaginal delivery of anti-HIV microbicide drugs," *Journal of Controlled Release,* vol. 243, pp. 43-53, 2016.
[224] M. J. Gomes, C. Fernandes, S. Martins, F. Borges, and B. Sarmento, "Tailoring Lipid and Polymeric Nanoparticles as siRNA Carriers towards the Blood-Brain Barrier–from Targeting to Safe Administration," *Journal of Neuroimmune Pharmacology,* pp. 1-13, 2016.
[225] A. M. Pinto, C. Gonçalves, D. M. Sousa, A. R. Ferreira, J. A. Moreira, I. C. Gonçalves, *et al.*, "Smaller particle size and higher oxidation improves biocompatibility of graphene-based materials," *Carbon,* vol. 99, pp. 318-329, 2016.
[226] M.-A. Shahbazi, M. Hamidi, E. M. Mäkilä, H. Zhang, P. V. Almeida, M. Kaasalainen, *et al.*, "The mechanisms of surface chemistry effects of mesoporous silicon nanoparticles on immunotoxicity and biocompatibility," *Biomaterials,* vol. 34, pp. 7776-7789, 2013.
[227] B. Mendes, C. Marques, I. Carvalho, P. Costa, S. Martins, D. Ferreira, *et al.*, "Influence of glioma cells on a new co-culture in vitro blood–brain barrier model for characterization and validation of permeability," *International Journal of Pharmaceutics,* vol. 490, pp. 94-101, 2015.
[228] M. J. Gomes, P. J. Kennedy, S. Martins, and B. Sarmento, "Delivery of siRNA silencing P-gp in peptide-functionalized nanoparticles causes efflux modulation at the blood–brain barrier," *Nanomedicine,* vol. 12, pp. 1385-1399, 2017.
[229] U. Bilati, E. Allémann, and E. Doelker, "Nanoprecipitation versus emulsion-based techniques for the encapsulation of proteins into biodegradable nanoparticles and process-related stability issues," *American Association of Pharmaceutical Scientists PharmSciTech,* vol. 6, pp. E594-E604, 2005.
[230] X. Tian, F. Wei, T. Wang, P. Wang, X. Lin, J. Wang, *et al.*, "In vitro and in vivo studies on gelatin-siloxane nanoparticles conjugated with SynB peptide to increase drug delivery to the brain," *International Journal of Nanomedicine,* vol. 7, pp. 1031-1041, 2012.
[231] I. M. Adjei, C. Peetla, and V. Labhasetwar, "Heterogeneity in nanoparticles influences biodistribution and targeting," *Nanomedicine,* vol. 9, pp. 267-278, 2014.
[232] Y. Monsalve, G. Tosi, B. Ruozi, D. Belletti, A. Vilella, M. Zoli, *et al.*, "PEG-g-chitosan nanoparticles functionalized with the monoclonal antibody OX26 for brain drug targeting," *Nanomedicine,* vol. 10, pp. 1735-1750, 2015.
[233] S. Stolnik, M. Garnett, M. Davies, L. Illum, M. Bousta, M. Vert, *et al.*, "The colloidal properties of surfactant-free biodegradable nanospheres from poly(ß-malic acid-co-benzyl malate)s and poly(lactic acid-co-glycolide)," *Colloids and Surfaces A: Physicochemical and Engineering Aspects,* vol. 97, pp. 235-245, 1995.
[234] M. R. Kulterer, M. Reischl, V. E. Reichel, S. Hribernik, M. Wu, S. Köstler, *et al.*, "Nanoprecipitation of cellulose acetate using solvent/nonsolvent mixtures as dispersive media," *Colloids and Surfaces A: Physicochemical and Engineering Aspects,* vol. 375, pp. 23-29, 2011.
[235] N. García, R. Rubio-Presa, P. García-García, M. A. Fernández-Rodríguez, M. R. Pedrosa, F. J. Arnáiz, *et al.*, "A selective, efficient and environmentally friendly method for the oxidative cleavage of glycols," *Green Chemistry,* vol. 18, pp. 2335-2340, 2016.
[236] R. Alyautdin, I. Khalin, M. I. Nafeeza, M. H. Haron, and D. Kuznetsov, "Nanoscale drug delivery systems and the blood–brain barrier," *International Journal of Nanomedicine,* vol. 9, pp. 795-811, 2014.

[237] K. Gao and X. Jiang, "Influence of particle size on transport of methotrexate across blood brain barrier by polysorbate 80-coated polybutylcyanoacrylate nanoparticles," *International Journal of Pharmaceutics,* vol. 310, pp. 213-9, 2006.

[238] E. Dashtimoghadam, H. Mirzadeh, F. A. Taromi, and B. Nyström, "Microfluidic self-assembly of polymeric nanoparticles with tunable compactness for controlled drug delivery," *Polymer,* vol. 54, pp. 4972-4979, 2013.

[239] A. Valério, D. S. Conti, P. H. Araújo, C. Sayer, and S. R. da Rocha, "Synthesis of PEG-PCL-based polyurethane nanoparticles by miniemulsion polymerization," *Colloids and Surfaces B: Biointerfaces,* vol. 135, pp. 35-41, 2015.

[240] M. Noubarani, F. Keyhanfar, M. Motevalian, and M. Mahmoudian, "Improved HPLC method for determination of four PPIs, omeprazole, pantoprazole, lansoprazole and rabeprazole in human plasma," *Journal of Pharmacy & Pharmaceutical Sciences,* vol. 13, pp. 1-10, 2010.

[241] L. Martín-Banderas, E. Sáez-Fernández, M. Á. Holgado, M. M. Durán-Lobato, J. C. Prados, C. Melguizo, *et al.*, "Biocompatible gemcitabine-based nanomedicine engineered by Flow Focusing for efficient antitumor activity," *International Journal of Pharmaceutics,* vol. 443, pp. 103-109, 2013.

[242] X. Song, Y. Zhao, W. Wu, Y. Bi, Z. Cai, Q. Chen, *et al.*, "PLGA nanoparticles simultaneously loaded with vincristine sulfate and verapamil hydrochloride: systematic study of particle size and drug entrapment efficiency," *International Journal of Pharmaceutics,* vol. 350, pp. 320-329, 2008.

[243] J. Della Rocca, D. Liu, and W. Lin, "Are high drug loading nanoparticles the next step forward for chemotherapy?," *Nanomedicine,* vol. 7, pp. 303-305, 2012.

[244] D. Liu, H. Zhang, S. Cito, J. Fan, E. M. Mäkilä, J. J. Salonen, *et al.*, "Core/shell nanocomposites produced by superfast sequential microfluidic nanoprecipitation," *Nano Letters,* vol. 17, pp. 606-614, 2017.

[245] C. F. Brayton, "Dimethyl sulfoxide (DMSO): a review," *The Cornell Veterinarian,* vol. 76, pp. 61-90, 1986.

[246] B. Wang, W. Jiang, H. Yan, X. Zhang, L. Yang, L. Deng, *et al.*, "Novel PEG-graft-PLA nanoparticles with the potential for encapsulation and controlled release of hydrophobic and hydrophilic medications in aqueous medium," *International Journal of Nanomedicine,* vol. 6, pp. 1443-1451, 2011.

[247] L. K. Shah and M. M. Amiji, "Intracellular delivery of saquinavir in biodegradable polymeric nanoparticles for HIV/AIDS," *Pharmaceutical Research,* vol. 23, pp. 2638-2645, 2006.

[248] M. V. Patel and F.-J. Chen, "Triglyceride-free compositions and methods for improved delivery of hydrophobic therapeutic agents," *US Patent 6, 294, 192,* 2001.

[249] F. Araújo, N. Shrestha, M.-A. Shahbazi, P. Fonte, E. M. Mäkilä, J. J. Salonen, *et al.*, "The impact of nanoparticles on the mucosal translocation and transport of GLP-1 across the intestinal epithelium," *Biomaterials,* vol. 35, pp. 9199-9207, 2014.

[250] J. Emami, H. Hamishehkar, A. R. Najafabadi, K. Gilani, M. Minaiyan, H. Mahdavi, *et al.*, "A novel approach to prepare insulin-loaded poly(lactic-co-glycolic acid) microcapsules and the protein stability study," *Journal of Pharmaceutical Sciences,* vol. 98, pp. 1712-1731, 2009.

[251] S. Salatin, J. Barar, M. Barzegar-Jalali, K. Adibkia, F. Kiafar, and M. Jelvehgari, "Development of a nanoprecipitation method for the entrapment of a very water soluble drug into Eudragit RL nanoparticles," *Pharmaceutical Research,* vol. 12, p. 1, 2017.

[252] J. das Neves, M. Amiji, M. F. Bahia, and B. Sarmento, "Assessing the physical–chemical properties and stability of dapivirine-loaded polymeric nanoparticles," *International Journal of Pharmaceutics,* vol. 456, pp. 307-314, 2013.

[253] I. Takeuchi, K. Tomoda, A. Hamano, and K. Makino, "Effects of physicochemical properties of poly(lactide-co-glycolide) on drug release behavior of hydrophobic drug-loaded nanoparticles," *Colloids and Surfaces A: Physicochemical and Engineering Aspects,* vol. 520, pp. 771-778, 2017.

[254] P. Sansdrap and A. Moes, "In vitro evaluation of the hydrolytic degradation of dispersed and aggregated poly(DL-lactide-co-glycolide) microspheres," *Journal of Controlled Release,* vol. 43, pp. 47-58, 1997.

[255] A. Trapani, J. Sitterberg, U. Bakowsky, and T. Kissel, "The potential of glycol chitosan nanoparticles as carrier for low water soluble drugs," *International Journal of Pharmaceutics,* vol. 375, pp. 97-106, 2009.

[256] A. Dankowska and M. Małecka, "Application of synchronous fluorescence spectroscopy for determination of extra virgin olive oil adulteration," *European Journal of Lipid Science and Technology,* vol. 111, pp. 1233-1239, 2009.
[257] (June 2, 2017). *http://pepbank.mgh.harvard.edu/interactions/details/45306*.
[258] J. Bart, R. Tiggelaar, M. Yang, S. Schlautmann, H. Zuilhof, and H. Gardeniers, "Room-temperature intermediate layer bonding for microfluidic devices," *Lab on a Chip,* vol. 9, pp. 3481-3488, 2009.
[259] C. Velasco-Aguirre, F. Morales, E. Gallardo-Toledo, S. Guerrero, E. Giralt, E. Araya, *et al.*, "Peptides and proteins used to enhance gold nanoparticle delivery to the brain: preclinical approaches," *International Journal of Nanomedicine,* vol. 10, p. 4919, 2015.
[260] J. M. Silva, G. Vandermeulen, V. G. Oliveira, S. N. Pinto, C. Rodrigues, A. Salgado, *et al.*, "Development of functionalized nanoparticles for vaccine delivery to dendritic cells: a mechanistic approach," *Nanomedicine,* vol. 9, pp. 2639-2656, 2014.
[261] J. A. Berges, A. E. Fisher, and P. J. Harrison, "A comparison of Lowry, Bradford and Smith protein assays using different protein standards and protein isolated from the marine diatom Thalassiosira pseudonana," *Marine Biology,* vol. 115, pp. 187-193, 1993.
[262] V. Sanna, I. A. Siddiqui, M. Sechi, and H. Mukhtar, "Resveratrol-loaded nanoparticles based on poly(epsilon-caprolactone) and poly(d, l-lactic-co-glycolic acid)–poly(ethylene glycol) blend for prostate cancer treatment," *Molecular Pharmaceutics,* vol. 10, pp. 3871-3881, 2013.
[263] G. Platzer, M. Okon, and L. P. McIntosh, "pH-dependent random coil (1)H, (13)C, and (15)N chemical shifts of the ionizable amino acids: a guide for protein pK a measurements," *Journal of Biomolecular NMR,* vol. 60, pp. 109-129, 2014.
[264] T. J. Kinnari, A. Soininen, J. Esteban, N. Zamora, E. Alakoski, V. P. Kouri, *et al.*, "Adhesion of staphylococcal and Caco-2 cells on diamond-like carbon polymer hybrid coating," *Journal of Biomedical Materials Research Part A,* vol. 86, pp. 760-768, 2008.
[265] K. Gellynck, V. Kodeck, E. Van De Walle, K. Kersemans, F. De Vos, H. Declercq, *et al.*, "First step toward near-infrared continuous glucose monitoring: in vivo evaluation of antibody coupled biomaterials," *Experimental Biology and Medicine,* vol. 240, pp. 446-457, 2015.
[266] E. H. Decloedt and G. Maartens, "Neuronal toxicity of efavirenz: a systematic review," *Expert Opinion on Drug Safety,* vol. 12, pp. 841-846, 2013.
[267] R. G. Guan, I. Johnson, T. Cui, T. Zhao, Z. Y. Zhao, X. Li, *et al.*, "Electrodeposition of hydroxyapatite coating on Mg-4.0Zn-1.0Ca-0.6Zr alloy and in vitro evaluation of degradation, hemolysis, and cytotoxicity," *Journal of Biomedical Materials Research Part A,* vol. 100, pp. 999-1015, 2012.
[268] K. Amin and R. M. Dannenfelser, "In vitro hemolysis: guidance for the pharmaceutical scientist," *Journal of Pharmaceutical Sciences,* vol. 95, pp. 1173-6, 2006.
[269] S. A. McClave, "Nutritional assessment in inflammatory bowel disease: application of nutrition strategies to the management of the difficult Crohn's patient," *The American Journal of Gastroenterology,* vol. 102, pp. S88-S93, 2007.
[270] Z. Peng, S. Pati, D. Potter, R. Brown, J. B. Holcomb, R. Grill, *et al.*, "Fresh frozen plasma lessens pulmonary endothelial inflammation and hyperpermeability after hemorrhagic shock and is associated with loss of syndecan-1," *Shock (Augusta, Ga.),* vol. 40, pp. 195-202, 2013.
[271] L.-F. Blume, M. Denker, F. Gieseler, and T. Kunze, "Temperature corrected transepithelial electrical resistance (TEER) measurement to quantify rapid changes in paracellular permeability," *Die Pharmazie,* vol. 65, pp. 19-24, 2010.
[272] S. Van der Merwe, J. Verhoef, J. Verheijden, A. Kotzé, and H. Junginger, "Trimethylated chitosan as polymeric absorption enhancer for improved peroral delivery of peptide drugs," *European Journal of Pharmaceutics and Biopharmaceutics,* vol. 58, pp. 225-235, 2004.
[273] B. Weksler, E. Subileau, N. Perriere, P. Charneau, K. Holloway, M. Leveque, *et al.*, "Blood-brain barrier-specific properties of a human adult brain endothelial cell line," *The FASEB journal,* vol. 19, pp. 1872-1874, 2005.
[274] C. Förster, M. Burek, I. A. Romero, B. Weksler, P. O. Couraud, and D. Drenckhahn, "Differential effects of hydrocortisone and TNFα on tight junction proteins in an in vitro model of the human blood–brain barrier," *The Journal of Physiology,* vol. 586, pp. 1937-1949, 2008.